Involvement of intracellular signaling mechanisms in the pro-inflammatory response induced by amorphous silica nanoparticles in bronchial epithelial lung cells (BEAS-2B)

Thu Huong Thi Nguyen

Master thesis at School of Pharmacy

Department of Pharmaceutical Bioscience

Faculty of Mathematics and Natural Sciences

UNIVERSITY OF OSLO

May 2015

Involvement of intracellular signaling mechanisms in the pro-inflammatory response induced by amorphous silica nanoparticles in bronchial epithelial lung cells (BEAS-2B)

Master thesis in Pharmacology for the grade Master in Pharmacy at

Department of Pharmaceutical Biosciences
School of Pharmacy
Faculty of Mathematics and Natural Sciences
University of Oslo

The thesis was carried out at

Department of Air Pollution and Noise

Division of Environmental Medicine

Norwegian Institute of Public Health

Supervisors

Marit Låg

Magne Refsnes

Tonje Skuland

Ragnhild Paulsen

2015

Involvement of intracellular signaling mechanisms in the pro-inflammatory response induced by amorphous silica nanoparticles in bronchial epithelial lung cells (BEAS-2B)

Thu Huong Thi Nguyen

http://www.duo.uio.no/

Print: Reprosentralen, Universitetet i Oslo

Acknowledgements

The work on this thesis was carried out at the Department of Air Pollution and Noise at the Norwegian Institute of Public Health in the period August 2014 to May 2015. First, I would like to thank my main supervisors Magne Refsnes and Marit Låg for your enthusiasm for the subject, constructive feedback, and always being available for questions and discussions. A special gratitude goes to my co-supervisor Tonje Skuland for amazing technical guidance and supervision in the laboratory, giving me help with planning experiments, and for all your valuable comments. Thank you all for your knowledge, good mood and support through this whole period giving me calming words in a stressing writing period.

Furthermore, I would like to thank the head of the department, Per Schwarze, for welcoming me with open arms and giving me the opportunity to work on the thesis at the division. Special thanks is also extended to Hans Jørgen Dahlman for helping me with the ELISA method, and Leni Ekeren and Edel Lilleaas for always providing answers when help was most needed in the laboratory. I would also like to thank the rest of the research group at MILS for always being helpful, and for all the lovely conversations in the hallways. You guys helped making this thesis year an exciting and educational year.

I would also thank my parents who have supported me through my entire education, giving me motivation when I needed it the most and making it possible to reach my goals. Lastly, I would like to thank my brother for his encouragement and believing in me, especially in the last couple of weeks during moments of stress and frustration.

Thu Huong Thi Nguyen

Oslo, May 2015

Abstract

The presence of nanoparticles in commercially available products has increased drastically in the last decade. Nanoparticles, which are defined as particles with a diameter range from 1 to 100 nm in at least one dimension, have unique physicochemical properties compared to larger-sized particles of similar chemical composition. This might be due to their small size, large surface area, and surface reactivity. Because there is still limited knowledge on their effect on human health and environment, it is important to characterize their chemical properties and potential toxicity to confirm the safety of nanoparticles. The research group has previously demonstrated that amorphous silica nanoparticles (10 nm and 50 nm) have the potential to elicit marked pro-inflammatory cytokine responses mediated through mitogen-activated protein kinases (MAPKs) in a bronchial cell line (BEAS-2B). Si50 has also been shown to induce cytokine responses through nuclear factor (NF)-κB signaling pathways. In the present thesis, the pro-inflammatory and cytotoxic potential of SiNP of 10 nm and 50 nm size to induce gene expression and cytokine responses of IL-6, IL-8, IL-1β and TNF-α were compared at equal mass concentrations in the same bronchial cell line. Three different cell densities of BEAS-2B cells were used to determine if cytokine responses and cytotoxicity of SiNP-exposed cells were affected by cell density in culture. Furthermore, the involvement of the intracellular signaling pathways NF-κB and PKC in mediating the release of IL-6 and IL-8 were examined.

The study showed a size- and concentration-dependent increase in pro-inflammatory responses of IL-6, IL-8, RANTES, TNF-α and IL-1β, as well as cytotoxicity measured as LDH-release in BEAS-2B cells after exposure to Si10 and Si50. Si10 caused a stronger response of both IL-6 and IL-8 compared to Si50 at similar particle concentrations. The SiNP-induced RANTES-, IL-1β- and TNF-α responses were less clearly increased by the nanoparticles compared to IL-6 and IL-8, and with Si10 as most potent on mass basis. For both particle sizes, the pattern of release was similar for IL-6 and IL-8. This was different for RANTES showing different pattern of release between Si10 and Si50. Regarding cell density of BEAS-2B cells, cultures with the intermediate cell density induced the highest cytokine release for Si10. However, the effects of cell density upon exposure to Si50 were less distinct. The relative LDH-release was little affected by cell density. Gene expression showed a greater mRNA expression of IL-6 and IL-8 compared to IL-1β and TNF-α, with a more prolonged up-regulation for Si10 than Si50. The activation of NF-κB through the

phosphorylation of p65 and degradation of IκB-α was demonstrated in SiNP-exposed BEAS-2B cells. In addition to this, pre-treatment with inhibition of p65 showed the involvement of NF-κB in the release of IL-6 and IL-8 in Si10- and Si50-exposed cells, as demonstrated by the chemical NF-κB inhibitor PDT-p65, and siRNA against p65. It was also demonstrated by using the broad PKC-inhibitor GF109203X that PKC was partly involved in the induction of IL-6 and IL-8 release in BEAS-2B cells.

In conclusion, SiNP caused a size- and concentration-dependent increase in pro-inflammatory responses of IL-6, IL-8, RANTES, TNF-α and IL-1β, as well as LDH-release, with Si10 being more potent than Si50. The cell density was of importance for the cytokine responses, whereas cytotoxicity was little affected. A more prolonged gene expression of IL-6, IL-8, IL-1β and TNF-α was seen for Si10-exposed cells compared to Si50. Both Si10-and Si50 seemed to exert their effects on IL-6 and IL-8 via a mechanism involving NF-κB and possibly PKC.

Abbreviations

ADAM	A disintegrin and a metalloprotease domain
AP-1	Activator protein-1
AP antibody	Alkaline phosphatase antibody
BEAS-2B	Human bronchial epithelial cell line
BSA	Bovine serum albumin
CCL5	See RANTES
cDNA	Complementary DNA
CD28	Cluster of differentiation 28
CXCL8	See IL-8
C/EBP	CCAAT/enhancer-binding proteins
DAG	Diacylglycerol
DMEM/F12	Dulcobecco's Modified Eagle Medium: Nutrient Mixture F-12
EGFR	Epidermal growth factor receptor
ELISA	Enzyme-linked immunosorbent assay
ERK	Extracellular signal-regulated kinases
GM-CSF	Granulocyte macrophage colony-stimulating factor
IκB	Nuclear factor of kappa light polypeptide gene enhancer in B-cells inhibitor
IKK-β	Inhibitor of nuclear factor kappa-B kinase subunit beta
IL-1	Interleukin-1
IL-1R	Interleukin-1 receptor
IL-6	Interleukin-6
IL-8	Interleukin-8
JNK	c-JUN NH_2-terminal kinases
LDH	Lactate dehydrogenase
mRNA	Messenger ribonucleic acid
MAPK	Mitogen-activated protein kinase
MAPKKK	Mitogen-activated kinase kinase kinase

MIP-2	Macrophage inflammatory protein-1
MKK	Mitogen-activated protein kinase kinase
NALP3	NACHT, LRR and PYD containing protein 3
NLRP3	See NALP3
NF-κB	Nuclear factor kappa-light-chain-enhancer of activated B cells
NOD	Nucleotide-binding oligomerization domain
p38 MAPK	p38 mitogen-activated protein kinase
PBS	Phosphate buffered saline
PKA	Protein kinase A
PKC	Protein kinase C
RANTES	Regulated on Activation, Normal T Cell Expressed and Secreted
RIG	Retinoic acid-inducible gene
ROS	Reactive oxygen species
SiNP	Silica nanoparticle
Si10	Silica nanoparticle 10 nm
Si50	Silica nanoparticle 50 nm
siRNA	Small interfering RNA
SV40	Simian virus 40
TACE	Tumor necrosis factor-α converting enzyme
TGF-β	Transformed growth factor-β
TLR	Toll-like receptors
TNF-α	Tumor necrosis factor-α
TNFR	Tumor necrosis factor receptor

Table of content

1 Introduction

1.1 Background

In recent years, the number of nanoparticle-based materials has increased drastically in the marketplace [1]. Nanoparticles are defined as particles with a diameter range from 1 to 100 nm in at least one dimension, and exhibit unique features different than its bulky counterpart [2]. Nanoparticles exist naturally in the environment, but are also generated as by-products of anthropogenic processes, e.g. vaporization, combustion, welding fumes and from diesel- and petrol-fuelled vehicles [3].

Nanotechnology is used in a wide range of applications which includes food, cosmetics, electronics, and biomedical supplies for diagnostic, *in vivo* imaging and therapeutic purposes [4-8]. Physicochemical properties of nanoparticles such as their small size allow them to reach different biological compartments and target specific organs within the body [9]. This gives the advantage of a site-specific pulmonary delivery of inhaled drug particles in the airways [10], thus reducing the risk for adverse effects. Another approach to target specific cells is coating of nanoparticles with bioconjugates (i.e. DNA, proteins, and monoclonal antibodies). This emphasizes the importance of safety evaluation to ensure that these modifications do not cause any adverse effects *in vivo* [5]. Most nanoparticles are used as carriers in treating diseases such as asthma, tuberculosis, emphysema and cystic fibrosis, but have also been used in various cancer treatments [11].

However, the increased use of engineered nanoparticles and continuous discovery of new applications of nanoparticles have raised concerns about undesirable effects as there is still limited knowledge about their effect on human health and on the environment [8, 12]. Knowledge of health effects in miners and trade workers is useful, because they are vulnerable to inhalation of particulate matters through occupational exposure, [13]. Inhaled environmental and occupational pollutants such as silica have shown to produce alveolar epithelial injuries [14]. It is well known that the smaller the diameter of nanoparticles, the higher potency they have to induce inflammation in the lung [11]. It is therefore important to characterize their chemical properties and potential toxicity to confirm the safety of nanoparticles, especially in *in vivo* applications as they have the potential to penetrate intracellular targets in the lungs, and may also to a low extent reach the systemic circulation

[4-6]. This may in turn cause oxidative stress, inflammation, genotoxicity and fibrosis in the respiratory system, and thus potentially induce irreversible pulmonary diseases and injuries in other tissues [11]. Therefore, to ensure occupational and consumer safety, it is essential to gain information on biological reactivity [15] and possible toxic effects of nanoparticles[12].

1.2 Nanoparticles

1.2.1 Particle characterization

Nanoparticles are defined as particles with a diameter range from 1 to 100 nm in at least one dimension [16, 17], and may be divided in naturally occurring nanoparticles, anthropogenic nanoparticles and engineered nanomaterials. The physicochemical characterization of nanoparticles (e.g. size, shape, surface charge, chemical properties, crystal structure, solubility and degree of agglomeration) is important to characterize for the evaluation of the toxicological effect and thus safety of nanoparticles [18-20].

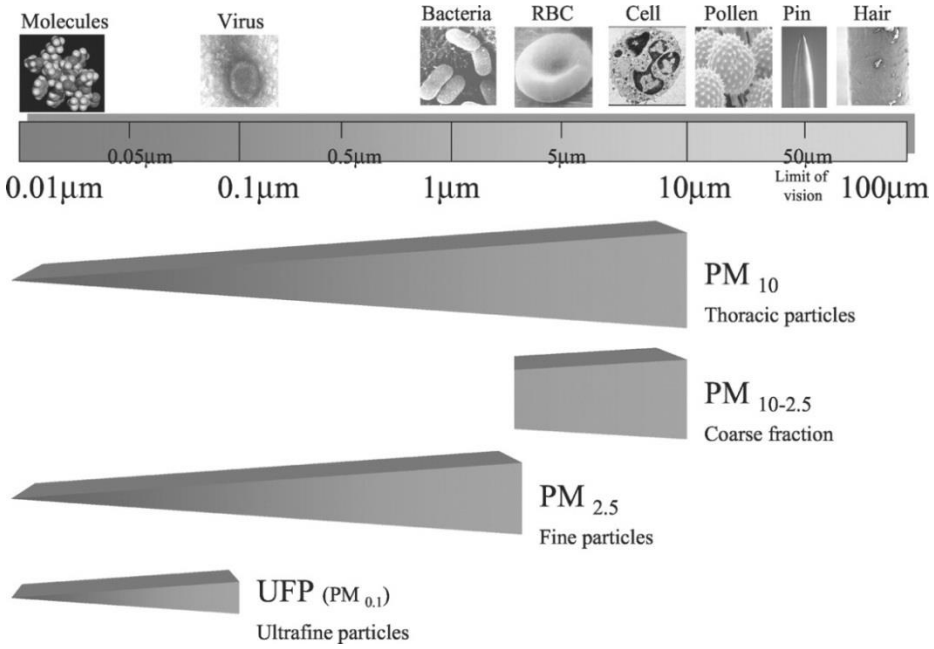

Figure 1: Size scale for different particles compared to various materials [21]

1.2.1.1 Particle size and surface area

From a toxicological point of view, particle size and surface area are important characteristics to evaluate, because the amount of reactive groups increases with decreasing particle size and increasing surface area [22].

Nanoparticles have a greater surface area per volume compared to larger particles with the same mass and similar chemical composition due to the higher amount of atoms on the surface available for chemical reactions. This increases the particles chemical and biological reactivity per given mass unit leading to a more intense airway inflammation [23-26]. A greater surface area may also increase the amount of adsorbed environmental pollutants, oxidant gases, organic substances and transition metals to the particle surface [27]. Nanoparticles are therefore associated with a greater production of reactive oxygen species, oxidative stress and secretion of pro-inflammatory cytokines compared to larger particles [28]. The surface area is also dependent of the chemistry and shape of particles, and thus small chemical alterations or defects of the nanoparticle surface may change its activity [23].

1.2.1.2 Particle shape

Engineered nanoparticles may be synthesized in different shapes such as particles, rods, fibers, sheets and wires [29]. It has been demonstrated that the shape of nanoparticles might affect their biological effect. *In vivo* and *in vitro* studies on micro-sized spherical and fibrous material have shown that fibrous materials (e.g. asbestos, fiberglass) induce higher cytotoxic and genotoxic effects, increasing the risk for lung fibrosis and lung cancer. Fibers have also greater biopersistence than spherical particles, giving longer interactions with cells and thus stronger biological effects. This has also been demonstrated for smaller particles where experiments with titanium dioxide (TiO_2) nanoparticles have shown greater toxicity with fibers than with spheres [28]

1.2.1.3 Surface charge

The surface charge of nanoparticles is important for tissue distribution, because the cell membrane is comprised of an anionic (negatively charged) and hydrophilic outer surface. Cationic (positively charged) nanomaterials may therefore be attracted to the cell surface and promote an internalization into cells [29]. Nanoparticles with a negative charge surface interact with cationic sites on cell surfaces. Neutral nanoparticles interact to a lesser extent with cell surfaces which may lead to a longer circulation time [17]. These properties will also determine which biomolecules will interact with the particle surface in the biological compartments [29]. Interaction forces that occur at the nanoscale are van der Waals, electrostatic, solvation and depletion forces [7]. Some nanomaterials have also the potential to

exert toxicity by releasing toxic ions. Their ability to dissociate in biological fluids is dependent on their chemical composition [17].

1.2.1.4 Protein corona

Surface coating of nanoparticles, either during manufacturing or by adsorption of lipids and proteins at the portal of entry and during translocation, may alter the effects and biokinetics of nanoparticles as well as their interaction with cells [23]. The amount of bound proteins may form a protein corona, which is a dynamic layer of proteins that covers the particle surface [9], depending on nanoparticle properties and physiological environment (e.g. respiratory system, gastrointestinal tract, blood lymph etc.). This leads to a negative net charge and zeta potential of the particles at physiological pH. Hydrophobicity, the higher surface charge and greater surface area of nanoparticles may potentially increase the adsorption of proteins to the nanoparticle surface [7, 17]. The protein corona may modify the properties of nanoparticles potentially altering their biodistribution and toxicity [17].

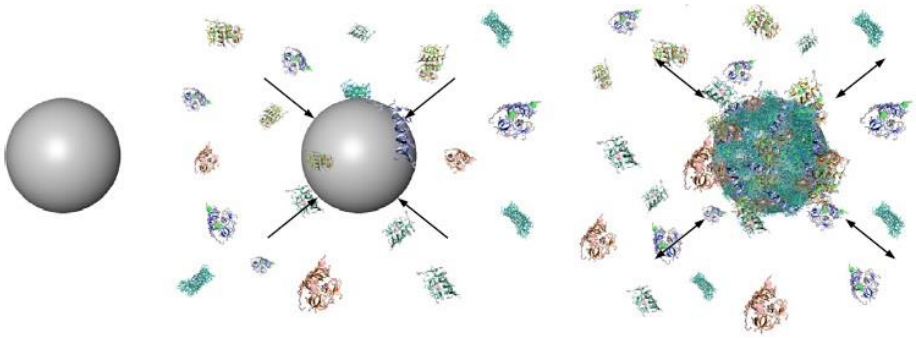

Figure 2: Formation of a protein corona on the nanoparticle surface *(http://mappingignorance.org/2013/06/05/nanohazards/)*

Protein coronas are normally divided in hard coronas and soft coronas. Hard coronas consist of tightly bound proteins that do not readily desorb, while soft coronas consist of loosely bound proteins that adsorb with low affinity. It is believed that hard corona proteins interact directly with the nanoparticle surface. On the other hand, soft corona proteins interact with the hard corona through weak protein-protein interactions. Proteins that are adsorbed to a nanoparticle, are in a continuous state of dynamic exchange, and may desorb at any time point allowing other proteins to interact with the nanoparticle surface. Proteins with a high association rate and a short residence time will adsorb stronger to a nanoparticle, but they will

also be replaced rapidly with other proteins that might have a slower association rate, but longer residence time [7] .

1.2.1.5 Agglomeration/aggregation

The particle dispersion and agglomeration state may be affected by the solvent or media used [29]. As the particle size decreases, the surface energy increases and facilitates stronger interactions between nanoparticles [9]. To reduce the surface tension, the particles adhere to each other by weak forces to increase their size and decrease their surface area which cause them to agglomerate [25, 30]. The agglomeration of airborne engineered nanomaterials or their attachment to ubiquitous background particles can cause rapid changes in their physicochemical characteristics [3] and thus influence their biological responses. The particles in the agglomerate are held together by weak forces, such as van der Waals forces, electrostatic interactions or surface tension [7]. Agglomerates can therefore be easily re-dispersed by ultrasonic treatment or in certain biological environments [16]. Other factors promoting agglomeration is the presence of salt and electrolytes in biological solution which may neutralize repulsion of surface charges on nanoparticles allowing them to agglomerate [7]. A study by Gosens et al [25] also showed that nanogold particles agglomerated to a larger extent in PBS than water, which was difficult to bring back to suspension by sonication. Consequently, the toxicity of nanoparticles varies depending on different medium used.

When nanoparticles are subjected to stronger forces, aggregates are formed making it more difficult to separate the particles. The state of agglomeration or aggregation may change the biological behavior of particles and thus probably influence airway deposition, clearance mechanisms as well as their immunological and toxicological effects [16, 28]. Despite this, it is believed that aggregates maintain the toxicity of the nanoparticles they comprise of due to the high surface area of nanoparticles which is retained in the aggregates [31].

1.3 The respiratory system

1.3.1 The anatomy

The respiratory system is divided into the upper and lower respiratory tract separated by the larynx. The lower respiratory tract is also commonly divided in the conducting airways and the peripheral airways, starting with the trachea, continues to the bronchi, branches to bronchioles and ends in the alveolar ducts and sacs (figure 3). With each branching of the bronchioles both the diameter and length of the tubules decreases, but concurrently the increased number of airways leads to a higher surface area [32].

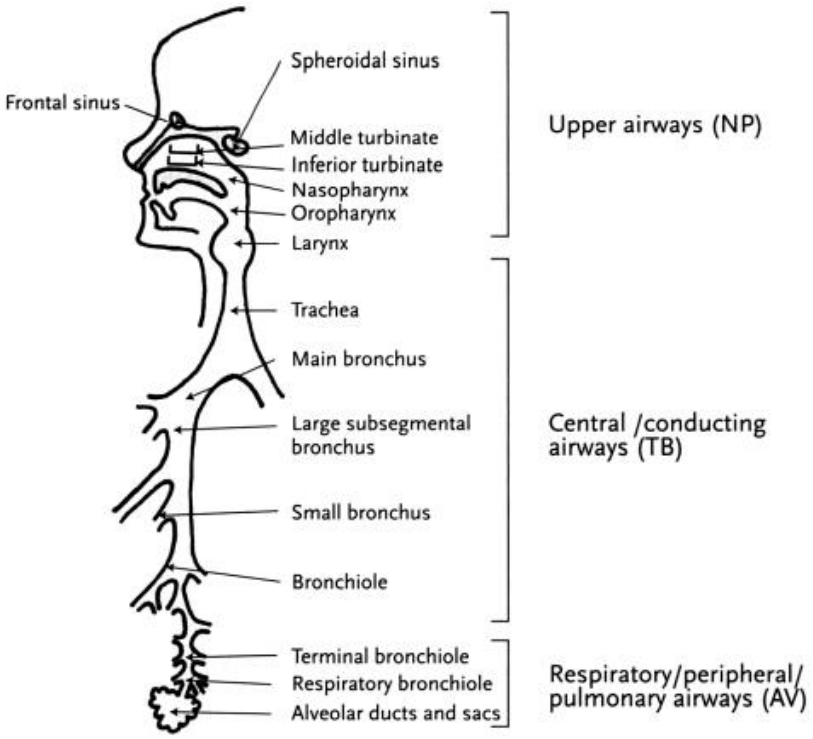

Figure 3: The respiratory tract [32]

1.3.2 Cells in the respiratory system

There are more than 40 distinct cell types in the respiratory system. The epithelial layer forms the interface between the respiratory system and the inspired air, i.e. the air-liquid interface. Both ciliated and non-ciliated cells such as bronchiolar Clara cells, goblet cells and basal cells cover the mucosa layer in the trachea, bronchi and bronchioles. This layer lies on a connective tissue substratum consisting of a basement membrane, lamina propria and submucosa, and

contains smooth muscle, glands and cartilage [33]. The cilia of the upper respiratory epithelium has the ability to remove microorganisms and other potentially hazardous substances by continuous transportation of mucus and foreign substances toward the larynx (mucociliar clearance) where they are swallowed [34]. Goblet cells (mucous cells) are the most important producers of mucus in the airways [33].

In the present study, a SV-transformed human bronchial epithelial cell line (BEAS-2B cells) is used. The bronchiolar epithelium consists of two cell populations - ciliated and non-ciliated cells - supported by a basement membrane. These cells are a part of the innate immune system which defends the airways against harmful substances [33]. Ciliated cells are most prone to injury and will lose cilia, die and degrade into the airway lumen after severe injury. Non-ciliated cells (Clara cells) are more resistant to injury, have a secretory function and can proliferate and differentiate to ciliated cells [35].

Type I cells (pneumocytes) are flat epithelial cells that cover approximately 90 percent of the alveolar area and are also involved in the gas exchange of O_2 and CO_2 between air and pulmonary capillary blood [10]. The alveolar epithelium is a part of the air-blood barrier which keeps circulating blood from direct exposure to airborne toxicants and pathogens [14]. On the other hand, type II cells are specialized cuboidal epithelial cells which synthetize and secrete the alveolar surfactant, consisting of a mixture of lipoproteins. This plays an important role of decreasing the surface tension to prevent an alveolar collapse [10]. In this way the morphology and function of the respiratory system is maintained. Type II cells are also precursors for type I cells, and have therefore the ability to proliferate and differentiate into new type I cells to restore damaged type I cells, and thereby maintain a normal alveolar epithelium [14].

1.4 Particle deposition in the respiratory tract

The lung is a major site of interaction with inhaled particulates because of its large surface area and thin air-blood tissue barrier [14]. The airways consist of epithelium protected by a thick layer of mucus, which forms a barrier preventing penetration of particles. The barrier between the alveolar wall and the capillaries are on the other hand thin and weak in gas exchange areas, making them less well protected against harmful substances from the environment [11]. After deposition on the alveolar wall, some nanoparticles might be able to penetrate the air-blood tissue barrier into the alveolar capillaries [14].

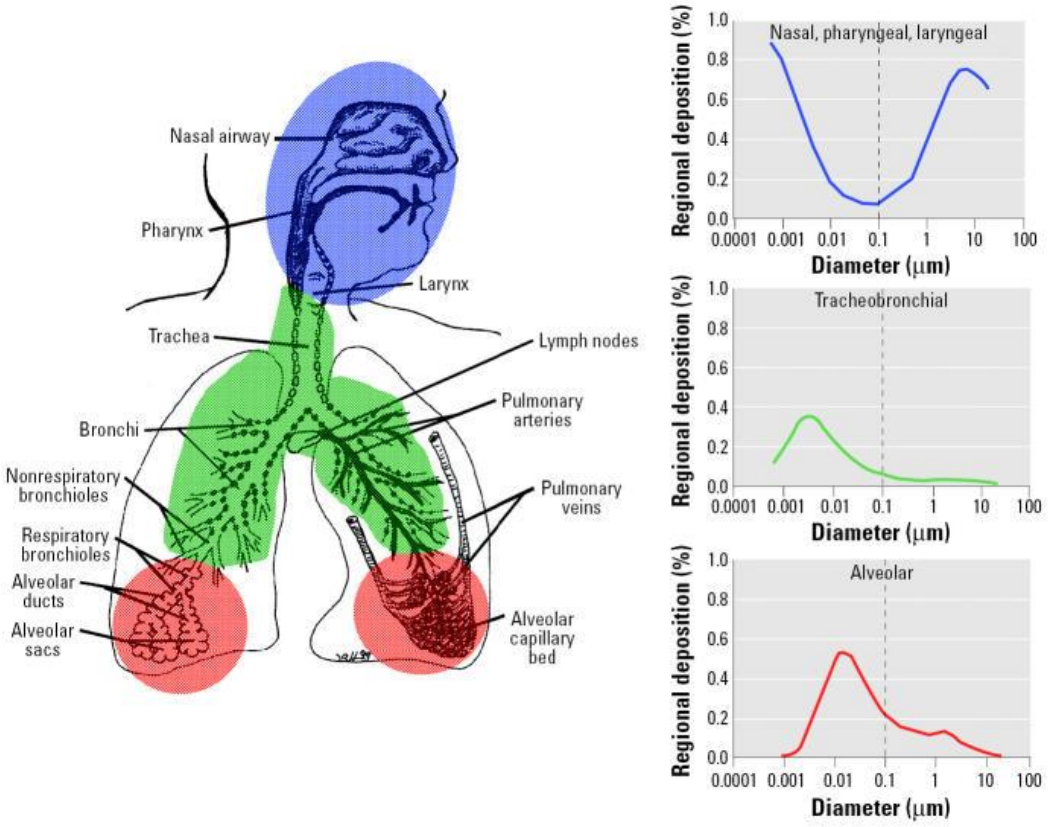

Figure 4: Site of deposition of inhaled particles with different particle sizes **[36]**

The site of deposition of inhaled particles is mainly determined by particle size and shape where large particles (> 10 µm) are distributed in the upper part of the respiratory system, while smaller particles (0.1-3 µm) can reach the conducting airways and alveoli [10, 37]. Furthermore, the smallest particles (1-5 nm) will also deposit in the nasal passage (see Fig 4). A fraction of ultrafine particles (< 0.1 µm), i.e. nanoparticles, might depending on the size have the ability to penetrate through the air-blood tissue barrier and enter the alveolar

capillaries after deposition on the alveolar wall [14]. In these regions, the residence time of deposited particles in the distal airways and alveoli are increased [38], which may in turn trigger inflammatory responses in the lung and potentially cause harmful responses in the circulatory system [10]. Different breathing patterns may also change the site of deposition of particles with a specific size. Particle density may also play a role in deposition [37].

1.4.1 Mechanisms of particle deposition

Within the respiratory tract, there are different deposition mechanisms of particles depending on particle size. The most important ones are interception, inertial impaction, sedimentation and Brownian diffusion [37].

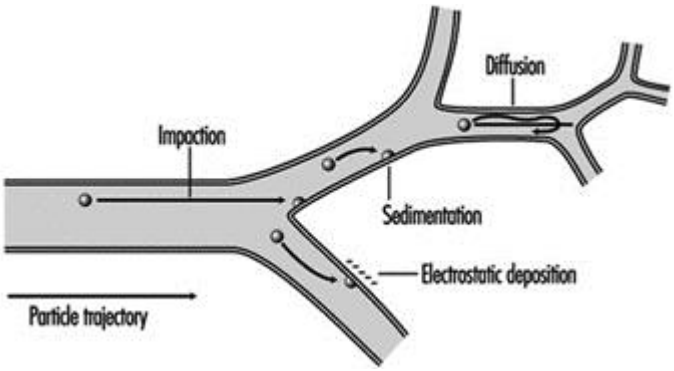

Figure 5: Deposition mechanisms in the lung
(http://www.ilo.org/iloenc/images/stories/enlarged/Part01/RES_imgs/RES010F2.jpg)

Interception forces (particle-surface contact) are relevant for fibers that can attach to the airways' walls when they pass through the respiratory tract. Particles in the size range 0.5-3 µm will deposit by sedimentation and reach bronchioles and alveoli which have a lower airstream velocity. Deposition of particles is dependent on their residence time in the airways as well as its size and density. This occurs especially during slow and deep breathing.

Inertial impaction is mainly the deposition mechanisms for particles > 5 µm in the upper respiratory tract and conducting airways. Upon a bifurcation in the respiratory tract, a change in direction of the air stream causes particles with high velocity to impact on the airway's

walls instead of changing the direction with the air stream. A greater impaction is seen for larger particles, particles with high densities or those travelling in higher velocities [32, 39] .

Particles greater than 10 µm impact in the upper airways and are removed by coughing, swallowing and mucociliary mechanisms. Smaller particles (0.5-5 µm), which avoid impaction in the upper respiratory tract, may deposit by impaction and sedimentation in the lower airways. The velocity of the air stream decreases with the branching of the conducting airways, and the impaction becomes less important as a deposition mechanism [39].

Particle deposition by diffusion is significant as the particle size decreases (< 0.3 µm) [40] and is relevant for regions where the airflow is low or absent, e.g. in distal airways and alveoli [32, 38, 39]. Brownian movement occurs when there is a collision of small particles by gas molecules in the respiratory tract. The movement from a high to a low concentration causes the particles to change the direction from the aerosol to the airways' walls. The rate of diffusion is inversely proportional to the particle size. Particles of 0.5 µm are usually immediately exhaled, because they are too small for effective impaction or sedimentation and too large for deposition by Brownian diffusion [39].

Inhaled nanoparticles deposit mainly by Brownian diffusion and may be deposited both in the upper and the lower respiratory tract. The particles do not usually distribute evenly in the respiratory system, but seem to be concentrated in certain areas [41]. Where they are deposited is mostly determined by their particle size. A model developed by the International Commission on Radiobiological Protection (ICRP) have suggested that nanoparticles of 1 nm in diameter deposit to a higher degree in the nasopharynx and in some degree in the tracheobronchial tree because of a higher diffusion velocity [28]. During aggregation or agglomeration, the nanoparticle size may change from the nano-size to the micro-size range [28]. Nanoparticles with a primary or agglomerate particle size with a diameter of 10-100 nm are believed to deposit more efficiently in the alveolar region compared to larger particles with a diameter of 0.1-1 µm [42].

It has also been suggested that small nanoparticles with a size of 10-40 nm will deposit mainly in the bronchioles, but also in the nose, trachea, throat, pharynx and in the alveoli. Nanoparticles with a size of 50 nm deposit as equally in the alveoli as in the bronchioles, while greater nanoparticles (> 50 nm) deposit in a larger extent in the alveolar region [43].

Because the highest deposition of nanoparticles is in the bronchi and bronchioles, studying the effects of inhaled nanoparticles in these areas are therefore relevant.

1.4.2 Physiological factors affecting particle deposition in the airways

The method of breathing is an important factor that could affect the deposition of particles. Both breathe holding and quiet breathing leads to a larger inhaled volume and thus greater peripheral distribution of particles. During heavy breathing (e.g. during exercise), deposition of particles in the larger airways increases by inertial impaction, because larger volumes are inhaled at higher velocities [37, 39]. The increase in ventilation may also cause a switch from nasal to mouth breathing which may in turn increase the exposure to particulate matter or pulmonary dose of a compound [10]. Particle deposition by sedimentation and diffusion are enhanced during breath holding after inhalation, because it increases the time between the end of inspiration and the start of exhalation, and thereby increases the time for sedimentation to occur [39].

Particle deposition may be altered by factors modifying the diameter of the conducting airways, such as in patients with lung diseases because of changes in breathing patterns and fine pulmonary structures [44]. For example, the mucous layer in patients with chronic bronchitis is thickened and extended peripherally and may partially block the airways in some areas. This can potentially alter the airflow and increase the risk of deposition of particles in the respiratory system [37]. It is suggested that nanoparticles have a higher deposition in alveoli in individuals with chronic inflammatory diseases such as asthma and chronic obstructive pulmonary disease compared to healthy individuals [14, 45, 46]. This may be due an increased residence time of particles in the alveolar region because of non-uniform ventilation, distribution, damaged clearance ability and flow perturbations [29, 47].

1.4.3 Interaction of nanoparticles with the pulmonary surfactant system

The surfactant layer, existing in the alveolar region and peripheral airways, is the initial contact area during deposition of inhaled nanoparticles. Binding of nanoparticles to surfactant components, such as phospholipids or surfactant protein, may alter the particles' toxic effects and/or particle clearance, as well as the surfactants biophysical function [31, 48]. However, there are still little knowledge on nanoparticles' effect on the biophysical function of the

pulmonary surfactant and their potential to alter the respiratory system [49, 50]. It has been suggested that particle size and surface area is of importance in causing severe damage to the lung surfactant structure [51]. This is due to their high surface area per mass unit, which gives them the ability to bind more surfactant components [31]. For example Schleh et al [48] demonstrated that TiO_2 nanoparticles may adjust both the structure and function of the pulmonary surfactant system compared to micro-sized particles, indicating that particle size and surface area might have a critical role for the biophysical response of the surfactant in the respiratory system.

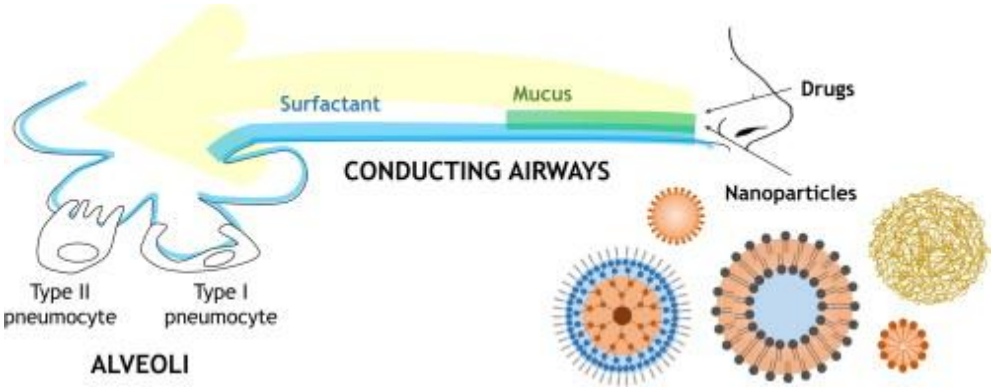

Figure 6: Possible targets for inhaled nanoparticles in the pulmonary surfactant system [52]

Other factors potentially affecting nanoparticles translocation and interaction with the pulmonary surfactant film are solubility and surface charge of nanoparticles. Hydrophilic nanoparticles may submerge in the aqueous phase of the lining layer of the surfactant film [53] where they are coated with surfactant components. This may in turn cause an alteration of the cytotoxic potential and lead to a rapid translocation to other organs. In contrast, hydrophobic nanoparticles may be trapped in the surfactant layer and brought in close proximity with epithelial cells and cells in the immune system, e.g. type I and type II alveolar cells, alveolar macrophages and alveolar dendritic cells [49, 54]. This may in turn lead to interference with specific cellular functions such as surfactant metabolisms of type II alveolar cells [31], or cause secretion of pro-inflammatory cytokines [54]. The physiological barriers of the respiratory system might therefore not be effective for protecting the body from nanoparticles [14].

1.4.4 Translocation to and accumulation in secondary organs

The respiratory system's large absorptive and highly vascularized surface area can promote a rapid and extensive systemic exposure [10] as the entire cardiac output flows through pulmonary capillaries, increasing the risk for exposure to toxic substances and thus causing adverse effects [14]. Because distribution of nanoparticles through the systemic circulation is plausible, endothelial cells might come into direct contact with these substances [55].

The alveoli consist of tight junction gaps of 1 nm between type I alveolar cells which contributes to the transportation of smaller molecules through the paracellular route [32]. It has been suggested that nanoparticles might cross the alveolar epithelium through the transcellular route in form of endocytosis, which may be the main mechanisms for cellular particle uptake [16]. Inhaled nanoparticles can partly escape engulfment of alveolar macrophages and transmigrate to the pulmonary interstices or the systemic circulation by translocation processes [9]. Decreased ability of lung macrophages to remove inhaled nanoparticles may facilitate contact of increased duration between nanoparticles and airway epithelial and endothelial cells [56]. Because nanoparticles have sizes comparable to proteins, they can deposit in biological compartments that are usually protected from bigger particles, such as the cardiovascular system, lymph nodes, bone marrow and the brain, through the circulatory system [6, 9, 14]. Nanoparticles have the potential to cause inflammation, oxidative stress and molecular activation both in primary organ of entry as well as secondary target organs to a lesser extent. It is unlikely that these effects occur with larger particles except in particle overload conditions, e.g. silicosis of the liver, spleen and bone marrow [23].

Some studies have also reported that nanoparticles may have the ability to translocate to the brain through the olfactory nerve endings in the nose [19, 46] or via the vascular system from the pulmonary capillary and thus passing the blood-brain barrier [14]. Loss of olfactory function and neurodegenerative pathology has been found in the brain of individuals exposed to severe air pollution, and it is speculated that air pollution is a contributing factor to the development of diseases such as Parkinson's, Alzheimer's and Huntington's disease [14, 46]. This suggest that neurotoxic or neurodegenerative effects may occur following inhalation of certain nanoparticles [23].

To what extend nanoparticles are able to translocate to other tissues are still under discussion [28]. There are several studies on nanoparticle translocation both in rats and human lungs which show conflicting results. In the human lung, Nemmar et al [57] reported rapid uptake of radiolabelled carbon nanoparticles into the bloodstream and deposition into the liver**,** but in contrast, other studies only detected a small fraction of translocation of carbon [58-60] and iridium nanoparticles [61]. Kreyling et al [61] also demonstrated that in *in vivo* studies in rats exposed to nanoparticles (15-20 nm) radiolabeled with iridium, less than 1 % of the nanoparticles entered the bloodstream and reached the liver, spleen, brain, kidneys and heart. Based on these studies, one may conclude that a small fraction of nanoparticles might potentially translocate across the air-blood barrier to the circulatory system, but the significance of this translocation regarding human health requires further studies.

1.4.5 Defense mechanisms in the airways

The respiratory system is especially vulnerable to the effects of harmful compounds because it has direct contact with inhaled air that may contain toxic pollutants, noxious gases, dust, fibers and tobacco smoke from the environment and/or industries, as well as airborne viruses, bacteria and fungi [10]. The respiratory system has different mechanisms to protect against permeation of foreign substances, which will be discussed further.

1.4.5.1 Barrier functions

Bronchial epithelial cells are a part of the non-specific immune system. Within the bronchial epithelium, the epithelial cells form a continuous physical barrier and will thus defend the airways against entry of foreign substances. Its secretory and ciliary function gives an effective mucociliary clearance and the secretion of mediators gives protection against noxious substances. Tight junctions *(zonula occludens)* surrounding each cell at the apical pole provide a physical barrier which prevents leakage [33].

1.4.5.2 Particle clearance

It has been postulated that clearance, in addition to solubility, adsorption ability and surface activity, is an important factor for the ability of nanoparticles to induce lung toxicity [45]. Because nanoparticles move by diffusion, they may also deposit in the entire respiratory tract [29]. Deposited nanoparticles can be cleared from the airways through different mechanisms

to rapidly reduce the degree of local absorption or remove potentially toxic particles that can cause damage to pulmonary tissues. Clearance of particles that are deposited in the nose, depend on their solubility in the mucus and site of deposition [37]. In this area, soluble particles are dissolved in the mucus, absorbed by the epithelium and then removed by the circulatory system. Even though dissolved parts of particles may reach other organs, it is assumed that their toxic potential is low due to a high degree of dilution in body fluids. For many types of particles the toxicity is mainly associated with the insoluble parts of the particle, which may potentially cause high doses of toxins in the lungs, and possibly in other organs through a translocation mechanism [62].

Insoluble particles deposited in the nasal and bronchial mucus are usually transferred by mucociliary epithelium towards the glottis within 24-48 hours where they are swallowed [10], which has been shown in rats exposed to radiolabeled iridium (15 and 80 nm) nanoparticles [28]. The underlying cilia in the tracheobronchial tree also push deposited particles and particle-bound macrophages to the oropharynx by impaction forces, where they are swallowed and enter the gastrointestinal (GI) tract for excretion [37].

Because cilia are not found beyond the terminal bronchioles, small particles deposited in the alveoli are phagocytized by alveolar macrophages and removed via lymphatic systems to lymph nodes and bloodstream. The alveolar macrophages can also be transported to the bronchioles by the alveolar fluid and removed by mucociliary clearance or retained in the alveolar walls over a longer period of time [10, 37]. If these macrophages are later activated, release of reactive oxygen species (ROS) and lysosomal enzymes may occur and cause damage of pulmonary tissues [10]. It is believed that clearance of nanoparticles from the respiratory system occurs mainly through phagocytosis by alveolar macrophages. The efficiency of this process in dependent on nanoparticle size, shape and agglomeration potential [28].

When particle deposition in the lungs is high, a slowing of alveolar clearance occurs. This causes nanoparticles that reach the lower respiratory tract to sequester for months or years which in turn may cause alterations in lung physiology [37] and possibly subsequent lung injury [11]. Several studies in rats showed that non-agglomerated nanoparticles were less efficiently cleared by macrophage phagocytosis compared to micro-sized particles, which caused a significant accumulation of nanoparticles within the alveoli [28]. This was further demonstrated by Oberdörster et al [47] in a study exposing rats to TiO_2 nanoparticles (20 nm).

Compared to fine TiO_2 particles (250 nm), TiO_2 nanoparticles caused a slower clearance, as well as a higher degree of translocation to interstitial sites and regional lymph nodes. Another author suggested that phagocytosis of nanoparticles might be unintentional and occurs during phagocytosis of other materials [63].

1.5 Inflammation

Inflammation is a localized and protective response triggered by damage to tissues and cells by pathogens, noxious stimuli or physical injury. The inflammatory response has the ability to eliminate injurious substances, and thus facilitate the repair and regeneration of damaged tissues. Inflammation is divided into acute inflammation and chronic inflammation. Acute inflammation is a short-term response where leukocytes infiltrate the damaged region, remove the stimulus and promotes healing by repairing tissues. In contrast, chronic inflammation is a prolonged, dysregulated and maladaptive response that involves active inflammation, tissue destruction and incomplete tissue repair [64].

There are done several extensive studies on how nanoparticles affect the immune system. *In vivo* studies in rats have also shown that compared to larger-sized particles of identical chemical composition at equivalent mass concentrations, exposure to nanoparticles may elevate inflammatory responses [30].

1.5.1 Acute inflammation

After an acute injury, there is an increased permeability of blood vessels, vasodilatation, increased blood flow towards damaged areas and migration of fluid, proteins and leukocytes from the circulation to the site of tissue damage. The accumulation of fluid outside blood vessels leads to edema causing pain and discomfort [65]. Cells in the innate immune system, such as macrophages, neutrophil granulocytes and soluble signaling molecules, are recruited to the site of injury by chemotactic factors (i.e. chemotaxis) and are believed to control the acute inflammatory response [3]. The mechanisms of acute lung injury by toxic substances are not fully understood, but it is likely that oxidant stress is involved. An acute toxic injury to the lung can damage its epithelial side by inhalation or its endothelial side via circulation[14].

1.5.2 Chronic inflammation

If the inflammatory response is excessive or persistent, i.e. chronic inflammation, the function or morphology of tissues may be altered [35]. The characteristics of a chronic inflammation are the infiltration of macrophages, lymphocytes and plasma cells (B-lymphocytes) recruited from the circulation to the site of injury by chemotactic factors. Macrophages contribute to the progression of tissue damage and functional impairment upon inhalation of foreign agents such as silica dust, which is usually not removed by phagocytosis or enzymatic breakdown, causing the particles to retain in the alveolar wall for long periods of time [65]. This may induce excessive tissue damage and chronic inflammation within the body [14]. Chronic inflammation is associated with several chronic conditions and diseases such as allergy, atherosclerosis, cancer, fibrosis and autoimmune diseases [64]. In contrast, interactions that induce immune suppression may reduce the response to recognize pathogens and mutated cells, possibly causing severe diseases such as cancer [14]. The cause of chronic inflammation is yet not fully understood [64].

After an injury, damaged cells, which are capable of proliferation, regenerate to promote healing of tissues. However, the increase in fibroblasts and extracellular matrix in the interstitium has the potential to cause a thickening of the alveolar septa, which may in turn affect the gas exchange in the respiratory system [35]. Deposition of nanoparticles in the respiratory system may lead to chronic inflammation, epithelial injury and pulmonary fibrosis. Engineered nanoparticles (e.g. carbon nanotubes) have been demonstrated to cause fibrosis in rats [66]**.**

1.5.2.1 Pulmonary fibrosis

Pulmonary fibrosis is a chronic and incurable respiratory disease affecting alveolar and respiratory regions. Acute or chronic exposure to fumes and dust at work places are able to cause inflammatory reactions and influx of polymorph and other cells into the airways. This may trigger the release of TNF-α and IL-1β, and subsequent activate the expression of pro-fibrotic growth factors such as transforming growth factor-β (TGF-β) [67]. Production of TGF-β, which mediates the regeneration of the extracellular matrix leading to reparation of injured tissues, is normally ceased when repair is complete. Failure to halt TGF-β production causes fibrosis which is characterized by excessive deposition of extracellular matrix of abnormal composition following tissue damage [37, 68]. This can be caused by continuous

injury or a defect in the regulation of TGF-β. Collagen and laminin are also increased during fibrinogenesis and changes the composition of extracellular matrix, which may interfere with gas exchanges across the air-blood barrier, making it comprised as lung volume and diffusion capacity are decreased [37, 68]. Occupational exposure to asbestos and crystalline silica (e.g. quartz) have been reported to cause pulmonary fibrosis [14].

Silicosis is an example of pulmonary fibrosis that occurs after inhalation and deposition of dust containing crystalline silica particles, even after the workers leave the source of exposure [69]. Increased risk for lung cancer has been seen among workers with silicosis, and it is therefore important to limit exposure to silica dust even though there is few quantitative data about lung cancer risk in relation to silica exposures [70].

1.5.3 Proinflammatory cytokines

Cytokines are a group of proteins that regulate inflammation, as well as repair of damaged tissue, by serving as communication signals and thus influencing the response of the respiratory system to foreign substances. Cytokines exert their effect by interacting with specific cell-membrane receptors on target cells. An activation of initiating cytokines triggers a cascade of events resulting in cell recruitment. Cell differentiation, secretion, replication and apoptosis are maintained by intercellular signals. This shows that cytokines have an important role in maintaining normal tissue homeostasis.

Cytokines are produced by both immune effector cells (e.g. monocytes, lymphocytes, neutrophils) as well as non-immune cells (e.g. endothelial cells, fibroblasts, epithelial cells). Even though they play an important role in normal physiology, an alteration in their expression may contribute to the pathophysiology of disease. During an inflammatory response, initiating cytokines are rapidly induced and trigger a cascade of events such as the production of chemotactic cytokines and expression of cell-surface adhesion molecules. Pro-inflammatory cytokines such as TNF-α, IL-1 and IL-6 act as initiators for inflammatory processes [35].

TNF-α plays an important role as a macrophage-derived cytokine in the respiratory system, that initiates inflammatory cascades through a cytokine network involving induction of other proteins and cytokines that could directly interact with inflammatory and immune cells to facilitate their recruitment. By signaling through its two receptors (TNFR-1 and TNFR-2) and

by activating several transcription factors, such as NF-κB, TNF-α exerts its biological activity [71]. TNF-α mediates cell recruitment indirectly by activating a network of cell-cell and cytokine interactions resulting in the infiltration of inflammatory cells. This induces cytokines that are chemotactic for inflammatory cells, as well as the release of interleukins, which functions as mediators of cell infiltration in conjunction with an inflammatory response. As an initiator of inflammatory cascades, TNF-α may also stimulates the production of other mediators such as platelet-derived growth factor, TGF-β, prostaglandin E2, prostacyclin, and reactive oxygen and nitrogen species by leukocytes [35, 71, 72].

There are two types of IL-1 based on its structural form: **IL-1α** and **IL-1β**, both of which are produced by macrophages, monocytes and dendritic cells as pro-forms, which are further processed upon activation. Their pro-inflammatory effects are mediated by binding to IL-1 receptor type I [33]. Production of pro-IL-1α and pro-IL-1β are induced by Toll-like receptors (TLR), which are regulated through the activation of NF-κB [73]. The clustering of multiprotein complexes, called inflammasomes, trigger the protease caspase-1 to cleave pro-IL-1β to a mature and biologically active form which are secreted [74]. The mechanisms leading to processing of IL-1α is not yet fully characterized in detail, but it is believed that IL-1α is active both as a cell surface-associated form (pro-IL-1α) and as a mature secreted form. Only the latter triggers the secretion of IL-6/IL-8. Pro-IL-α only requires NF-κB for activation, while secretion of mature IL-1α is also dependent on activation of the inflammasome and caspase-1. It has been shown in IL-1β-deficient mice that the presence of IL-1β is required for the secretion of IL-1α [73].

IL-1β is usually released in response to infection or injury. However, it has been reported in *in vivo* studies that IL-1β may induce alveolar epithelial repair, inhibit apoptosis or stimulate proliferation of pneumocytes. An enhanced alveolar epithelial repair has been suggested to be partly regulated by the IL-1R via an epidermal growth factor (EGF)-receptor dependent mechanism [75]. It is also believed that IL-1 may induce various transcription factors such as NF-κB and AP-1 [76].

IL-1β and TNF-α act synergistically to initiate the cascade of inflammatory mediators by targeting the endothelium [76]. They may also indirectly trigger cell proliferation or migration of certain cell types which contribute to tissue repair mechanisms [77]. Increased levels of TNF-α and IL-1β elicit the production of other pro-inflammatory cytokines such as IL-6 and IL-8 by binding to and activating their respective receptors (TNF-R and IL-1R) [75]. IL-1 and

TNF-a simultaneously activate different mitogen-activated protein kinases (MAPK) and nuclear factor (NF)-kB [78]

IL-6 is a cytokine that activate the immune system and regulate various functions in different cell types such as activating other cytokines to produce greater amounts of acute-phase response proteins or reactant in the circulatory system. IL-6 also mediates maturation of B-lymphocytes, complement activation, proliferate T-lymphocytes and further induce cytokine release [71]. It has also been reported that IL-6 plays a role in the epithelial repair process by regulating vascular responses and enhance fibroblast proliferation [75, 79].

1.5.4 Chemokines

Chemokines are small heparin-binding, chemotactic cytokines that mediates the recruitment and activation of leukocytes and other cells to the site of injury with a high degree of specificity in the cells they attract [35, 71]. They are divided into three subfamilies based on their structure and functions: Cystein-X-amino acid cysteine (CXC) chemokines, cysteine-cysteine (CC) chemokines and C chemokines, which have chemotactic activity for neutrophils, mononuclear cells and lymphocytes. Chemokines are considered to be key mediators of cell recruitment in the lung, and increased expression of several chemokines may be induced by TNF-α under inflammatory conditions [35].

IL-8, also referred to as **CXCL8**, is a pro-inflammatory mediator whose main function is to attract and activate neutrophils to the site of acute inflammation which is a key process for protection against pathogens [78, 80]. In normal non-inflamed tissues, production of IL-8 is low or absent, but during a response to external stimuli such as proinflammatory cytokines (IL-1 and TNF-α), pathogens and cellular stress, a rapid and significant increase in IL-8 levels are found. Stimulation with TNF-α and IL-1 cause a 100-fold up-regulation of IL-8, while certain bacteria or EGF cause a five- to tenfold increase in IL-8 secretion [78, 81]. Both MAPK and NF-κB are involved in the increased expression of IL-6 and IL-8 [82].

RANTES, also called **CCL5**, is a CC chemokine that plays an important role in the immune response by recruiting leukocytes to the site of inflammation by functioning as a chemoattractant for T cells (especially CD4 T cells), eosinophils and basophils. RANTES has also the potential to activate eosinophils and upregulate the expression of adhesion molecules on these cells. Because it has been demonstrated that epithelial cells produce RANTES in

response to infection with influenza virus A, it may indicate that RANTES have a role in regulating protective immune responses against viral infections [83].

1.6 Activation of cytokines through intracellular signaling pathways

The release of proinflammatory cytokines in response to inflammatory stimuli are dependent on intracellular signaling pathways which carry the signal needed to activate the production of inflammatory mediators. It has been demonstrated that the stress-activated intracellular signaling pathways NF-κB and MAPK are triggered in response to pro-inflammatory cytokines [84, 85].

1.6.1 Mitogen-activated protein kinase signaling pathways

MAPK is a family of protein serine/threonine kinases that are involved in the regulation of cell growth, differentiation, immune activation and different cellular stress responses such as inflammation and apoptosis, in response to extracellular stimuli (growth factors, cytokines, oxidants, toxins etc.) [86]. There are three major MAPKs signaling pathways, extracellular signal-regulated kinase-1 and -2 (ERK1/2), and the stress activated protein kinases c-Jun NH_2-terminal kinases (JNK) and p38 mitogen activated protein kinases (p38 MAPKs). It has been reported that ERK is activated by growth factors and are associated with cell survival and proliferation, while p38 and JNK are activated by cellular stress and are associated with inflammation and apoptosis [87]. During activation of MAPK by MAP kinase kinase (MKK), transcription factors in the cytoplasm or nucleus are phosphorylated and activated. This leads to expression of target genes giving a biological response [85].

1.6.2 Transcription factor NF-κB

Nuclear factor (NF)-κB is a dimeric protein that comprises members of the Rel transcription protein family [35]. These proteins play a key role for normal immune and inflammatory response, cell survival and proliferation, as well as maintaining cellular and tissue homeostasis [88], but is also found chronically activated in inflammatory diseases causing tissue destruction [89]. The Rel homology domain (RHD) in NF-κB proteins has the ability to bind to DNA, form dimers and produce nuclear localization signals. NF-kB is comprised of

five subunits: p65 (also known as RelA), c-Rel, p50, p52 and RelB. Each NF-kB subunit has the ability to form hetero- and homodimers [90].

In the inactivated state, NF-κB transcription factors are sequestered in the cytoplasm by binding to inhibitory IκB proteins (IκB-α, IκB-β and IκB-ε). IκB prevents NF-κB from entering the nucleus by covering the nuclear localization signal on Rel proteins [35, 91]. In most cells, p65/p50 heterodimer is the most regular NF-kB dimer and is bound to IκB-α in resting cells [88].

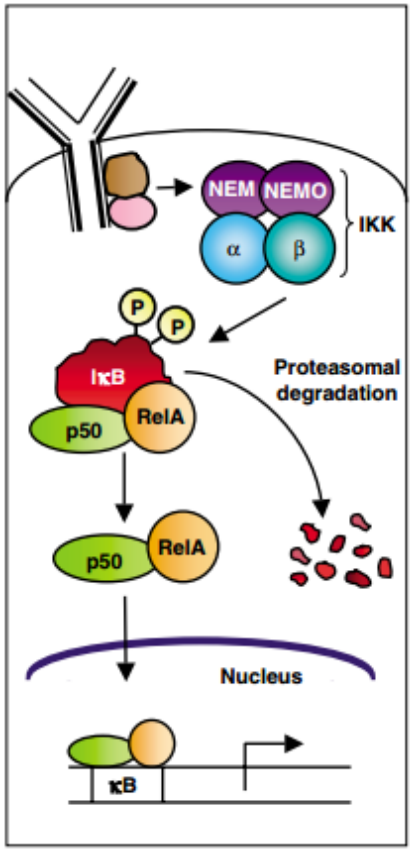

Figure 7: The classical NF-κB signaling pathway[92]

During an immune and inflammatory response, activation of pattern recognition receptors (e.g. Toll-like receptors, NOD-like receptors, RIG-I-like receptors) and different pro-inflammatory stimuli [e.g. reactive oxygen species (ROS), reactive nitrogen species (RNS), TNF-α, IL-1β, MAPKs p38], activate NF-κB transcription [71, 93] through its kinase complex, IκB kinase (IKK) [35, 94]. This causes phosphorylation of two adjacent serines [81] and ubiquitination of IκB, and triggers a proteasome-mediated degradation of IκB which allows the translocation of NF-κB dimers to the nucleus, where they regulate gene

transcription coding for proteins involved in inflammatory and immune responses [95] such as TNF-α, IL-2, IL-8, MIP-2 and GM-CSF [35, 94]. The nuclear transport of NF-κB is dependent of Rho protein signaling [71].

After activation, transcription is terminated when p65 returns to cytoplasm in an inactivated state [94]. A balance of ubiquitination and deubiquitination controls the stability of DNA-bound NF-κB [89].

TNF-α have shown to trigger the activation of NF-κB through the stimulation of a serine-kinase cascade of upstream activating kinases, such as protein kinase C (PKC) isoform and MAPK kinase kinases (MAPKKK). IκB are phosphorylated by these kinases via IKK-β, which will then induce its own proteolytic proteasome-mediated degradation through the proteolytic ubiquitin-proteasome pathway [71].

1.6.2.1 Activity of NF-κB

After translocation to the nucleus NF-κB binds to DNA and functions as positive transcriptional regulators of pro-inflammatory genes which have binding sites for NF-κB on their promotor regions. Upon binding to these regions, NF-κB has the ability to induce or increase the gene transcription of proinflammatory cytokines, chemokines, interferons, growth factor and other inflammatory mediators. These mediators may in turn activate NF-κB in a positive feedback loop [71]. Enhanced NF-κB-induced transcriptional activity may additionally require phosphorylation of the subunits as well as binding of coactivators [78, 81]. IκB kinases α and β are phosphorylated by NF-κB-inducing kinase (NIK), which is a recently identified protein activated by IL-1, TNF and Fas [78].

Defects in the regulation of NF-κB signaling pathways are linked to development of cancer, aging, ineffective response to microbial infection, and inflammatory and autoimmune disorders [96, 97]. Increased expression of NF-κB is associated with vascular disease [71]. Development and immune defects may occur as a result of interruption of IκB degradation and subsequent defects of the NF-κB signaling pathways [98]. This emphasizes the critical role IκB has in activating NF-κB pathways.

1.6.3 Intracellular signaling mechanisms involved in the activation of IL-8

Expression of IL-8 is mediated by binding to NF-κB, AP-1 and CCAAT/enhancer-binding protein (C/EBP) sites on the IL-8 promotor region. Both the AP-1 and C/EBP sites are required for maximal gene expression, but they are not essential for induction of gene expression [78, 81]. Unlike NF-κB, AP-1 proteins are usually bound to their equivalent DNA element. Their transcriptional activity is regulated by phosphorylation of transactivation domains and by binding to protein kinase [81].

In inactivated cells, the IL-8 promoter is repressed by processes such as deacetylation of histones, octamer (OCT)-1 binding and activation of NF-κB repressing factor (NRF), preventing transcription of IL-8. An optimal IL-8 gene expression is dependent of three different mechanisms which includes de-repression of the gene promoter, activation of transcription factor NF-κB and JNK pathways, and stabilization of posttranscriptional mechanisms such as IL-8 mRNA by p38 MAPK. It has been previously shown that an active form of MKK6 selectively activates p38 MAPK and induces a significant stabilization of the IL-8 transcript [81]. Another MAPK family member, ERK1/2, is also involved in the regulation of IL-8 [81, 86]. All of these MAPK are activated by phosphorylation through MKK. It is believed that the p65 subunit of NF-κB is bound to the IL-8 promoter, which translocate to the nucleus upon induction of IL-8 transcription triggered by TNF-α and IL-1. Blockage of either NF-κB or JNK reduces IL-8 secretion drastically [81]. It has also been suggested that IL-8 regulation may also be regulated via EGFR signaling, possibly through an ectodomain of TGF-α catalyzed by the metalloprotease TACE/ADAM-17 [99].

Elevated levels of IL-8 are associated lung diseases, acute lung injury, chronic obstructive pulmonary disease (COPD), chronic bronchitis and worsening of asthma, especially in children [80]. It is therefore important to control chemokine production to regulate the infiltration of leukocytes and thus the intensity of an inflammatory response [78]. The expression of IL-6 during an inflammatory response is regulated through similar mechanisms as IL-8 [81]. There are not many studies published for which intracellular mechanisms RANTES are mediated through, but a study by Pham et al [100] showed that EGFR, MAPKs p38, JNK and ERK might have a role in regulating the expression of RANTES after exposure to silica nanoparticles.

1.6.4 Protein kinase C

Protein kinases C (PKC) are a family of serine/threonine kinases that plays a central role in signal transduction, as well as controlling many aspects of cell function such as cell proliferation, differentiation and apoptosis [101]. In addition to this, PKC may regulate the function of various proteins by controlling protein phosphorylation.

The PKC family is comprised of at least 12 isozymes with specific means of regulation and tissue distribution patterns. PKC is ubiquitously distributed in tissues and organs, and have the highest activity in the brain [102]. The different isoforms of PKC have shown to regulate a number of signaling pathways in different immune cells [103, 104], and exert both inhibitory (e.g. α, β, ε and atypical isoforms) and stimulatory effects (e.g. δ and θ isoforms) on apoptosis [87]. This makes it possible for the PKC isozymes to respond differently to a variety of cellular stimuli [105].

Under physiological conditions, most of the PKC isoforms are activated in the presence of diacylglycerol (DAG), which may arise from the receptor-mediated hydrolysis of inositol phospholipids and increased levels of Ca^{2+}, both of which is regulated through the activation of G-protein-coupled receptors (GCPRs). Unlike the inositol phosphates, DAG is highly lipophilic and remains within the membrane. During activation of PKC, DAG binds to a specific site on the PKC molecule and leads to migration of the enzyme from the cytosol to the cell membrane where it can catalyze the phosphorylation of different intracellular proteins [102, 106]. Based on their activation mechanisms, the PKC isoforms may additional be divided into three subclasses:

- The conventional PKCs (α, β1, β2 and γ) require Ca^{2+}, DAG and phospholipids for activation.
- Novel PKCs (δ, ε, η and μ) are calcium independent.
- Atypical PKCs (ζ and λ) are independent of both Ca^{2+} and DAG.

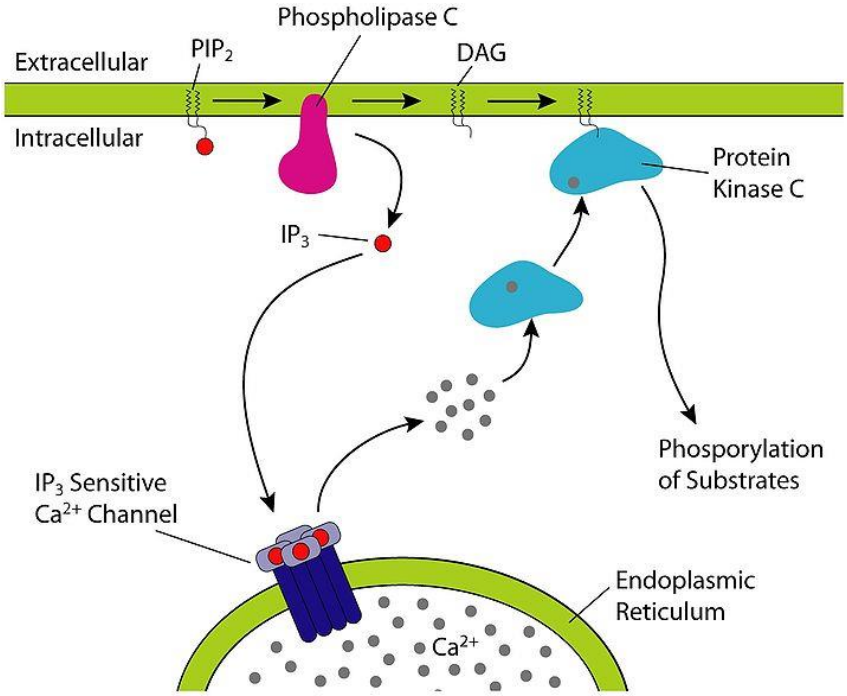

Figure 8: Activation mechanisms of protein kinase C

(http://en.wikipedia.org/wiki/Inositol_trisphosphate)

Activation of PKC signal transduction proteins are considered to be one of the earliest events leading to cellular responses such as the release of cytokines [105]. In conjunction to this, previous studies have reported that proinflammatory cytokines and environmental stress may trigger IL-8 responses via G-protein-linked signal transduction systems, such as PKA-, PKC-, Ca^{2+}-dependent protein kinase- and tyrosine kinase-linked mechanisms [107]. For example, it is shown that PKC-δ and other PKC isoforms may trigger cell signaling events that leads to the synthesis of pro-inflammatory cytokines, such as TNF-α, IL-1β and IL-6 in human monocytes [102]. Another study postulates that PKC might work via negative feedback control mechanisms, e.g. by phosphorylating growth factors such as EGF which leads to the decrease of a protein-specific protein kinase as well as growth factor-binding activities [102]. Different chemicals and carcinogens, such as asbestos, have been reported to induce PKC activation [105]. Recent studies have suggested that PKC isotypes might be a regulator of nanomaterial responses [102], but there are few published studies that assess the involvement of PKC in nanoparticles.

1.6.5 Oxidative stress

Under normal conditions, ROS is produced in essential processes, such as cell signaling, photosynthesis and respiration, forming superoxide (O_2^-, $HO_2^{\cdot}$), hydrogen peroxide (H_2O_2) and hydroxyl radicals ($OH^{\cdot}$). These reactive species are rapidly removed by non-enzymatic antioxidants (e.g. vitamin C, vitamin E, glutathione, beta-carotene, uric acid) and enzymatic systems (e.g. catalase, peroxidase and superoxide dismutase [SOD]), which works as a first line defense against oxidants [102]. An imbalance between antioxidant and oxidant production due to an excessive production of ROS has the potential to interact with critical macromolecules and cause harmful effects on biological systems [108, 109].

Because the lung epithelium are exposed to oxidants produced internally during normal metabolism as well as oxidants in the ambient air (e.g. mineral dust, ozone, nitrogen dioxide, cigarette smoke and diesel exhaust), oxidative stress may cause the development of a range of respiratory diseases such as chronic obstructive pulmonary disease (COPD), asthma, acute respiratory distress syndrome and idiopathic pulmonary fibrosis. Neutrophils, eosinophils, alveolar macrophages as well as alveolar epithelial cells, bronchial epithelial cells and endothelial cells are the main cellular sources of ROS in the lung [110].

Several studies have reported that formation of ROS and subsequent oxidative stress are early cellular responses to nanoparticles, which have an important role in the cytotoxic potential of these particles [8, 22, 111-114]. Furthermore, it has been demonstrated that compared to larger particles, nanoparticles have a greater potential to elicit the production of ROS and thus cause toxicity in biological systems, which may be explained by the significant increase in relative surface area with decreasing particle size [115]. Reactivity of a given amount of material increases concomitant with the relative surface area because the reactive portion of the particle is on the surface [26]. The increased levels of ROS could also be due intracellular processes from phagocytic cells [108].

The induction of oxidative stress might be associated with the activation of signaling pathways which lead to the expression of pro-inflammatory genes in macrophages [113]. ROS generated by nanoparticle exposure may function as signaling intermediates to activate redox-sensitive intracellular signaling pathways, such receptor tyrosine kinases, MAPK [67] and transcription factors (NF-κB and AP-1) [35, 113], which may in turn induce inflammation and thus cellular release of pro-inflammatory mediators [56, 115]. A recent study has shown

that both carbon black and silica nanoparticles induce the activation of NF-κB in A549 lung epithelial cells and macrophages [113]. Other *in vitro* studies with silver nanoparticles (Ag NP) have shown reduction in GSH, elevated ROS levels, lipid peroxidation and increased expression of ROS responsive genes. This was furthermore associated with DNA damage, apoptosis and necrosis [116]. It is therefore reasonable to indicate that there is a direct relationship between surface area, ROS generating potential and pro-inflammatory effects of nanoparticles in the respiratory system [67].

1.7 The potential of amorphous silica nanoparticles to elicit inflammatory responses

Silicosis is one of the most prevalent occupational diseases worldwide which is caused by inhalation of silica, especially crystalline silica which is a component in sand and rocks [69]. Crystalline silica (e.g. quartz), which are classified as a class 1 human carcinogen [20, 105], has been demonstrated to induce more persistent inflammatory reactions and toxicity compared to amorphous (non-crystalline) silica particles [72, 117]. The effects of amorphous silica nanoparticles appear to be transient and reversible depending on the concentration [12, 118], and are therefore regarded to be safer with no or less chronic effects [119]. The use of amorphous silica nanoparticles have therefore increased in a broad range of industries such as additives to cosmetics, drugs, printer toners, varnishes and food, as well as for biomedical and biotechnological applications (e.g. cancer therapy, DNA transfection, drug delivery and enzyme immobilization) [6, 120]. Unlike crystalline micron-sized silica which is well-studied, there is still limited knowledge of the toxicity of amorphous and nano-sized silica particles [6]. Even though amorphous silica is regarded as less toxic compared to their crystalline counterparts, there is still a possibility for amorphous silica nanoparticles to elicit harmful effects [82].

Previous studies have demonstrated that silica nanoparticles on a mass basis elicited stronger inflammatory responses compared to fine particles [6, 55, 121]. Lin et al [122] investigated the cytotoxicity of amorphous silica nanoparticles (15 and 46 nm) in human alveolar epithelial cells (A549 cells) and concluded that both nanoparticle sizes were more cytotoxic than fine quartz particles. In the same study, it was demonstrated that exposure to 15 nm silica nanoparticles generated oxidative stress in A549 cells, causing lipid peroxidation and membrane leakage. Similar was shown in BEAS-2B cells [120]. It has also been suggested

that SiNP-induced ROS generation acted as second messengers, which stimulated the translocation of the stress-responsive transcription factor NF-κB [123].

Amorphous silica nanoparticles have shown to induce transient inflammatory response after intratracheal instillation, causing release of pro-inflammatory cytokines such as TNF-α, IL-1β, IL-6 and IL-8 [124]. Several cell culture studies have also shown that amorphous silica nanoparticles have the potential to induce marked pro-inflammatory cytokine responses, such as IL-6 and IL-8, and that this might be regulated through MAPKs and NF-κB signaling pathways. We have previously demonstrated the potential of amorphous silica nanoparticles with particle sizes of 10 nm, 12 nm and 50 nm to induce cytotoxicity and pro-inflammatory response in human bronchial epithelial cells (BEAS-2B) [100]. The study of Pham et al [100] showed that the inductions of all three SiNP in cytokine responses (IL-6, IL-8 and RANTES) were partly dependent on particle size, with smaller particle sizes giving the a highest increases in cytokine release. Both Si10 and Si50 mediated IL-6 and IL-8 responses through MAPKs p38 and JNK pathways [100].

We have also compared the effects of Si50 with Si500, where Si50 gave on a mass basis greater cytokine responses than submicro-sized nanoparticles (Si500) [125]. Exposure to Si50 also induced the transcription of IL-6 and IL-8 involving signaling mechanisms such as MAPKs p38, NF-κB and TGF-α/EFGR. JNK seem to also be involved, but was dependent on the exposure conditions [82].

Chen and von Mikecz [126] reported that all silica nanoparticles with particle sizes between 40 nm and 5 μm penetrated to the cytoplasm, but nuclear localization was only observed for SiNP between 40 and 70 nm. Larger particles were mainly located in the cytoplasm and accumulated around the nucleus. Hornung et al [127] showed that silica particles might disrupt lysosomes after internalization by macrophages, leading to the release of lysosomal enzyme, cathepsin, into the cytosol which may trigger the NALP3 inflammasome and cause IL-1β responses.

Even though several studies have shown that PKC may be activated by various environmental substances and inflammatory cytokines, and is thus involved in inflammation in the respiratory system, the direct role of PKC in the inflammatory response is not yet fully investigated [128]. To date, there are no studies done to evaluate the involvement of PKC in the cytotoxic response of silica nanoparticles. However, existing studies have evaluated the

involvement of this signaling mechanism in asbestos-induced diseases. PKC-δ, which is involved in the regulation of collagen synthesis and fibrosis, has been reported to be activated in bronchial and alveolar epithelial cells both in vivo and in vitro after exposure to asbestos fibers and mechanical wounding [103]. Several studies have also reported that PKCs modulate MAPK pathways in different cell types through the activation of fos/jun response genes, which causes injury and proliferation of epithelial cells [129]. Other studies showed that exposure of fractured crystalline silica to murine epidermal cells (JB6 cells) triggered the translocation of PKCα and PKCε from the cytosol to the membrane, which thereby activated AP-1 transcription activity. Both ERK and p38 played an important role in regulating silica-induced AP-1 activation [105]. It has also been suggested that PKC activation might induce pro-inflammatory responses through NF-κB pathways in human bronchial epithelial cells [128]. Previous studies have demonstrated that crystalline silica has the potential to increase intracellular calcium levels *in vitro* [130-132] which is a known activator of NF-κB [133, 134].

Because these particulates are also associated with various respiratory diseases through the release of ROS and cytokines from alveolar macrophages and epithelial cells [103], similar intracellular PKC-related mechanisms, possibly mediated via activation of MAPK and NF-κB, might also be involved upon exposure to silica nanoparticles.

2 Aims of the study

The purpose of this study is to gain better understanding of the pro-inflammatory and cytotoxic response of silica nanoparticles, and to determine which cellular mechanisms could be involved. Cellular effects of SiNP of 10 nm (Si10) were compared with SiNP of 50 nm (Si50) in SV-40 transformed human bronchial epithelial cells (BEAS-2B). To shed light on these issues, we raise the following questions:

- To what extent will cell density in culture affect the cytokine responses and cytotoxicity to silica nanoparticles?

- How are the potentials of small amorphous silica nanoparticles (Si10) to elicit the cytokine response of IL-6, IL-8, RANTES, IL-1β and TNF-α, and cytotoxicity (LDH-release), compared to larger silica nanoparticles (Si50)?

- Does silica nanoparticles induce an increased gene expression of the cytokines IL-6, IL-8, TNF-α and IL-1β, and how is the gene expression time-dependent? Is there a difference in response for silica nanoparticles with different particle sizes (Si10 vs Si50)?

- Is the transcription factor NF-κB involved in the Si10- and Si50-induced cytokine release of IL-6 and IL-8?

- Is protein kinase C (PKC) involved in the Si10- and Si50-induced cytokine release of IL-6 and IL-8?

3 Materials and methods

3.1 Materials

3.1.1 Silica nanoparticles

In this study, two different commercially produced amorphous silica nanoparticles were used. Both the 10 nm and 50 nm particles were bought as water suspensions. The particles used were

Si10 Amorphous silica nanoparticle, 10 nm (Kisker Biotech)

Si50 Amorphous silica nanoparticle, 50 nm (Kisker Biotech)

The particle properties for Si10 and Si50 was characterised by Skuland et al [82, 125] and Pham et al [100], by analysing the particle working solution of Si10 and Si50 (as prepared according to section 3.3.1) with respect to zeta-potentials (Electrophoretic light scattering, ELS) and hydrodynamic diameter (Dynamic light scattering, DLS) in water and in medium. Table 1 summarizes the measured values for amorphous silica nanoparticles with nominal sizes of 10 nm and 50 nm.

Particle characterizations		
	Si10	**Si50**
Hydrodynamic size in water	7.5 nm	75 nm
Zeta potential in water	- 41.6 mV	- 29.5 mV
Hydrodynamic size in medium	8.7 nm	77 nm

Table 1: Characterization of the particle properties for Si10 and Si50. *Table 1 summarizes the measured hydrodynamic size and zeta-potential for amorphous silica nanoparticles with a nominal size of 10 nm and 50 nm.*

3.1.2 Cell lines and culture medium

In this study a SV-40 transformed bronchial epithelial cell line (BEAS-2B) was used. The cells were bought from European Collection of Cell Cultures (ECACC) in Salisbury in the United Kingdom, while the medium (LHC-9 and DMEM/F12) were bought from Life Technologies (a Gibco Thermo Fisher brand) in Grand Island in the USA.

3.1.3 Materials used in the study

See Appendix 1.

3.1.4 Solutions used in the study

See Appendix 2.

3.2 Methods: The principles

3.2.1 Enzyme-linked immunosorbent assay (ELISA)

Enzyme-linked immunosorbent assay, also referred to as ELISA, is a biochemical analytic method that is used to quantify and detect the presence of an antigen in a complex mixture. The most important step in the detection is the highly specific antibody-antigen interaction. An antibody, also known as an immunoglobulin (Ig), is a protein produced by the immune system when it encounters foreign substances, called antigens. The antibody recognizes a particular part of the antigen, called epitopes, allowing these structures to bind together with precision. Of this reason, antibodies can only interact with a fitting antigen. There are different variations with respect to the ELISA method. We can divide these in direct, indirect, competitive and sandwich ELISA. The two latter are based on the indirect concept. Only sandwich ELISA is used in this thesis and will be further discussed.

In sandwich ELISA, antigens is quantified between two layers of antibodies, i.e. capture and detection antibody. The antigen (target protein) to be quantified has to contain at least two antigenic epitopes, where one active site has the ability to bind to a capture antibody and the other to a detection antibody (figure 9). Either monoclonal or polyclonal antibodies can be used as capture or detection antibodies.

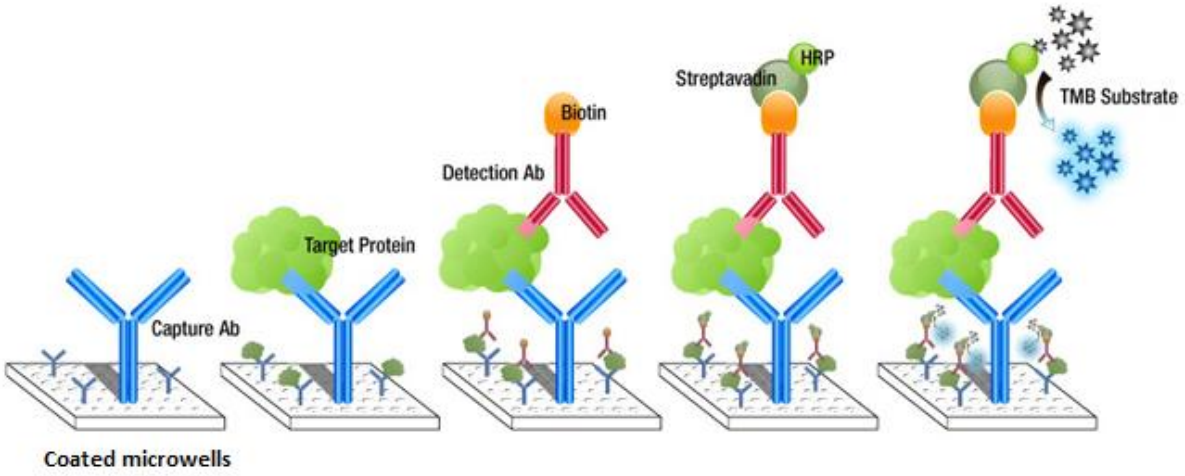

Figure 9: Principles of sandwich ELISA

(http://www.epitomics.com/products/product_info/1257)

Indirect sandwich ELISAs are often performed in positively charged 96-well polystyrene plates, which will passively bind antibodies and proteins (figure 9). This requires a immobilization of an unknown amount of antigen (samples) to a solid surface by pre-coating the surface with a "capture" antibody. This is followed by adding a labelled antibody for detection ("detection" antibody), which has specificity for the antigen. These three capture antibody-antigen-detection antibody will form a complex (figure 9). Between each step, the plate is washed with a detergent solution to remove unbound proteins or antibodies. In the final step an enzymatic substrate is added to convert the enzyme to a detectable signal, often as a colour change in a chemical substrate.

In this study, streptavidin-HRP (horseradish peroxidise) are used as an enzyme label in conjunction with a secondary antibody to detect proteins through a colour development. Streptavidin is a protein with a high affinity for biotin, which enables the streptavidin-HRP complex to bind to the biotin-labelled detection antibody. The enzyme HRP oxidizes the chromogenic substrate tetramethylbenzidine (TMB), which is catalysed by the oxidizing agent hydrogen peroxide, from a colourless to a blue substrate. The colour development is dependent of the amount of HRP bound to the detection antibody. Before spectrophotometric measurements are made, a stop solution of sulphuric acid is added. This changes the colour

from blue to yellow. By making a standard curve, the concentration of unknown samples can be determined as the amount of colour produced is proportional to the amount of antigen in the sample.

3.2.2 Colorimetric lactate dehydrogenase (LDH) assay

Lactate dehydrogenase (LDH) is a cytosolic enzyme that is released from the cytoplasm to the bloodstream or medium when tissues are damaged by disease, injury or toxic materials. The released LDH can be measured by a coupled enzymatic reaction. LDH catalyses the interconversion of lactate to pyruvate through the reduction of NAD^+ to NADH and H^+ (figure 10). In the next step diaphorase uses NADH to reduce a yellow tetrazolium salt (INT) to a red formazan product. The intensity of the colour development can be measured spectrophotometrically.

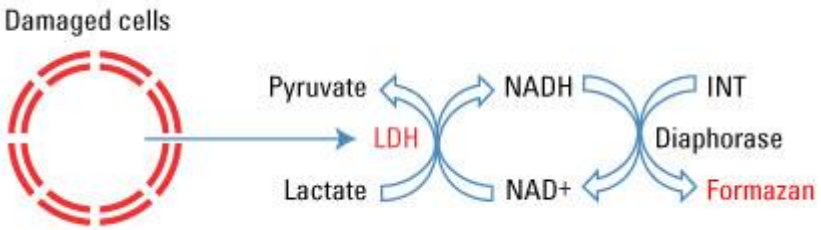

Figure 10: The principle of LDH assay

(https://www.lifetechnologies.com/order/catalog/product/88953)

The amount of produced formazan is directly proportional to the amount of released LDH in the medium. Because LDH is a stable enzyme, it has been used as an indicator for the presence of membrane damage and toxicity of tissues and cells, as it is also elevated in certain pathological conditions such as cancer [135].

3.2.3 Western blotting

Western analysis is a method that is used to measure the expression and phosphorylation of proteins by using specific antibodies. This is done by separating and identifying specific proteins from a complex mixture of proteins that are extracted from cells through cell lysis. Western blotting is divided in four important steps: Cell lysis, electrophoresis, immunoblotting and immunodetection.

3.2.3.1 Cell lysis and sample preparation

Cell lysis disrupts the cell membrane and solubilizes intracellular proteins. To ensure low cell activity and to prevent denaturing, proteolysis and de-phosphorylation of proteins, it is important to add inhibitors of protein-denaturation and protein-phosphatases as well as keeping the cells and the cell-lysates on ice at every time during the denaturation process. After lysis the cell-lysate have to be denaturized at 95 °C to ensure a linear structure. Also the cell-lysate has to be diluted to the same protein concentration (to ensure that the samples are compared on an equivalent basis) in lysis buffer, containing glycerol, 2-mercaptoethanol and sodium dodecyl sulfate (SDS). 2-mercaptoethanol prevents the re-binding of disulfide bonds and thereby keeps the denaturized structure intact after the denaturation process. Glycerol is added to make the samples sink easily into the wells of the gel, while SDS is an anionic detergent that both disrupts non-covalent bonds in proteins and gives the sample proteins a negative charge. This enables the proteins to move in an electric field that is applied during electrophoresis.

3.2.3.2 Gel electrophoresis

There are two different gel-layers in a Western gel, called stacking gel and separating gel, both of which are comprised of acrylamide/bis-acrylamide. The stacking gel has a lower acrylamide concentration and is somewhat acidic (pH 6.8). Even though it separates proteins poorly, the low acrylamide concentration makes a porous gel that forms thin and defined bands when applying voltage at 100V. The separating gel, which is basic (pH 8.8) makes the gel's pores narrower because of its higher polyacrylamide content. This separates proteins by their size, whereas small proteins migrate more easily and rapidly than larger proteins through the acrylamide gel. Ammonium persulphate (APS) and TEMED are added lastly to the gel solutions of acrylamide/bis-acrylamide to initiate the polymerization process and turn the

solution into a solid gel. When voltage is applied, the diluted proteins will travel towards the positive electrode because they are negatively charged.

3.2.3.3 Immunoblotting

After separating the protein mixture, the proteins are transferred by current from the gel to a membrane producing a band for each protein. The membrane is normally either made of nitrocellulose or PVDF (polyvinylidene fluoride). It is important that the membrane is placed between the gel surface and the positive electrode in a "sandwich" to ensure the migration of the negative charged proteins from the gel to the membrane (figure 11).

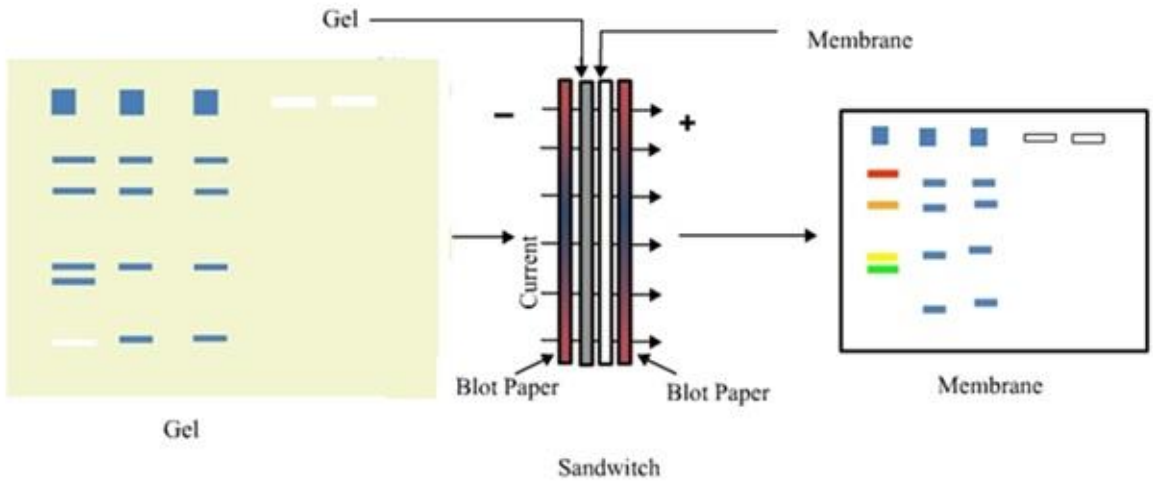

Figure 11: Schematic illustration of immunoblotting

(http://vlab.amrita.edu/?sub=3&brch=187&sim=1331&cnt=1)

3.2.3.4 Immunodetection

In the immunodetection, antigens of interest are detected by an antigen-antibody reaction. To prevent antibodies from binding nonspecifically to the membrane, the membranes are blocked with 3 % dry milk before it is incubated with a primary antibody specific for the targeted protein (antigen). Then a secondary antibody, which is usually conjugated with an enzyme (e.g. Horse Radish Peroxidase, HRP), is added to make an antibody-antigen-complex (figure 12). The primary antibody is incubated with BSA rather than dry milk because milk contains casein, which is itself a phosphoprotein and biotin. This may in turn cause an interference

with the assay results when combined with certain detection labels (e.g. biotin and AP antibody labels).

Unbound antibodies are washed off leaving only bound antibodies to the targeted protein. These bands are detected by chemiluminescene when treating the membranes with chemiluminesensing reagents. Because Western blotting is a semi-quantitative method, it can only be used to compare protein levels, but not measure the absolute quantity. For a more precise comparison, the differences need to be standardized. A loading control (β-actin) was therefore used to interpret the results and to normalize the levels of protein detected by confirming that protein loading is uniform across the gel.

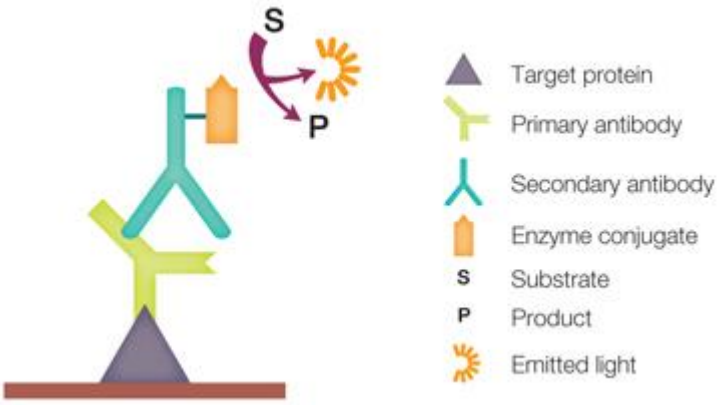

Figure 12: Illustration of a protein detection with Western analysis

(http://www.bio-rad.com/en-us/product/clarity-ecl-western-blotting-substrate)

3.2.4 Real time PCR

Real-time polymerase chain reaction is a technique used to amplify and consecutively detect or quantify a targeted DNA or RNA (as cDNA) molecule. Gene expression is regulated in cells by turnover gene transcripts, called messenger RNA (mRNA). The number of mRNA transcript of a targeted gene can be used to measure the amount of an expressed gene in a cell. To be able to run a real time PCR analysis, mRNA has to be reverse-transcribed to cDNA in a reaction by an RNA-dependent DNA polymerase enzyme, called reverse-transcriptase, with random hexamers. cDNA is then used as a template during the PCR process. In the real time PCR process, the cDNAs were mixed with forward and reverse primers, a fluorogenic probe, buffer, a thermo-stable DNA polymerase, dNTPs and water. This mixture called mastermix

was made prior to the PCR assay and distributed to a PCR plate before adding cDNA template, no-template control or no-reverse-transcriptase control. The two latter are negative controls that confirms the absence of contaminants in the PCR reagents and RNA samples. To give a detection of a specific PCR product as it accumulates during PCR cycles, a fluorogenic probe (f. eks TaqMan) was used. Real time PCR allows us therefore to measure the generation of amplified products at each PCR cycle, unlike standard PCR where the product is detected at the end. Primers that are specific to the target are mixed with the master mix solution, before the gene expression is analysed using computer software.

A standard PCR process is consisting of a cycling process (often 30 cycles) of three steps (figure 13):

- Step 1: Denaturation of cDNA at 95 °C. This disrupts hydrogen bonds between complementary strands and yields single-stranded molecules.
- Step 2: Annealing of primers which causes the primers to complementary bind to the targeted sequences (often at 50 cycles).
- Step 3: DNA synthesis (at 74 cycles) mediated by DNA polymerase.

In real time PCR the annealing and DNA synthesis are merged into one step, and annealing and DNA extension occurs at approximately 50-60 °C

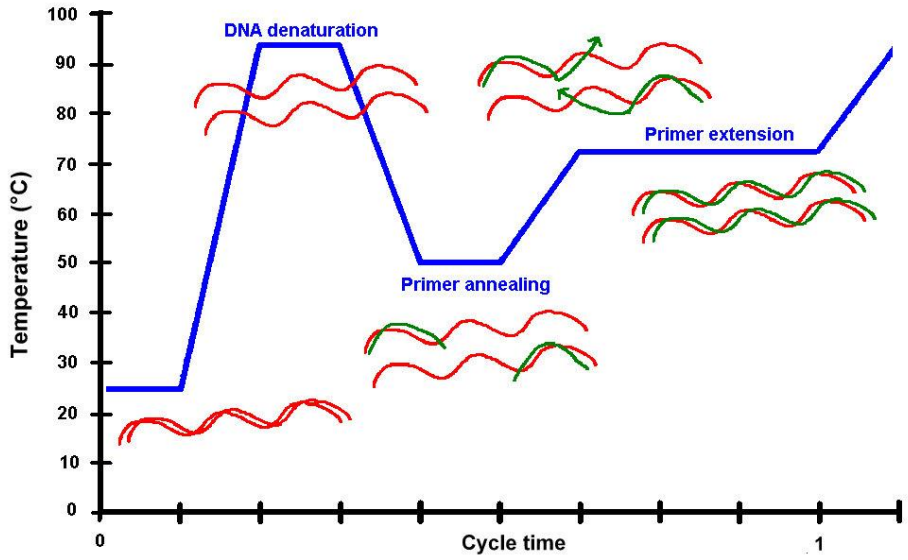

Figure 13: Thermal cycles during a PCR process

(http://biosistemika.com/workshops/qpcr-basics/)

By making use of a fluorogenic probe each new PCR product can be detected (instead of a fluorogenic probe one can use fluorogenic mastermix). At first the accumulation of PCR products is linear and under threshold, but at some point the DNA synthesis will be exponential and cross the threshold (figure 14). The more material there is at the starting point, the faster the exponential phase will occur. This is described by the Ct-value (cycle threshold), which is defined as the number of cycles required for the fluorescent signal to cross the threshold. The lower the Ct level, the greater are the amount of target nucleic acid in the sample. Real time PCR gives therefore an accurate quantification of the amount of starting material added to the reaction. In this study β-actin was used as an endogen control to determine the difference of gene expression (RQ) between two samples. The following formulas can be used to calculate this:

$$RQ = 2^{-(\Delta\Delta Ct)}$$

$$\Delta\Delta Ct = (Ct_{mRNA}\text{-}Ct_{18S})_{exposed} - (Ct_{mRNA} - Ct_{18S\ rRNA})_{control}$$

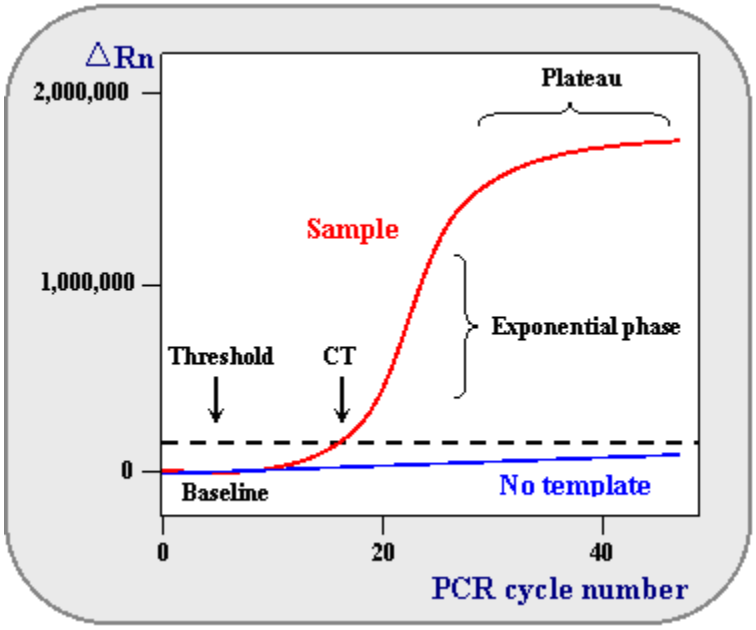

Figure 14: Model of a Real Time PCR plot

(http://www.ncbi.nlm.nih.gov/genome/probe/doc/TechQPCR.shtml)

3.2.5 Small interfering RNA (siRNA)

Small interfering RNA, also called silence RNA (siRNA), are short double stranded RNA molecules with 20-25 base pairs that are used to selectively silence the expression of specific genes and prevent the translation of a target protein message through RNA degradation. This is based on the concept of post-transcriptional gene silencing. SiRNA can induce RNA interference (RNAi) and down regulate mRNA expression of genes in eukaryote cells without an antiviral response. RNAi is initiated when double-stranded RNA (dsRNA) molecules activates the ribonuclease protein Dicer, which binds and cleaves dsRNAs to produce siRNAs. Each siRNA are separated into two single-stranded RNAs (ssRNAs), called the passenger strand (also the anti-guide strand) and the guide strand (figure 15). The passenger strand is degraded during the activation of RNA-induced silencing complex (RISC), while the guide strand of the siRNA becomes a part of RISC after the transfection. The guide strand then pairs with a complementary sequence in the targeted mRNA molecule and induce cleavage of the catalytic RISC component Argonaute. In this way, the RISC complex can find DNA and RNA in the targeted cell and can either join, destroy or inhibits its translation.

In this study the transfection reagent, HiPerFect, which is a mixture of cationic and neutral lipids, was used. HiPerfect fuses with the cell membrane and release siRNA intracellularly. This enables an effective siRNA uptake and efficient release of siRNA inside cells.

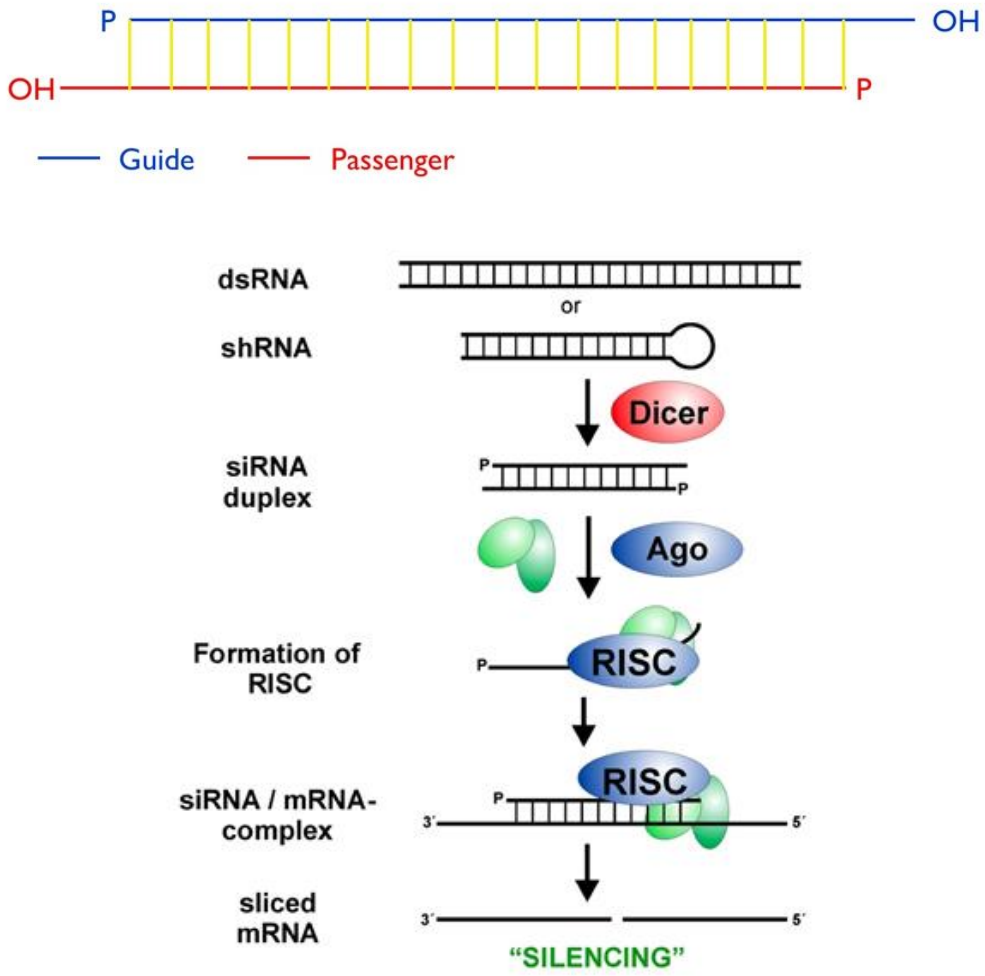

Figure 15: Illustration of the main steps in siRNA-mediated gene silencing

(http://mcmanuslab.ucsf.edu/node/268)

3.3 Methods: The procedures

3.3.1 Preparation of the particle solutions

Stock solutions of Si10 and Si50 were dispersed in distilled water to a concentration of 2.3 mg/ml. Based on the method of Bihari et al [136], the particle dispersion was made by sonicating 1 ml of the stock solution with 420 kJ/ml (50 % amplitude) on ice to dissolve any agglomerates present in the solution. Then 34.5 µl 50 mg/ml BSA and 115 µl 10x PBS were added to the particle solution to prevent agglomeration and stabilize the dispersion. The final concentration of the particle solution was 2.0 mg/ml with 0.15 % BSA and 1x PBS. The dispersions prepared with this method were stable for at least 1 week.

3.3.2 Cell culture

BEAS-2B cells were maintained in LHC-9 medium in collagen-coated cell culture bottles at 37 °C. Two days prior to particle exposure, the cells were either plated on collagen-coated 6-well plates for ELISA or Real time PCR, or 10 cm dishes for Western analysis. One day before exposure, the LHC-9 medium was substituted with DMEM/F12 medium which does not consist of growth factors and serum additives. This is done because previous studies have shown that agglomeration has occurred for Si50 nanoparticles in LHC-9 medium [82]. Furthermore, the sensitivity for the particles was higher in DMEM/F12 than LHC-9, both with respect to cell toxicity and cytokine responses [43]. At the time of seeding, each well in a 6-well plate consisted of approximately 24.200 cells/cm^2 in 1.5 ml medium, while each 10 cm dish consisted approximately of 19.400 cells/cm^2 in 10 ml medium.

3.3.3 Sample preparations prior to analysis

3.3.3.1 Exposure and harvesting of cell supernatant for measuring cytotoxicity and cytokines

To determine whether the exposure of silica particles induced release of IL-6, IL-8, IL-1β, TNF-α and RANTES or affected the cell-viability, and if the cell-density affected the cytokine release/cytotoxicity, BEAS-2B cells were exposed with different concentrations of Si10 (0-100 µg/ml) and Si50 (0-200 µg/ml) 1, 2 and 3 days after seeding. The cell supernatant was then harvested 20 hours after particle exposure, centrifuged at 300 g for 10 min to remove dead cells and thereafter at 8000 g for 10 min to remove particles. The cytokine release was measured by ELISA. Cytotoxicity was determined as the leakage of LDH by a Cytotoxicity Detection Kit (Roche).

In experiments using chemical inhibitors, BEAS-2B cells were pre-treated with inhibitors of PKC (GF109203X, 1 µM and 3 µM) and p65 (PDT-p65, 30 µM) 1 hour prior to exposure to Si10 (25 µg/ml) and Si50 (100 µg/ml) for 20 hours. The cell supernatants were harvested with the same procedure as mentioned above.

3.3.3.2 Exposure and preparation of cells for Western analysis

To study the involvement of NF-κB in the SiNP-induced responses of IL-6 and IL-8, BEAS-2B cells were exposed to either Si10 (25 µg/ml) or Si50 (100 µg/ml) for 1, 2, 4, 6 or 8 hours 2

days after seeding. After each time point, the plates/dishes were put on ice, the supernatants were removed and the dishes were washed 2 times with ice-cold Dulbeccos PBS before they were frozen. To make cell lysates, the frozen dishes were put on ice, added 200 µl of 1x lysis buffer in each dish and scraped for cells. The lysates were sonicated 10 times in 30 seconds in a BioRuptor®, and centrifuged in 8000 g for 15 min to remove cell/membrane residues. The supernatants were placed in fresh tubes and the pellets were discarded.

The protein concentrations in each lysate were determined with a DC-protein assay (BioRad), and then diluted in lysis buffer containing glycerol (10%), mercaptoethanol (5%), SDS (2%) and bromophenol blue (0.01%) to a concentration between 0.5-1.25 µg/ml before they were denaturated in 95 °C for 5 min.

3.3.3.3 Exposure and preparation of cells for Real time PCR

To investigate if SiNP induced gene expression of IL-6, IL-8, TNF-α and IL-1β, BEAS-2B cells were exposed to Si10 (25 µg/ml) and Si50 (100 µg/ml) for 1.5, 3, 6 and 8 hours 2 days after seeding. The supernatants were removed and each well were washed 2 times with ice cold Dulbeccos PBS, before the cells were frozen for at least 2 hours. Cellular RNA was then isolated from cells with an RNA isolation kit (PerfectPure). The cells were treated with 200 µl lysis buffer for approximately 5 min, and the wells were scraped for cells. To reduce the viscosity in the samples, a cannula with 26 G was used to cleave the RNA and DNA molecules.

Cell lysates were added to purification columns and washed with Wash 1 solution (see Appendix 2) to further destroy RNases and remove proteins, DNA and other contaminants from the column. To destroy bound DNA, the columns were treated with DNase for 15 min. Thereafter the column filters were washed with DNase wash solution and Wash 2 solution. After the washing process, RNA was eluted with an elution buffer for 1 minute. Between each step the column filters were centrifuged at 8000 g for 1-2 min, and before adding a new solution, the filters were added to new columns. Small quantities of the samples were used to determine the purity and concentration of RNA on a micro spectrophotometer (NanoDrop2000). The rest of the samples were stored in the freezer at -70℃.

3.3.4 Sandwich ELISA

One day prior to the analysis, a 96-well microtiter plate was pre-coated with a coating/capture antibody solution against the targeted protein using sandwich ELISA. The plate was washed with a blend of Dulbeccos PBS and Tween-20, and treated with a blocking solution (0.5 % BSA in PBS) for 1-2 hours at room temperature before adding the supernatants. Duplicates of the standard solution and the supernatants of each sample were added to the plate, and then incubated with a detection antibody for 2 hours (IL-6, IL-8 and TNF-α) in a shaking device. The wells were washed 4 times with a washing buffer (PBS and Tween) to remove unattached antibodies and proteins, and incubated with Streptavidin HRP for 30 min in a dark room at room temperature while shaking (IL-6/IL-8/TNF-α Cytoset, Invitrogen Life Technologies). The plate was washed again and incubated with a mixture of 3,3',5,5'-tetramethylbenzidine (TMB), citrate buffer and 30% H_2O_2 . When a satisfactory colour development had occurred, the stopping solution, 5% H_2SO_4, was added. The absorbance was measured spectrophotometrically at 450 nm (Sunrice Absorbance Reader, TECAN).

For detection of RANTES and IL-1β, the first step were divided into two stages, the supernatant of each sample were first incubated for 2 hours and washed with PBS/Tween before adding the detection antibody. The plate was then incubated for another 2 hours, following addition of an incubation with Streptavidin HRP for 20 min (CCL5/RANTES and IL-1β Duoset, R&D systems). The subsequent procedure was similar as described above.

3.3.5 Harvesting cells to determine cell density

To determine the exact cell density at the start of particle exposure for each experiment, the cell-number in two control wells were determined at the start of each exposure. This was done by a trypsinization process. The wells were washed 2 times with PBS, treated with trypsin/EDTA (0.025%/0.1%) and incubated for 2 min at 37 °C. When the cells had detached from the surface, a stop solution (20% FCS in PBS) was added, and the cell suspension was then collected. To measure the viability, 10 µl of the cell solution was mixed with 10 µl of trypan blue (0.4%) solution, which selectively colour dead cells blue. A TC 10 Automated cell counter (Biorad) was used to count viable cells.

3.3.6 The LDH assay

To measure the cytotoxicity in BEAS-2B cells after exposure to silica nanoparticles, the amounts of LDH in cell supernatants was quantified according to the supplier's

recommendations with a LDH assay detection kit (Roche). First, 100 µl of the standard and cell-sample solutions were added onto a 96-well polystyrene plate. Thereafter, 100 µl reaction mixture of catalyst and dye solution was added, and the plates were incubated dark in 5-30 min until the colour development was satisfactory. The absorbance was then measured and quantified at a wavelength of 490 nm with a TECAN Sunrise Absorbance Reader equipped with suitable software (Magellan V 1.10). To relate the LDH amount to cytotoxicity (% necrosis) a maximum LDH release was obtained. This was done by exposing the BEAS-2B cells to 1% Triton x-100 in medium for 5-30 min to give 100 % cell necrosis. To confirm the effect of Triton, as seen as shrinkage of cells to small grains, the cells were investigated under a microscope. The supernatant was then centrifuged at 300 g for 10 min and diluted for analysis.

The percentage of cytotoxicity was calculated with the following formula:

$$Cytotoxicity(\%) = \frac{ABSsample - ABSmedium}{ABS\ \max - ABSmedium} * 100$$

3.3.7 Western analysis

To separate the proteins, 15-30 µg proteins were applied on a 10% polyacrylamid gel (see Appendix 2) and the electrophoresis was run at 200 V for approximately 1 hour. The proteins were then blotted onto a nitrocellulose membrane at 100 or 70 V for 60-90 min dependent of the blotting equipment, blocked with 3% dry milk for 30 min and incubated with a primary antibody (1/1000 in 5 % BSA), targeting the desired protein, overnight. The membranes were then washed 3 times for 5-10 min with a TBS buffer before incubating with a HRP-conjugated secondary antibody (1/2000 in 3 % dry milk) at room temperature for 1-2 hours. After a second wash, the membrane was treated with a Super Signal West Dura (Pierce) solution to give chemiluminescence to the targeted antigen/antibody complex. The immunodetection was done in a ChemiDoc platform (Bio Rad), and analysed with Image Lab. To determine the loading control (β-actin), the membranes were incubated with a stripping solution for 15 min to remove primary and secondary antibodies, and rinsed with Tris-buffered saline (TBS) solution before they were incubated with a primary antibody against β–actin (1/200.000 in 3 % dry milk) overnight. The membranes were then incubated with a secondary antibody (1/5000 in 3 % dry milk) against β-actin, and the immune complex was detected in a ChemiDoc platform as described above.

3.3.8 Real time Polymerase Chain Reaction (PCR)

3.3.8.1 cDNA synthesis

Prior to the detection of the targeted DNA molecule, the mRNAs was transcribed to cDNA through a process called reverse transcription. A mixture of reverse transcriptases, random primers, dNTP mix, buffer and RNase free water were made and distributed to small PCR tubes together with RNA (1000 ng). Two additional tubes were made, one which does not consist of reverse transcriptase (called NRC), and one without RNA (called NTC). The NRC was made to control the presence of DNA contaminants, and the NTC was made to control the presence of contaminants from DNA and RNA. The cDNA synthesis was performed in a Gene Amp PCR System 2400 machine (Perkin Elmer) at 37° C for 2 hours. The cDNAs were then stored in the refrigerator overnight or in the freezer for a longer period.

3.3.8.2 REAL TIME PCR

To analyse the expression of IL-6, IL-8, TNF-α and IL-1β mRNA after silica nanoparticle exposure, the cDNA solutions were first diluted 1:9 with RNase free water. A Real time master mix, consisting of a blend of TaqMan master mix and primers for the genes of interest, were made. Both the diluted cDNA solution and real time master mix were added to a optical Fast Real Time PCR 96-well plate, covered with an optical adhesive cover, centrifuged at 300 g in 1 minute and analysed in a 7500 Fast System Real Time PCR machine (Applied Biosystems) with a standard 7500 PCR run mode with 1 minute extension at 60 °C.

3.3.9 Small interfering RNA (siRNA)

On the same day that BEAS-2B cells were plated on 6-well plates, the cells were transfected with a mixture of HiPerfect and siRNA against p65. Each well contained 250.000 cells in 2.3 ml LHC-9 medium. The transfection mixture was made for each well, consisting of a blend of 100 µl LHC-9 medium, 6 µl HiPerfect and 10-20 nM siRNA. It was thereafter mixed, rested for 10 min and added drop wise to each well. The cells were incubated for 20 hours before replacing it with DMEM/F12 medium. Nonsense siRNA (SignalSilence Control siRNA, 15 ng) was used as a negative control to verify that there was no specific degradation of cellular messages. Approximately 48 hours after transfections, the cells were exposed to Si10 (25 µg/ml) and Si50 (100 µg/ml) for 20 hours. The cell supernatants were harvested and used for

cytokine and cytotoxicity measurements (as described in section 3.3.4 and 3.3.6). Western analysis (as described in section 3.3.7) were used to control the effectively of the transfection after 48 and 72 hours.

3.4 Statistical considerations

In the present study, the software GraphPad Prism (version 5 for Windows) has been used for statistical analysis. All data are given as mean $\pm$ standard error of the mean (SEM) for at least 3-4 independent experiments. We used parametric tests and assumed that the datasets were normally distributed. In experiments where three or more groups were compared, one-way or two-way analyses of variance (ANOVA) with Dunnet's or Turkey's multiple comparison post-test were used to see if there was a significant difference between the datasets. Generally, P-values < 0.05 were considered to be statistically significant. This indicates that there was a 95 % probability that the difference between the compared groups was significant. If there was a large variation in the dataset, statistical analyses were done on log transformed data to ensure normal distribution.

4 Results

4.1 The effect of cell density in culture on the release of cytokines and cytotoxicity

The effect of cell density on the release of three different pro-inflammatory cytokines (IL-6, IL-8 and RANTES) in BEAS-2B cells after exposure to SiNP, were evaluated. The exact cell density, which is denoted as the number of living cells per well, was determined by counting the cells after trypsinization 1, 2 and 3 days after seeding. The effect of cell density on the potential of SiNPs to induce cytotoxic effects in BEAS-2B cells, measured as cell viability, was also examined.

Table 2 shows the mean cell density for four independent experiments on different days after seeding. The cell number per well were nearly doubled each day (Table 2). The cell cultures with intermediate cell density were approximately 80 % confluent, while cultures with the highest cell density were completely dense (100 % confluent).

	Day in culture		
	Day 1 **(low density)**	**Day 2** **(intermediate density)**	**Day 3** **(high density)**
Mean cell density (cells per well)	367 313 ± 57 139	613 000 ± 106 574	1 180 375 ± 235 339

Table 2: Cell number of BEAS-2B cells in DMEM/F12 media on different days after seeding. *The cells were plated on 6-well plates in LHC-9 medium. The cell density was determined in two wells in each experiment by trypsinization 1, 2 and 3 days after seeding. The table shows the mean cell density for 4 experiments and the standard deviations.*

BEAS-2B cells with the three different cell-densities were exposed for 20 h to increasing concentrations of SiNPs with sizes of 10 nm (0-100 µg/ml) and 50 nm (0-200 µg/ml). The release of IL-6, IL-8 and RANTES were measured with sandwich ELISA (figure 16 and 18), and the release of LDH with a cytotoxicity detection kit (figure 17).

With respect to cell density, exposing the cells at the intermediate density gave the highest relative fold increase of both IL-6 and IL-8 for Si10 (figure 16A and B). With respect to Si50 the effects of cell density upon exposure was less distinct, but the results indicated that Si50 gave the highest release of IL-6 at the intermediate density and of IL-8 at the intermediate and the highest density (figure 16D and E). The cells with the lowest cell density gave the lowest relative cytokine response for both particle sizes, but this was especially evident for Si10. For Si10 particles, the difference between intermediate density compared to low density and high density was statistically significant at all concentrations between 50-100 µg/ml for both cytokines (figure 16A and B). For Si50, the difference between the intermediate density and the high density was statistically significant for IL-8 at 100 µg/ml (figure 16E).

BEAS-2B cells appeared to be more sensitive to smaller nanoparticles, responding to lower concentrations of Si10, which elicited a stronger response of both IL-6 and IL-8 compared to Si50 at similar particle concentrations (figure 16). Even at the highest concentration of Si50 (200 µg/ml), the release of cytokines was much less than for Si10. For cell cultures with an intermediate density, Si10 gave a 100-fold increase, whereas Si50 gave a 2-fold increase of IL-6 at a concentration of 50 µg/ml (figure 16A and D). This was also similar for IL-8, giving a 328-fold increase for Si10 and 2.5-fold increase for Si50 at the same concentration (figure 16B and E). For both Si10 and Si50, the pattern of release was similar for IL-6 and IL-8. The release of cytokines was concentration-dependent, giving increasing amount of cytokine release with increasing concentrations.

Both Si10 and Si50 showed a lower response to RANTES than for IL-6 and IL-8 (figure 16C and F). For Si10-induced cytokine release, cells at the intermediate density caused the highest release of RANTES, but led to a more decline of cytokine release at higher concentrations. However, Si50 was not as potent as Si10 in inducing the release of RANTES, but caused a higher cytokine release on the lower density in culture compared to other densities. At the concentration 25 µg/ml, Si10 gave a 3-fold increase on the intermediate density compared to control, whereas Si50 gave a fold increase of 0.5 at the same density. However at the lowest

cell density Si50 gained a 2.6 fold increase at Si50 particle concentration of 25 µg/ml. The levels of RANTES were reduced at concentrations above 25 µg/ml for both particle sizes.

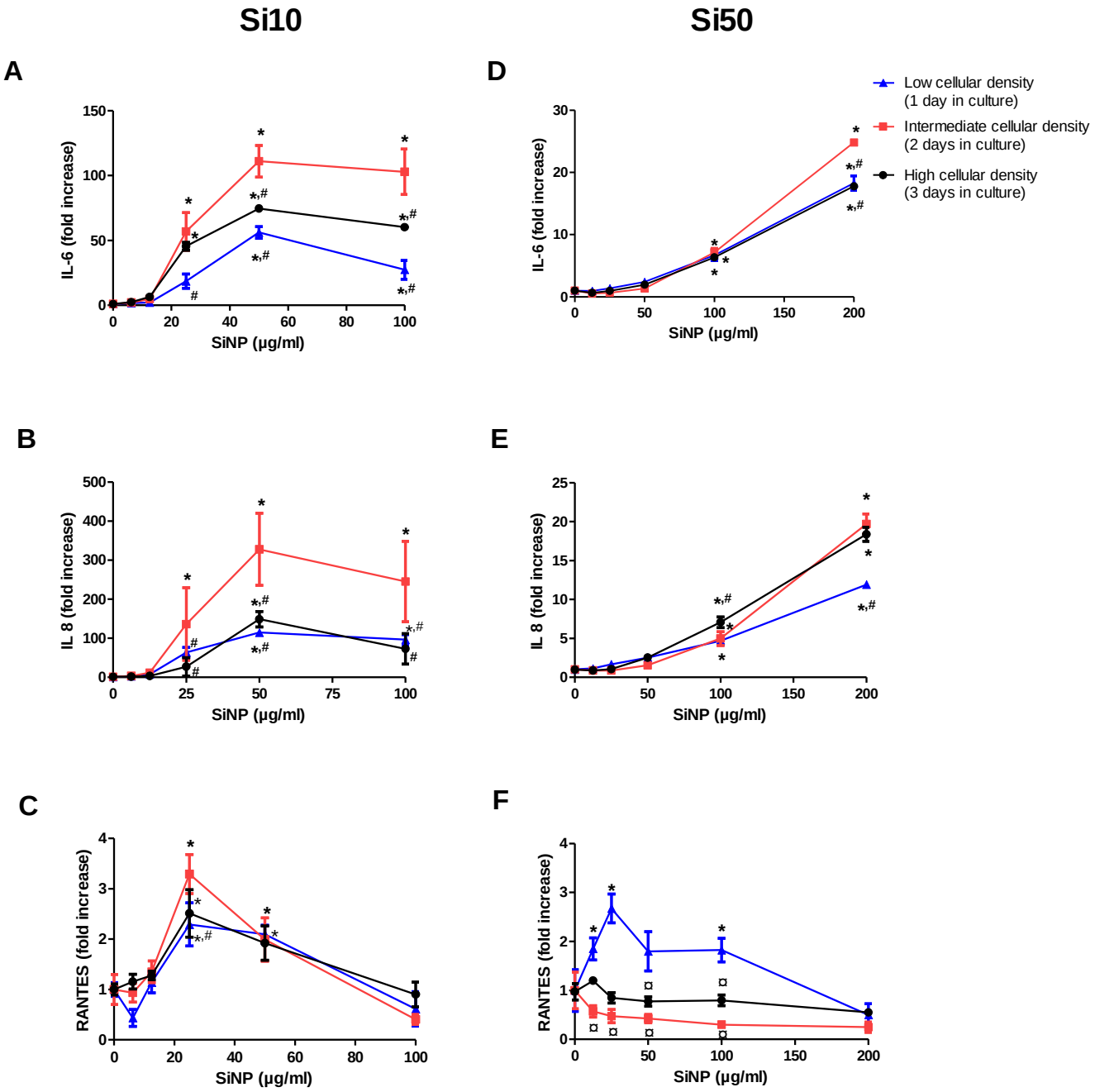

Figure 16: The release of pro-inflammatory cytokines from BEAS-2B cells after exposure to increasing concentrations of SiNP at different cell densities. *The cells were seeded on 6-well plates in LHC-9 medium and exposed at different cell densities (low, intermediate, high) to increasing concentration of Si10 (0-100 µg/ml) and Si50 (0-200 µg/ml) in DMEM/F12 media for 20 hours. The supernatants were harvested 20 hours after exposure. IL- 6, IL-8 and RANTES were measured by ELISA. The data are presented as mean value ± SEM of at least 4*

*experiments. The results are shown as fold increase relative to control. * is significant difference relative to control, p < 0.05 for Two way ANOVA with Dunnett's Multiple comparison test. # is significant difference relative to cells with intermediate density, p < 0.05 for Two way ANOVA with Dunnett's Multiple comparison test. ¤ is significant difference relative to cells with low density, p < 0.05 for Two way ANOVA with Dunnet's Multiple comparison test.*

The cytotoxicity, measured as the release of LDH, increased with increasing concentrations of SiNP. With respect to cell density, a greater cytotoxicity is observed for cell cultures with high density for both Si10 and Si50, but these cells had a higher basal level of cell death. At the highest cell density, the basal toxicity was approximately 13 %, while at low and intermediate densities the basal toxicity was approximately 7 %. Even though cell death is increasing proportionally with increased concentrations, it seems as the pattern of LDH release was similar for all densities. The result indicates that the higher amount of cells in a culture, the greater release of LDH occurs.

As seen in figure 17, Si10 is markedly more cytotoxic than Si50 at lower concentrations. This shows that particle size influences the toxic potential of nanoparticles. For Si10, the percentage necrosis increased from 13-70 % for cultures with high density, 6-54 % for intermediate density and 6-46 % for low density. In comparison, Si50 induced lower cytotoxicity where the percentage necrosis increased from 13-42 % for high density, 7-30 % for intermediate density and 7-27 % for low density. The difference the two nanoparticles caused LDH-release was in line with the release of cytokines.

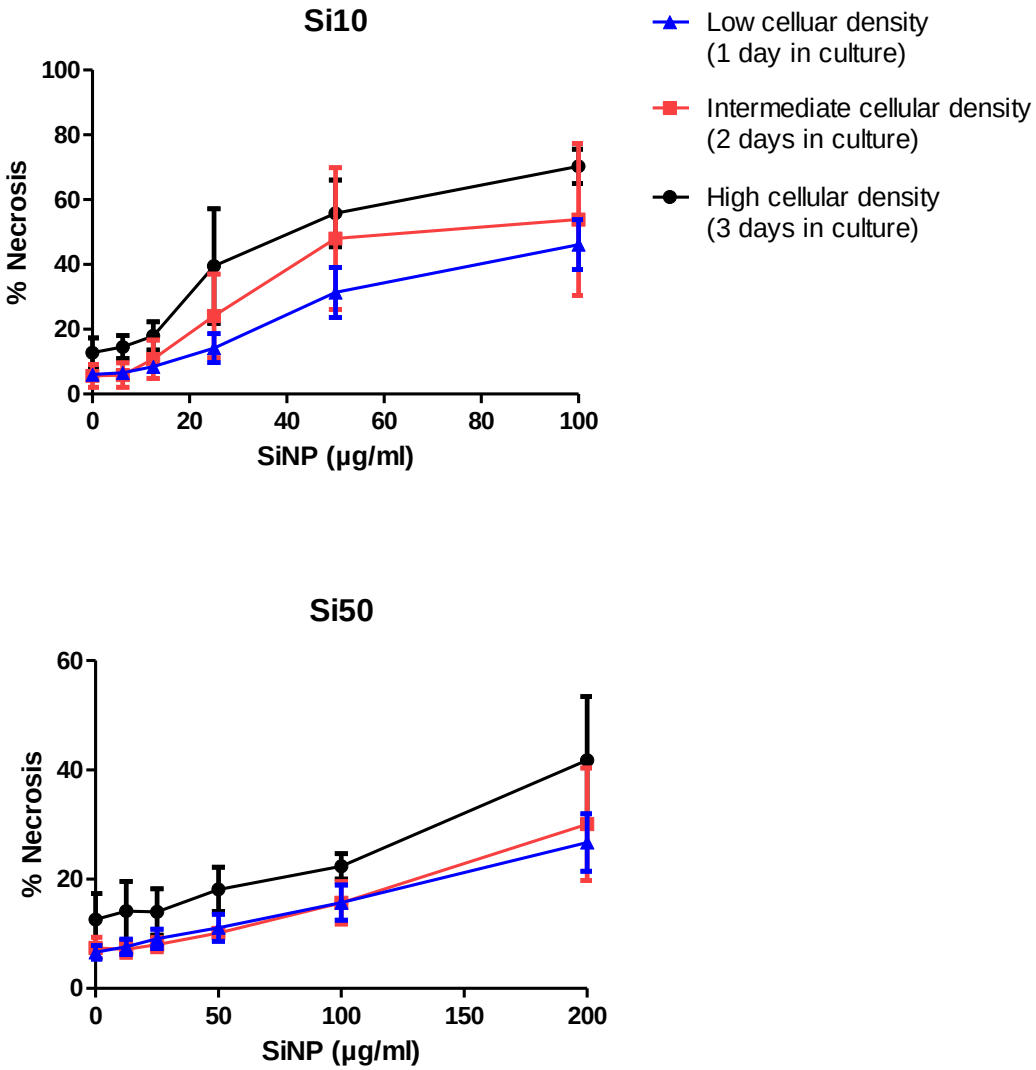

Figure 17: The release of LDH from BEAS-2B cells on different cell densities after exposure to an increasing concentration of Si10 and Si50. *The cells were exposed to an increasing dose of SiNP in DMEM/F12 media 1, 2 or 3 days in culture, and then harvested after 20 hours. The release of LDH was then measured with a cytotoxicity detection kit. The results are shown as percentage (%) necrosis, where LDH release from cells lysed with 1 % Triton X-100 was considered as 100 %. Percent cytotoxicity of the samples was determined relative to the control group. For both particle sizes, the basal toxicity for cultures in low and intermediate density was approximately 7 %, and approximately 13 % for cultures in high density. The data are presented as mean values ± SEM of at least 4 experiments.*

The pro-inflammatory cytokines, IL-6 and IL-8, have been extensively studied, but there was also of interest to examine the responses of IL-1β and TNF-α. Because cultures with an intermediate cell density induced the highest cytokine release after exposure to SiNP, we decided to measure the release of IL-1β and TNF-α with this cell density. The presented data are therefore only with intermediate cell density. This experiment also showed that Si10 was more potent compared to Si50, giving a 64-fold increase of IL-1β compared to Si50, which gave a 3-fold increase at a concentration of 50 µg/ml. The results from TNF-α response are not shown, because the cytokine release was under detection limit.

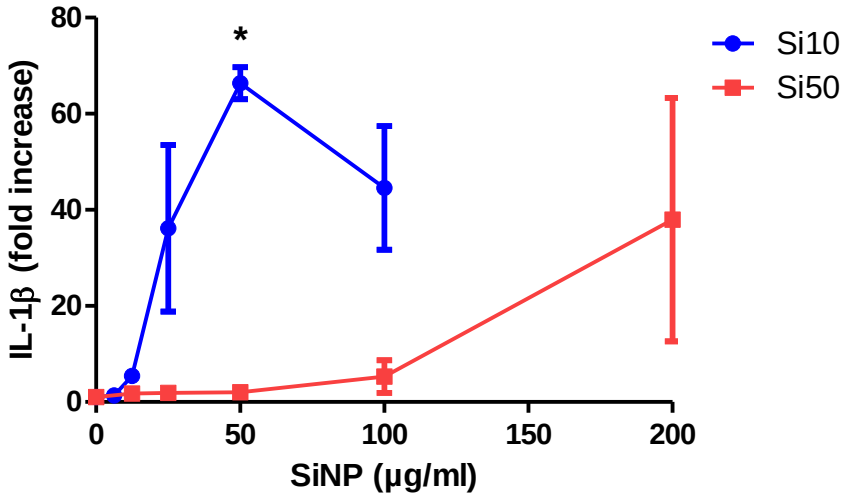

Figure 18: The release of IL-1β from BEAS-2B cells with an intermediate cell density after exposure to increasing concentrations of SiNP*. The cells were seeded on 6-well plates in LHC-9 medium, and substituted with DMEM/F12 20 hours after seeding. Cell cultures with an intermediate cell density were exposed to increasing concentration of Si10 (0-100 µg/ml) and Si50 (0-200 µg/ml) in DMEM/F12 media for 20 hours. The supernatants were then harvested, and the release of IL-1β was measured by ELISA. The data are presented as mean value ± range of 2 experiments. * is significant difference relative to control, $p < 0.05$ for One-way ANOVA with Turkey's Multiple comparison test.*

Based on the experiments with different cell density in the culture, we also decided to further study the effects on mRNA expression and involvement of intracellular signaling mechanisms after SiNP exposure in cultures with an intermediate density.

4.2 Gene expression of pro-inflammatory cytokines

To examine how the two different SiNPs affect the gene expression of IL-6, IL-8, TNF-α and IL-1β, mRNA analysis was performed using Real Time PCR after 1.5, 3, 6 and 8 hours of exposure with Si10 (25 µg/ml) and Si50 (100 µg/ml). The concentrations were chosen based on the measurements of cytokine responses by ELISA and cytotoxicity by LDH, as they gave a low cytotoxicity and a high release of pro-inflammatory cytokines.

Real Time PCR analysis of IL-6, IL-8, IL-1β and TNF-α showed that Si10 and Si50 induced a different gene expression pattern. The mRNA expression of these cytokines was highest when the cells were exposed to Si10 giving a prolonged and increasing mRNA-production towards 8 hours with a 144-fold increase of IL-8, 34-fold increase of IL-6 and approximately 6-fold increase of both IL-1β and TNF-α, compared to control cells. The gene expression of these cytokines were observed earlier for Si50, where the peak of exposure was already reached after 1.5 hours, giving fold increases of 6.5 for IL-8, 6 for IL-6, 3 for IL-1β and 2 for TNF-α. At this time-point the gene expression was approximately similar as observed for Si10.

However, the mRNA production was rather short lasting and reduced gradually after this time point compared to Si10. The Si10 induced mRNA expression of IL-8 was also stronger than for IL-6, IL-1β and TNF-α, with the production of IL-1β and TNF-α mRNA being the lowest for both particle sizes. The pattern regarding the time course for Si10-induced mRNA expression of IL-6 and IL-8 was similar compared to each other. Furthermore, the pattern of IL-1β and TNF-α was also similar to each other. For Si50, the time courses for all cytokines were similar.

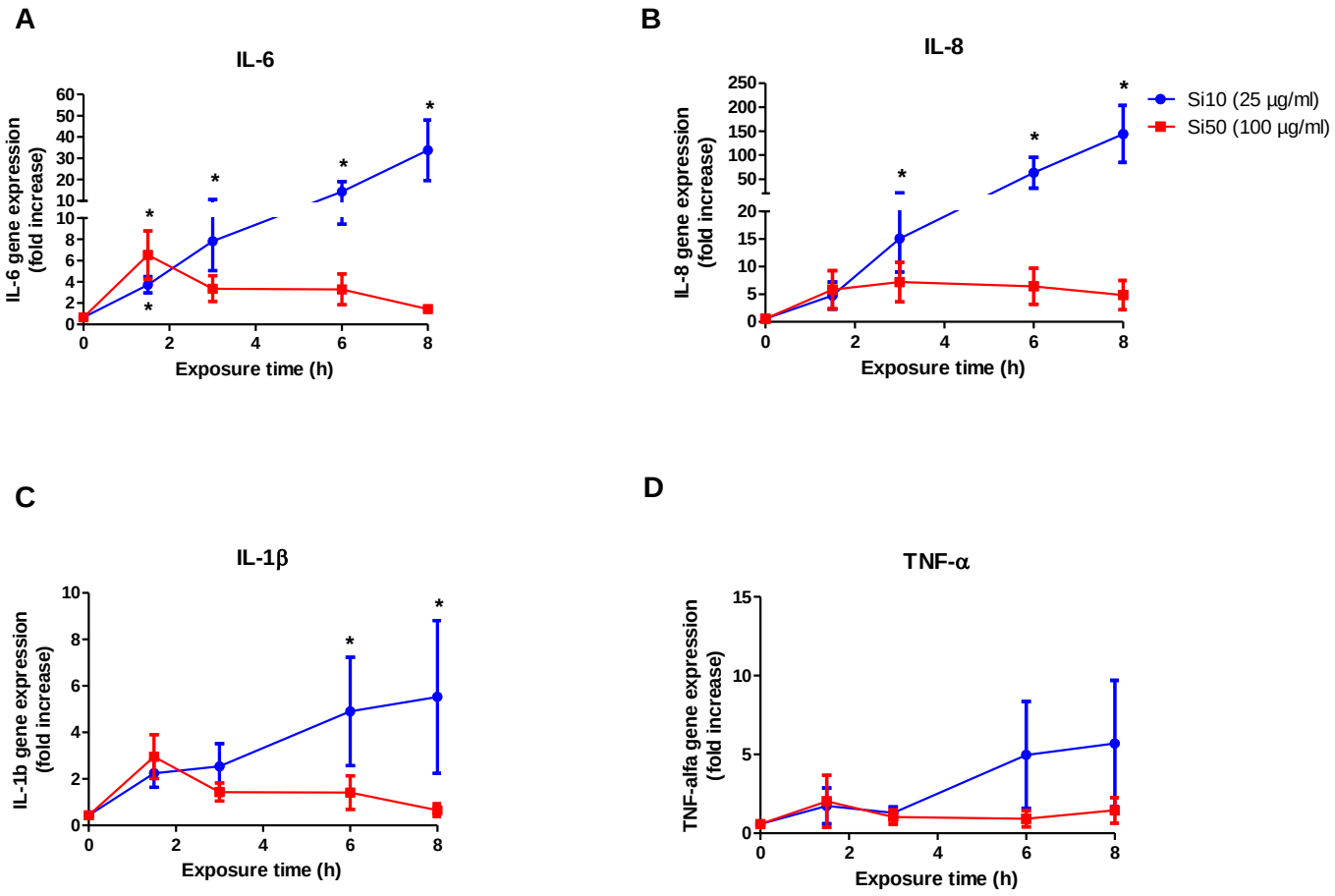

Figure 19: IL-6, IL-8, TNF-α and IL-1β mRNA-expression after exposing BEAS-2B cells to SiNP. *The cells were exposed to Si10 (25 µg/ml) and Si50 (100 µg/ml) for 1.5, 3, 6 and 8 hours. Cellular RNA was isolated from the cells with an RNA isolation kit, and mRNA was then measured by reverse transcription followed by Real Time PCR with primers for IL-6, IL-8, TNF-α and IL-1β. The data are represented as the mean value ± SEM of 4 experiments, and the results are shown as fold increase of the control. * is significant difference relative to control, $p < 0.05$ for One way ANOVA with Turkey's Multiple Comparison test. The statistics were calculated on log-transformed data.*

4.3 Involvement of transcription factor NF-κB in cytokine release

NF-κB signaling is important in various cellular stress responses, including cytokine expression. It was therefore desirable to see if this stress-activated pathway is triggered after exposure to silica nanoparticles.

4.3.1 Activation of NF-κB (p65) after exposure to Si10 and Si50

To examine the activation of NF-κB signaling pathways, the time-dependent phosphorylation of p65 and degradation of the NF-κB inhibitory protein, IκB-α, were assessed by Western analysis after exposure to Si10 (25 µg/ml) and Si50 (100 µg/ml) for 1, 2, 4, 6 and 8 hours.

In this study, exposure to Si10 led to a an early phosphorylation of p65 after 1 hour and gave a prolonged phosphorylation that lasted up to 6 hours before it was down-regulated after 8 hours (figure 20A). The phosphorylation of p65 induced by Si50 was approximately as marked as Si10 at 1 and 2 hours, but did not last as long in comparison with Si10. The phosphorylation was down-regulated twice – first at 4 hours and then at 8 hours. For both Si10 and Si50, the degradation of IκB-α did not occur clearly before at 6 hours (figure 20B).

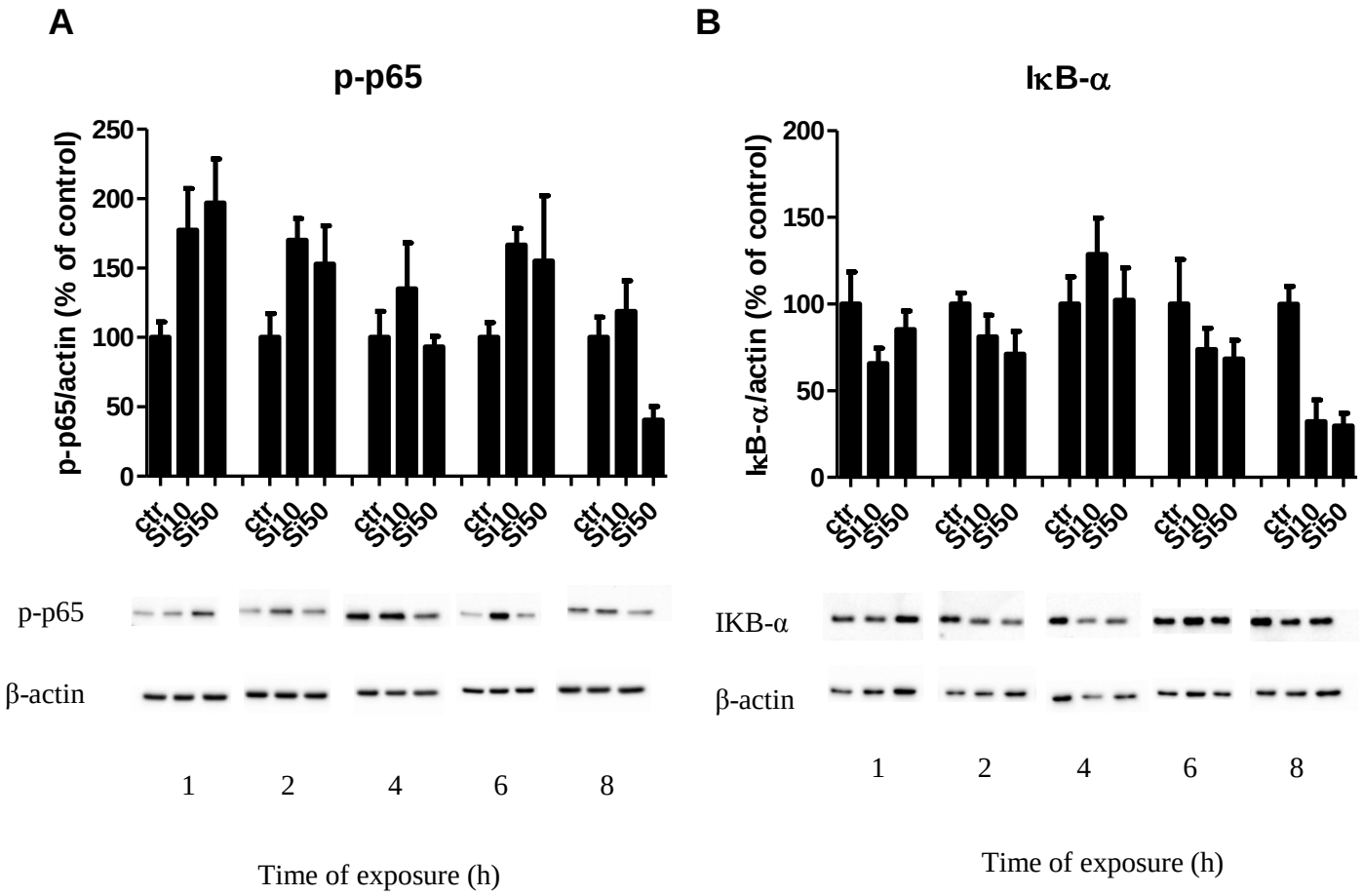

Figure 20: Activation of the NF-kB system presented as phosphorylation of NF-κB p65 and degradation of IκB-α in BEAS-2B cells after exposure to Si10 and Si50. *The cells were exposed to Si10 (25 µg/ml) and Si50 (100 µg/ml) for 1-8 hours, and the patterns of p65-phosphorylation and IκB-α degradation were examined by Western analysis. The data denote a representative blot for four experiments and the semi-quantification of the mean value ± SEM for at least 4 experiments. β-actin was used as a loading control. A: Quantification of p-p65 and a representative Western blot of p-p65/β-actin. B. Quantification of IκB-α and a representative Western blot of IκB-α/β-actin.*

4.3.2 The involvement NF-κB (p65) in cytokine release

To verify the involvement of NF-κB in IL-6 and IL-8 responses, BEAS-2B cells were pre-treated with a chemical inhibitor of p65 (PDT-p65, 30 µM) 1 hour prior to exposure to Si10 (25 µg/ml) and Si50 (100 µg/ml). Similar to p65, the PDT-p65 inhibitor contains a Ser276 site. During NF-κB activation, the Ser276 site on the inhibitor is phosphorylated instead of p65, which leads to an inhibited activity of p65 [137]. Figure 21A and 21B show the reduction in the SiNP-induced cytokine release after pre-treatment with PDT-p65. The reduction was greatest for Si10 with a significant decrease of IL-6 release by 73 % and a partial, but not significant reduction of IL-8 release by 42 % compared to the maximal response. Furthermore, the cytokine release of IL-6 was significantly reduced by 60 % in cells exposed by Si50. However, the Si50-induced IL-8 response was not affected by the NF-κB inhibitor.

PDT-p65 did not cause any significantly changes in cytotoxity after exposure to SiNP inBEAS-2B cells (figure 21C). However, it seemed as the cytotoxic effect of Si50 was to a small extent affected by the inhibitor, which is observed as a reduction in percentage necrosis.

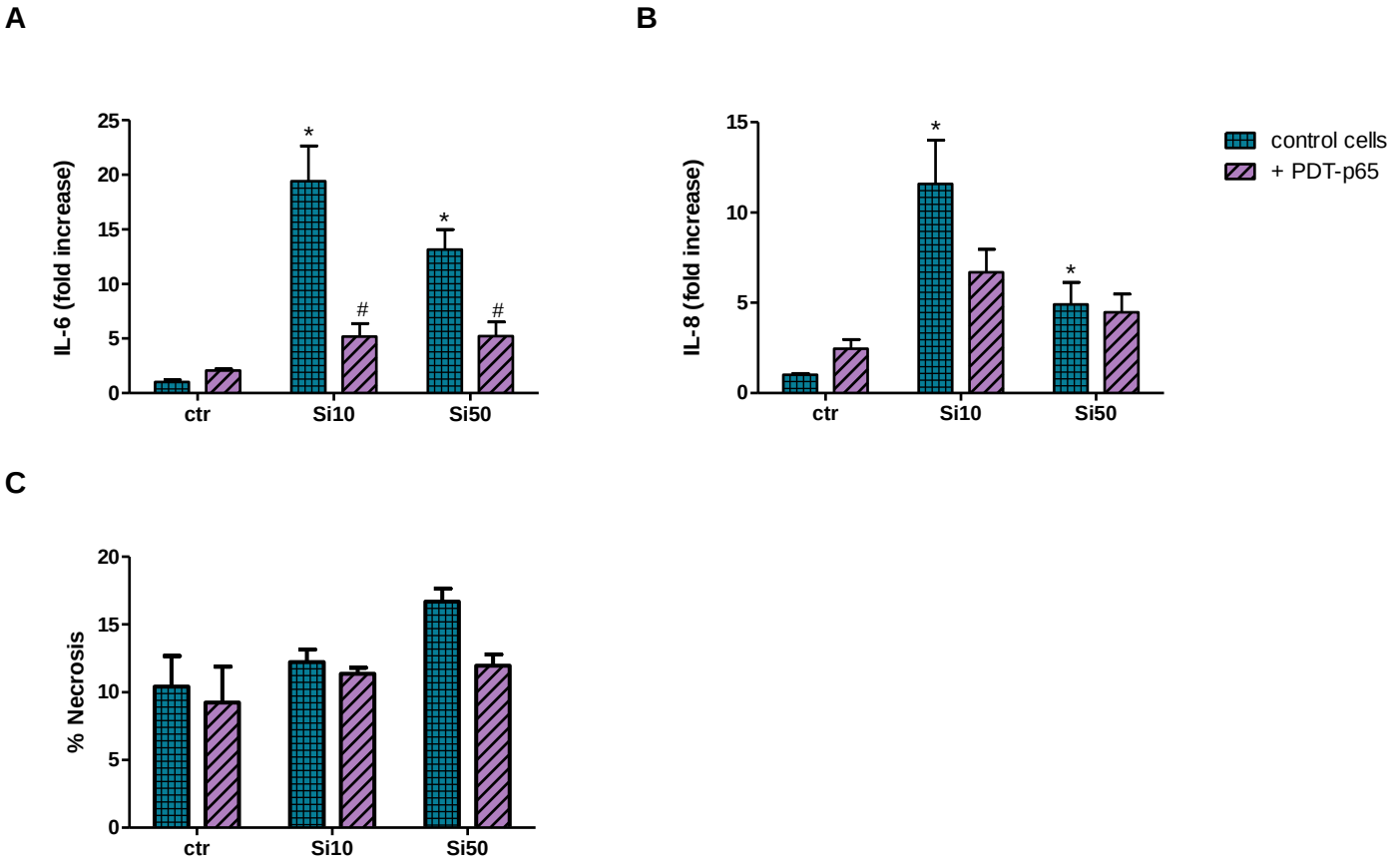

Figure 21: Effect of a p65-inhibitor on cytokine release and cytotoxicity induced by Si10 and Si50. *The cells were pre-treated with the chemical inhibitor, PDT-p65 (30 µM) for 1 hour before exposure to Si10 (25 µg/ml) and Si50 (100 µg/ml) for 20 hours in DMEM/F12 media. The release of cytokines and cytotoxicity was measured by ELISA and LDH as described in Materials and Methods (section 3.3.4 and 3.3.6). A and B: For IL-6 and IL-8, the data represents mean value ± SEM of 4 experiments. The results are shown as fold increase relative to control. C: The results are shown as percentage (%) necrosis, where LDH release from cells lysed with 1 % Triton X-100 was considered as 100 %. Percent cytotoxicity of the samples was determined relative to the control group. The LDH data represents mean value ± SEM of 3 experiments. * as significant difference relative to control, $p < 0.05$ for One way ANOVA with Turkey's Multiple Comparison test. # as significant difference for Si10/Si50 compared to Si10 with PDT-p65/ Si50 with PDT-p65, $p < 0.05$ for One way ANOVA with Turkey's Multiple Comparison test.*

To confirm the PDT-p65 results, BEAS-2B cells were also transfected with siRNA against p65 to knock down mRNA for p65. To ensure that the inhibition of IL-6 and IL-8 was due knock-down of p65 mRNA and not an unspecific reaction, the cells were also transfected with nonsense siRNA (10 µM) against p65, used as a control. The cells were transfected with three different concentration of siRNA (10, 15 and 20 nM) two days prior to exposure to Si10 (25 µg/ml) and Si50 (100 µg/ml). The supernatants were then analyzed for the release of IL-6 and IL-8 by ELISA. The protein levels of p65 were determined at the start and the end of exposure by Western analysis. The amount of siRNA was titrated to find the effective dose that gave knock-down of the protein levels of p65.

Treatment with 20 nM siRNA markedly knocked down p65 levels in the cells more efficiently compared to 10 and 15 nM siRNA (figure 22D). Figure 22 A, B and C showed that treatment with siRNA reduced the cytokine responses, which was most effective for 20 nM siRNA. The reduction in cytokine release was also greater in Si10-exposed cells compared to Si50-exposed cells. Using 20 nM siRNA, the Si10-induced IL-6 and IL-8 release were respectively reduced by approximately 60 and 70 %. In comparison, Si50-induced release was decreased by approximately 50 % for both cytokines (figure 22 C). Based on these experiments it can be concluded that NF-κB p65 contribute to SiNP-induced IL-6 and IL-8 release in BEAS-2B cells.

A) 10 nM

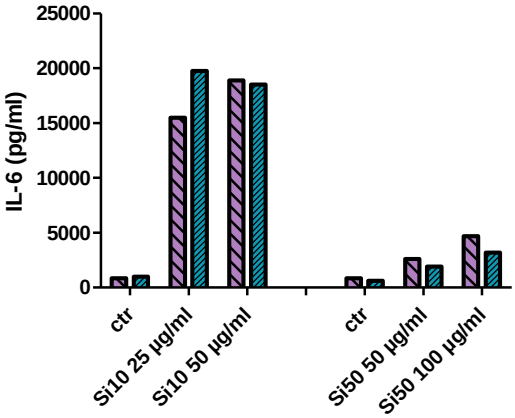

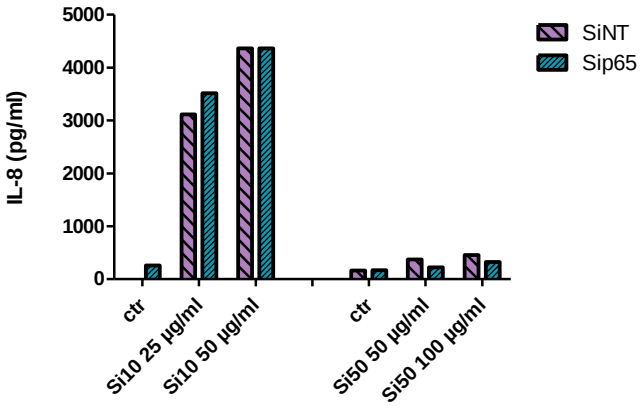

B) 15 nM

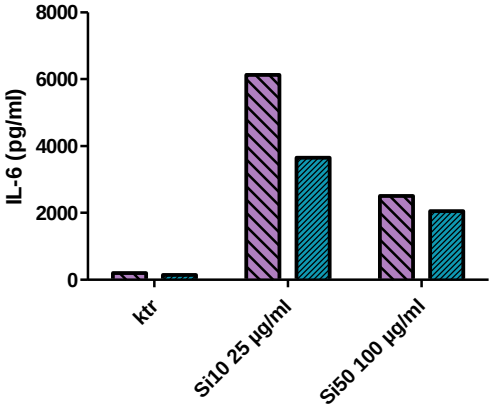

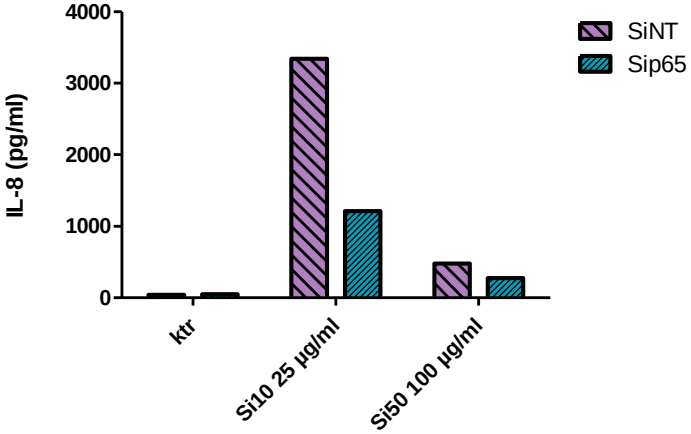

C) 20 nM

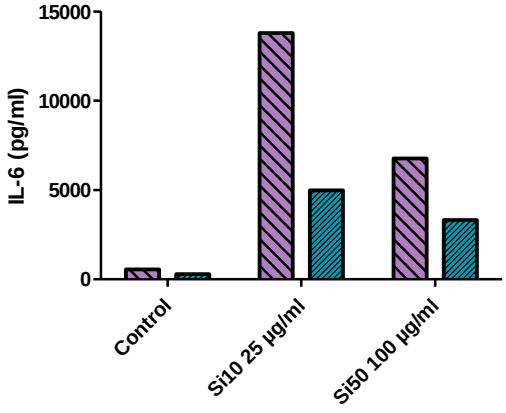

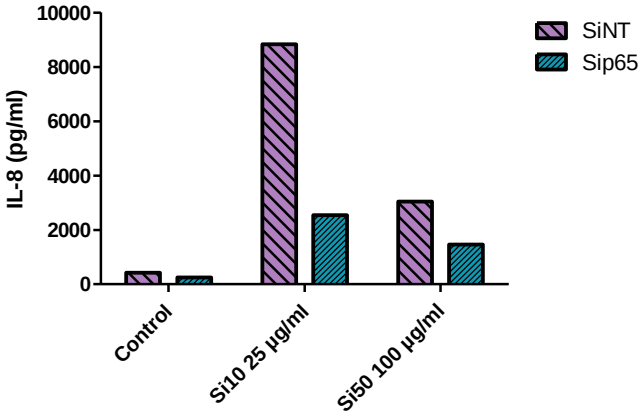

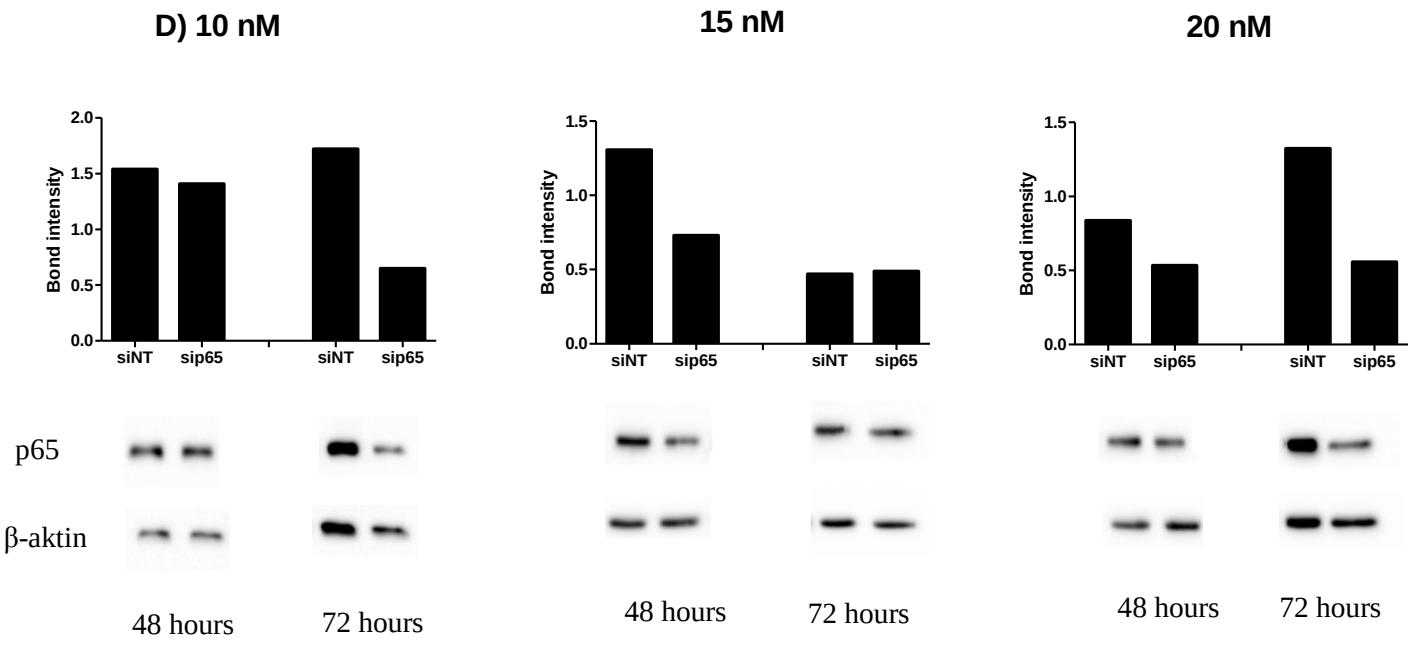

Figure 22: Effect of p65-inhibiton by siRNA on cytokine release induced by Si10 and Si50. *BEAS-2B cells were transfected with a blend of HiPerfect and siRNA against p65 in LHC-9 48 hours before exposure to Si10 (25 µg/ml) and Si50 (100 µg/ml) in DMEM/F12. The cell-supernatants were harvested after 72 hours and analyzed with sandwich ELISA according to the manufacturer's guidelines. Western analysis was used to control the efficiency of the transfection after 48 and 72 hours. Nonsense siRNA (SiNT) was used as a negative control. The results shown are only representative for one experiment per concentration.*

A. IL-6 and IL-8 release after transfection with 10 nM siRNA

B. IL-6 and IL-8 release after transfection with 15 nM siRNA

C. IL-6 and IL-8 release after transfection with 20 nM siRNA

D. Western blot of transfection efficiency after pre-treatment with 10, 15 and 20 nM siRNA

4.4 The involvement of PKC in cytokine release

Previously experiments by Skuland et al (unpublished study, 2015) have shown that Si10 and Si50 induced ROSgeneration in BEAS-2B cells, and that this contributed to the IL-8 and IL-6 releases after SiNP exposure. It has been suggested that silica particles may activate PKC and thus modulate cellular responses as ROS [105]. The role of PKC in the SiNP-induced cytokine response in BEAS-2B cells was examined with a broad inhibitor of PKC (GF109203X, 1 and 3 µM) 1 hour prior to particle exposure with Si10 (25 µg/ml) and Si50 (100 µg/ml) for 20 hours. Because the stock solution of the inhibitor also comprised of DMSO, the results were compared to DMSO concentrations equivalent to the GF109203X experiments to evaluate if DMSO affected the inhibitory effect of GF109203X on cytokine and LDH responses. Higher concentrations of the inhibitor was also used (6, 10 and 20 µM), but the amount of DMSO clearly affected the inhibition properties of GF109203X (not shown), and was therefore not used further in this study.

Figure 23A and B shows the effect of PKC inhibition on the cytokine release. The decrease in cytokine release was especially distinct for Si10 with a significant reduction of IL-6 and a marked, but not significant reduction of IL-8 after pre-treatment with 3 µM GF109203X. The reduced cytokine release for Si10-exposed cells was most marked for IL-6 (1 µM: 48 % reduction) compared to IL-8 (1 µM: 33 % reduction) relative to the maximal response. The release of IL-6 from Si50-exposed cells seemed to be partly reduced by GF109203X, but the inhibition was not statistically significant. The release of IL-8 in contrast did not seem to be affected.

Figure 23C shows that pre-treatment with GF109203X reduced the cytotoxicity in SiNP exposed cells especially for Si50 treated cells. In Si50-exposed cells, both concentrations of the PKC-inhibitor significantly reduced the cytotoxicity with approximately 12 %. For Si10 1 µM GF109203X reduced the cytotoxicity with 2 %, while the toxicity was reduced with 5 % in cells pre-treated with 3 µM inhibitor. This were however not significant.

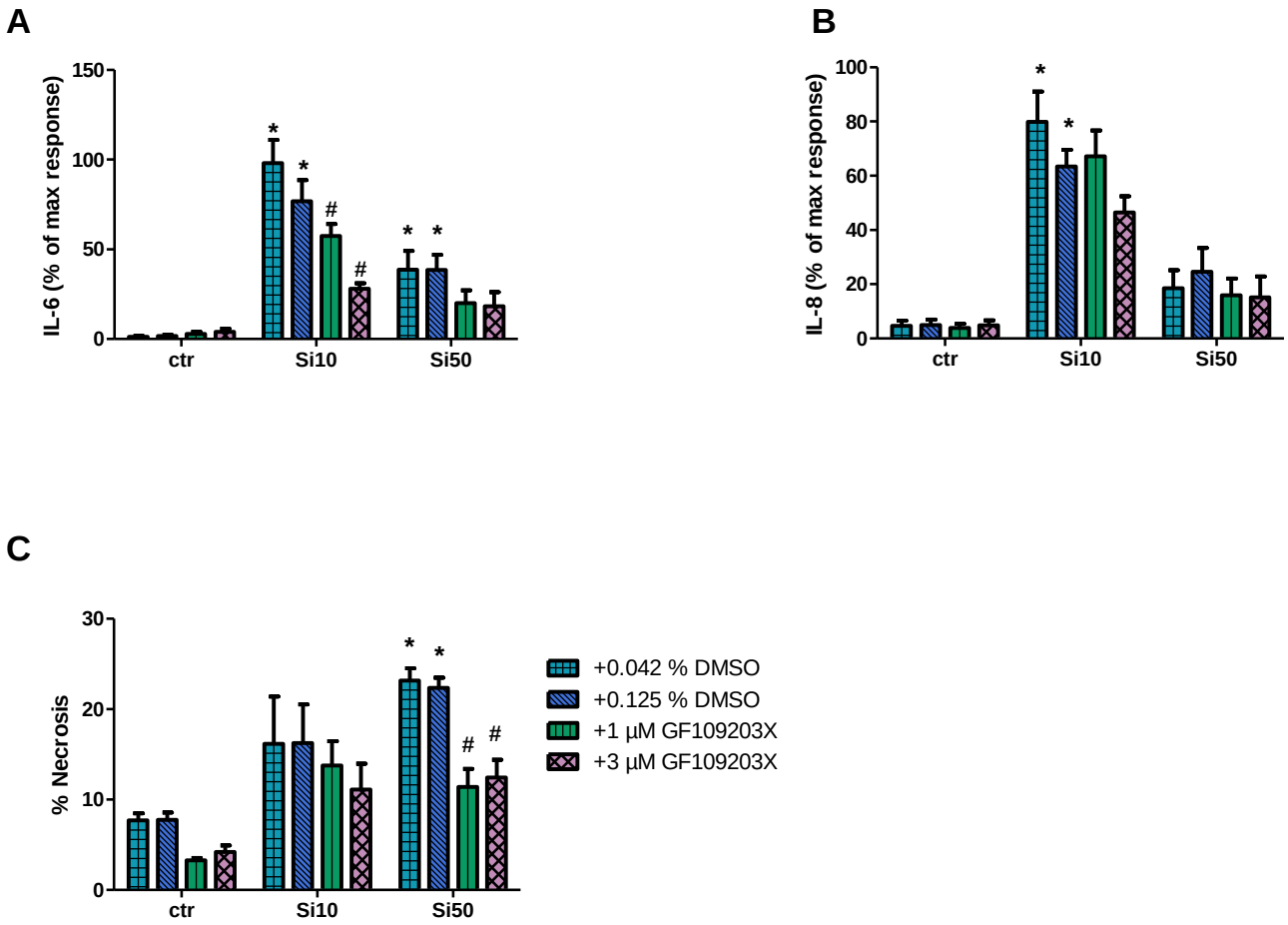

Figure 23: Effect of PKC-inhibitor and DMSO on the release of cytokines and cytotoxicity induced by Si10 and Si50. *BEAS-2B cells were pre-treated with the PKC-inhibitor, GF109203X (1 and 3 µM) or with the equally amount of DMSO, 1 hour prior to exposure to Si10 (25 µg/ml) and Si50 (100 µg/ml). The supernatant were then harvested after 20 hours and analyzed for cytokine response with ELISA and cytotoxicity with LDH cytotoxicity detection kit according to the manufacturer's guidelines. The results were compared to controls with DMSO concentrations, equivalent to the GF109203X experiments to evaluate the potential impact on cytokine and LDH release. The data represents mean value ± SEM of at least 4 experiments. A and B: IL-6 and IL-8 release after pre-treatment with GF109203X or DMSO. Percent inhibition of the samples was determined relative to the respective control (DMSO). The results were considered to be normally distributed. C: The release of LDH after pre-treatment with GF109203X or DMSO. The results are shown as percentage necrosis (%) relative to the respective control (DMSO). * is significant difference relative to control with DMSO (0.042 % or 0.125 %), $p < 0.05$ for One way ANOVA with Turkey's Multiple comparison test. # is significant difference compared to Si10+DMSO/Si50+DMSO, $p < 0.05$ for One way ANOVA with Turkey's Multiple comparison test.*

5 Discussion

The present thesis shows that smaller nano-sized amorphous silica nanoparticles (Si10) were more potent than larger silica nanoparticles (Si50) of similar composition in eliciting cytokine responses in BEAS-2B cells when compared at equal mass concentrations. Both particle sizes induced concentration-dependent pro-inflammatory responses. However, the release of IL-6 and IL-8 were increased upon decreasing particle size. Compared to IL-1β and TNF-α responses, the release of IL-8 and IL-6 were more marked. This was in accordance with the gene expression responses of these cytokines. Both Si10 and Si50 showed lower responses of RANTES. Results from LDH release also suggested a size-dependent cytotoxicity, with Si10 being the most potent.

With respect to cell density of the lung cell culture, the intermediate cell density induced the highest cytokine release for Si10, while the pro-inflammatory responses induced by Si50 were not as dependent on cell density compared to Si10. Our studies on the intracellular signaling pathways triggered by SiNP showed the involvement of NF-κB, and possibly PKC in the induction of cytokine release.

5.1 Methodological considerations

5.1.1 How well is a BEAS-2B cell culture model suitable for studying inflammatory responses in the airways?

To establish a relevant model for studying the effects of inhaled nanoparticles in the respiratory system, it is important that the cell line must closely resemble the phenotype of the original primary cell and exhibit specific epithelial cell characteristics *in vitro*. *In vitro* experiments with immortalized and normal cells have been broadly used to study the toxicological effects of particulate air pollution and the induction of pro-inflammatory cytokine signaling, which is essential for understanding the mechanisms causing various pulmonary diseases [138]. It has been speculated whether primary cells or continuous cell lines represent the most suitable model for toxicological studies in the airways.

In this thesis, we used BEAS-2B cell line that is derived from normal bronchial epithelium obtained from autopsy of non-cancerous individuals. The cells were immortalized by transfection with a 12-SV40 adenovirus hybrid and cloned, making it possible for investigation of carcinogenic processes such as DNA damage and cell transformation in the respiratory system. Lung epithelial cells are the first point of contact with respirable particles after inhalation. BEAS-2B cells have therefore been considered as a relevant cell line for *in vitro* toxicology testing upon exposure to tobacco, pollutants and nanomaterials [139]. The highest deposition of nanoparticles has also been reported in the bronchi and bronchioles, making it relevant for studying the effects of inhaled nanoparticles in these areas.

Compared to normal bronchial epithelial cells (NBHE), which are primary cells, BEAS-2B cells may present an alternative model with several advantages. They are usually considered stable and are well defined, which allow experimental replication over extended time periods. Because of their prolonged lifespan, immortalized cell lines also provide a constant supply of cells while maintaining the differentiation characteristics of the tissue of origin [138]. Gene expression in cell lines may also be more easily reproduced by various institutions [140]. However, primary cells are usually retrieved directly from tissues, organs or body fluids with no cell passages, and might therefore provide cell cultures that are more similar to the specific tissue. Such cultures might therefore be more suitable than immortalized cell lines for studying the toxic effects of harmful substances. Their characteristics are very close to the tissue of origin, making them more representative for *in vivo* responses [141]. Unger et al [142] also demonstrated in seven human endothelial cells in culture that the process leading to the capacity of cells to replicate indefinitely *in vitro* and to become a cell line, may cause a loss of expression of some specific endothelial characteristics in the cell line compared with primary endothelial cells in culture. But due to their relative homogeneity and ability to be maintained in culture indefinitely, immortalized cell lines still have been one of the preferred cell systems employed in the development and validation of *in vitro* toxicology assays [139].

Because of difficulties in replicating the interested effects in the respiratory system *in vivo,* BEAS-2B cells might be an alternative model to examine toxicity or pathogenicity in the lungs, which to some extent reflect biological aspects of primary cells. Since this is a human cell line, it is therefore possible to avoid extrapolation from animal models to human situations. Previous studies have also reported that this cell line behaves like primary

tracheobronchial epithelial cell cultures in response to pro-inflammatory mediators, secretion of cytokines and expression of adhesion molecules [143].

The altered phenotype of immortalized cell line may cause difficulties in interpreting cell responses to nanoparticles. There are also uncertainties when generalizing data obtained from immortalized cell lines in terms of responsiveness to untransformed respiratory epithelium. It has been reported that the magnitude of cytokine expression may differ significantly between primary bronchial epithelial cells and immortalized cell lines [144]. Ekstrom-Hammarström [145] reported that primary bronchial epithelial cells (NHBE) respond differently than the immortalized cell lines (BEAS-2B and A549) regarding the magnitude of cytokine expression, whereas cell viability and induction of oxidative stress were similar in all three cell types used.

Another approach might be the use of co-cultures to mimic the lung's complex mixture of various cells *in vivo*, which may give us a better understanding of how particles exert their effects in the respiratory system [79]. Kasper et al [53] showed that co-cultures simulating the alveolar-capillary barrier might provide a better model to predict *in vivo* toxicity caused by silica nanoparticles in the lower respiratory tract, compared to single-cell systems Co-cultures might therefore be important for developing better *in vitro* studies for risk assessment.

5.1.2 Does cell density affect cytokine responses and cytotoxicity?

In the present thesis, we have demonstrated that cell density may affect the release of pro-inflammatory cytokines in SiNP-exposed BEAS-2B cells. To our knowledge, this has not been previously described, neither in cells from the respiratory system nor in cells from other tissues or organs. To address whether the SiNP-induced cytokine responses were affected by cell density in culture, we examined this as the cells become more confluent over several days.

Numerous studies have shown a density-dependent association between cell density and inflammatory effects in various cells [146-149]. A study by Römer et al [148] reported that compared to a low cell density (1×10^6 cells/ml), a high cell density (1×10^7 cells/ml) of human peripheral blood mononuclear cells induced massive cytokine release during

subsequent stimulation with a soluble humanized CD28-spesific monoclonal antibody (TGN1412). Studies determining the effects of cell density on the secretion of nerve growth factor (NGF) from human lung fibroblast showed similar results. Olgart et al [147] showed that NGF from human pulmonary fibroblasts was cell density-dependent, where a higher NGF secretion was observed in pre-confluent cells (80 % confluent) compared to cells higher densities (100 % confluent). Interestingly, they showed that NGF secretion by human lung fibroblasts was not constant during culture. It was high at the very early stages of cell culture, lowering with the increase in cell number, and reaching the lowest level after confluence. It was suggested that cells with a less established cell-to-cell contact secreted more NGF than cells reaching confluence.

Correspondingly, our study showed that SiNP-induced cytokine responses of IL-6, IL-8 and RANTES might be influenced by cell density, in which Si10- and Si50-exposed cells were affected differently. Si10-induced cytokine responses were greatest in cell cultures with an intermediate cell density (approximately 80% confluent), and lowest for a low cell density. The explanation for this is unclear, but may be related to the findings described above, with different magnitude of responsiveness, dependent on the level of cell to cell contact.

Furthermore, it was suspected that a higher cell density in culture would lead to a greater fold increase of pro-inflammatory cytokines. In the present study, the highest cell density did not give a greater pro-inflammatory response, which might be because the cells were entirely dense in the culture dish (100 % confluent), forcing the cells to share the surface area. As cells become more confluent, the area of substrate each cell has to interact with decreases [150]. This may also cause a greater LDH-release due to growth arrest caused by the limited availability of nutrients in the culture dishes/plates, but this might also be due to the higher basal cell death observed in cell cultures with higher densities. This pattern suggests that in order for the cells to release high amounts of pro-inflammatory cytokines after exposure to Si10 particles, a certain cell density might be required, which is neither too low nor too high. Notably, it did not seem as the release of RANTES was as dependent of cell density, as observed for IL-6 and IL-8. This suggests that various cytokines might depend differently on cell density in the culture.

Overall, the responses to Si50 were not as dependent on the cell density as Si10, and the patterns differed for the different cytokines. Thus, the lowest cell density gave the highest response for RANTES, the intermediate cell density gave the greatest response for IL-6, and the highest cell density gave the greatest response for IL-8. Compared to IL-6 and IL-8, the pattern of released RANTES differed substantially. The lower fold increase of RANTES might explain that it has a less pronounced role in the induction of acute inflammatory responses after exposure to SiNP.

In vivo cell densities in the respiratory system are not well established. Within alveolar structures, interstitial cell densities are 19.4×10^6 cells/ml expressed by volume. However, the lung contains a considerable amount of air. It has been suggested that the alveolar structures may represent a low density area, while the airways correspond to a high density area. A study by Wang et al [151] suggested in their study that the response of cells may differ between these sites, in part because of differences in cell density. Whether the *in vitro* culture systems used in this thesis are relative to the densities existing in the respiratory system *in vivo* remains to be defined.

5.2 Differences in cytokine responses between Si10 and Si50 in cell cultures with various cell densities

When comparing the different particle sizes on a mass basis, Si10 caused a markedly greater fold-increase of all four cytokines compared to Si50. The higher fold increased induced by Si10 might be explained by the larger surface-to-mass ratio properties occurring with decreasing particle sizes. This effect has been shown to increase the reactivity of smaller particles due to the higher amount of atoms on the particle surface that are available for chemical reactions [23-25]. This study may also indicate that smaller nanoparticles might be more dependent on cell densities to induce their pro-inflammatory responses due to the greater interactions on the cell surface between adjacent cells. The difference in cytotoxicity between both particle sizes was correspondingly in line with the different release of cytokines. The induction of cell death at the highest concentrations clearly affected the cytokine and chemokine release induced by Si10, resulting in a progressive decrease in IL-6 and IL-8 responses. This did not apply to cells exposed to Si50, but might be due to a less responsiveness towards this particle size.

5.3 The relationship between gene expression and cytokine release of pro-inflammatory cytokines induced by SiNPs of different sizes

The present thesis has demonstrated that SiNP of 10 nm and 50 nm induced a time-dependent up-regulation in inflammatory-related genes such as IL-6, IL-8, TNF-α and IL-1β in BEAS-2B cells, which have been shown to be important regulators of inflammatory responses after exposure to harmful substances. In the cell cultures with an intermediate cell density, the maximal mRNA expression of these cytokines correlated well with the release of cytokines using the same nanoparticle concentrations.

The mRNA expression was dependent on particle size, where smaller nanoparticles (Si10) caused a significantly higher mRNA expression compared to Si50. Both particle sizes led to an early mRNA expression of all cytokines. Compared to Si50, prolonged and increasing mRNA expression of IL-6, IL-8, TNF-α and IL-1β towards 8 hours after exposure to Si10 was found. This was in accordance with the results from the cytokine analyses, where Si10 induced much higher responses than Si50 at equivalent concentrations. In contrast, Si50 induced a lower mRNA expression of all cytokines where the maximal gene expression was seen at 1.5 hours, before it was down-regulated and returned to control levels. Presumably this also indicates that a prolonged cytokine gene expression is needed for the marked cytokine release induced by Si10.

It is known that nanoparticles might be surrounded by a protein corona either during manufacturing or in biological environment, which may alter their toxicity, reactivity and cellular uptake as well as cellular responses [23, 152]. In our study, we used LHC-9 medium on the day of seeding and DMEM/F12 medium during exposure to SiNP. Both media were without added serum, and DMEM/F12 is known to be less enriched with proteins compared to LHC-9. Previous studies have shown little or no agglomeration of Si50 in DMEM/F12 in BEAS-2B cells [125]. This was in accordance with a study by Gualtieri et al [153], which showed that the less agglomerated amorphous SiNP induced marked responses in BEAS-2B cells. Convection and sedimentation/gravitation forces may contribute to the direct interaction of small agglomerates or single nanoparticles with the cells. Park et al [154] reported that SiNP tend to agglomerate in culture conditions during the time the experiment is performed, even though preventative measurements to avoid agglomeration of nanoparticles in the solutions has been made [153, 154]. Our research group has recently demonstrated that Si50

did not agglomerate more compared to Si10. The different time course of mRNA expression induced by Si10 and Si50 might therefore be due to different sedimentation properties of the particles. The prolonged increase of mRNA production induced by Si10 might suggest that it may exist as a suspension and does not sediment that easily compared to Si50. The faster and more easily sedimentation of Si50 may be because it is heavier and more compact than Si10, which in turn may explain the similar or relative high increase of Si50-induced mRNA production of IL-6, IL-8, TNF-α, and IL-1β compared to Si10 at 1.5 hours.

When investigating the mRNA levels of IL-6 and IL-8 for both cytokines, the results showed that the mRNA levels of IL-8 was clearly higher than IL-6. This was in line with our previous study comparing Si50 and Si500 based on equal mass and surface area concentrations. While Si50 was shown to significantly cause higher increased mRNA levels of both cytokines compared to Si500 on a mass basis, the differences was less distinct with respect to surface area concentrations [125]. The comparison of Si10 and Si50 based on a surface area concentration was not examined in this study, but several studies have indicated that opposed to equal mass concentrations, surface area may be a more appropriate parameter for dosing to determine the effects of fine and ultrafine particulates in biological systems [62, 117, 155, 156]. Recent studies with crystalline SiNP and TiO_2 nanoparticles supported that the toxicity of some nanoparticle-types may be related to the surface reactivity of the particles in influencing the development of inflammatory and cytotoxic responses in the lung [157]. This has also been demonstrated with unopsinized crystalline silica particles in A549 cells [158].

Interestingly TNF-α and IL-1β are pro-inflammatory mediators found to be released early in response to crystalline silica particles [79]. Increased levels of these cytokines are known to trigger the production of other pro-inflammatory cytokines such as IL-6 and IL-8, and thus attract neutrophils to inflammatory sites. We have previously shown that both IL-1β and TNF-α are released from monocytes upon exposure to crystalline silica, and that IL-1β mainly caused the induction of IL-8 responses [79]. This may explain the high IL-8 mRNA levels and IL-8 release after exposure to SiNP compared to the IL-6 mRNA and IL-6 levels.

In this study, TNF-α and IL-1β mRNA did not significantly increase compared to the mRNA expression of IL-6 and IL-8. This might indicate that only low levels TNF-α are needed to induce an activation of other cytokines important in the inflammatory response. With respect to IL-1β, low levels and a gradual increase in IL-1β mRNA may indicate a more complex mechanism for IL-1β release. Several studies have revealed that the IL-1β response is

regulated by two separate mechanisms. In the first signalling mechanism, ligation of pathogen-associated molecular pattern (PAMP) and danger associated molecular pattern (DAMP) molecules activates TLR, which leads to the gene expression of pro-IL-1β through the transcription factor NF-κB. The second signal includes activation of caspase-1, which cleaves pro-IL-1β to a mature form, and cause the secretion of IL-1β [69, 119]. It has been suggested that crystalline silica particles trigger the second signal through the NALP3 (also NLRP3) inflammasome response, which leads to the activation of caspase-1 and thus release of IL-1β [69, 119, 127, 159, 160]. Overexpression of IL-1β has been associated with silicosis upon chronic exposure. Sandberg et al [119] have also reported that amorphous silica particles may induce inflammasome activation, but the results differed depending on the particle size and cell types examined.

Recent studies have demonstrated that epithelial cell monolayers do not always require priming with LPS to induce IL-1β responses compared to the well-studied "two-signalling model" of IL-1β. Peeters et al [159] showed a modest increase of IL-1β levels after exposure to crystobalite silica particles in BEAS-2B cells without priming with LPS. Because the same cell line is used in the present study, similar mechanisms might be mediated through amorphous silica particles. The difference between the particles used is the surface characteristics. Similar effects were also reported after exposure to ambient particulate matter PM_{10} [161] and cigarette smoke [162] in BEAS-2B cells. Bronchial epithelial cells may therefore be considered as danger sensing cells that give small but relevant levels of biologically active IL-1β.

5.4 Involvement of NF-κB and MAPK in pro-inflammatory cytokine responses

We have previously shown that amorphous silica nanoparticles of different sizes induce marked cytokine responses of IL-6 and IL-8 mediated through intracellular signalling mechanisms such as MAPKs, EGFR, TNF-α and NF-κB [43, 82, 100]. It has been suggested that IL-8, as well as IL-6, have sites for NF-κB, AP-1 and C/EBP on their promoter regions, which are required for a maximal gene expression of these pro-inflammatory cytokines [78, 81].

The present study shows that both Si10 and Si50 mediate IL-6 and IL-8 responses through the phosphorylation of the NF-κB subunit p65 in BEAS-2B cells. Compared to Si50, lower concentrations of Si10 induced stronger and more prolonged phosphorylation of p65 that lasted up to 6 hours. On the other hand, the phosphorylation induced by Si50 was strong at 1-2 hours but the effect was short lasting, and reduced after this time point. These phosphorylations seem to precede the up-regulation of IL-6 and IL-8 mRNA, which led to an early expression of these cytokines in BEAS-2B cells already after 1 hour of exposure to Si10 and Si50. This may indicate that NF-κB plays a major role in the induction of critical pro-inflammatory cytokines during an acute inflammatory response.

A stronger up-regulation of IL-8 mRNA and thus release of IL-8 was observed after exposure to Si10, which may be due to additional posttranscriptional mechanisms such as mRNA stabilization by p38 MAPKs [81, 163]. In the absence of p38 activity, IL-8 mRNA has been reported to be very unstable and degrades rapidly [164]. An optimal IL-8 gene expression is dependent of three different mechanisms which include de-repression of the gene promoter, activation of transcription factor NF-κB and JNK pathways, and stabilization of posttranscriptional mechanisms such as IL-8 mRNA by p38 MAPK [81]. Furthermore, we have previously demonstrated that the MAPKs p38 and JNK are involved in the SiNP-induced responses of IL-6 and IL-8 [100], which furthermore support the higher expression of IL-8 observed in this study. Together, these studies suggest that expression of IL-8 requires activation of NF-κB in addition to MAPK pathways. It has also been shown that activation of NF-κB alone only caused marginal IL-8 responses [164].

The involvement of NF-κB was further supported by using a p65-spesific inhibitor (PDT-p65) as well as silencing of NF-κB p65 by siRNA. Pre-treatment of BEAS-2B cells with PDT-p65 caused a greater inhibition of IL-6 compared to IL-8 for Si10-exposed cells. Surprisingly, IL-8 responses induced by Si50 were not inhibited by PDT-p65. Other studies examining the potential of TPA and NaF to induce IL-8 responses in A549 cells showed unsuccessful inhibition of IL-8 after pre-treatment with commonly used chemical proteosomal inhibitors of IκB-α degradation, whereas PDT-p65 pretreatment induced a marked inhibition [164]. Notably, p65 knockdown by siRNA in the present study showed an even stronger suppression of SiNP-induced IL-6 and IL-8 releases, further supporting that NF-κB-activation is involved in the transcription of pro-inflammatory cytokines. A greater inhibition was seen for Si10

compared to Si50, which may be due to a stronger effect of Si10 on NF-κB-dependent mechanisms.

The precise mechanism of NF-κB translocation is not yet fully understood, but it is thought that the degradation of IκB-α is required for most cells [88], which is an important step in the activation of NF-κB. This makes it possible for p65 to translocate to the nucleus and thus promote gene expression of various pro-inflammatory cytokines such as IL-6 and IL-8 [35, 94, 95]. Interestingly, the present study shows a delayed degradation of IκB-α, which did not occur before at 6 hours. Our study may therefore indicate that amorphous silica nanoparticles phosphorylate p65 through mechanisms that are not dependent on the degradation of IκB-α. This is consistent with our previous findings for SiNP of 50 nm [43, 82].

These IκB-α-independent pathways may involve posttranslational modifications of NF-κB subunits, including site-specific phosphorylation of p65. It has therefore been suggested that gene transcription mediated by NF-κB might be regulated by serine or threonine phosphorylation or other modification of the Rel subunits that affect the transcription-activating function of NF-κB [165]. The IκB-independent activation of NF-κB has also been documented in other cell types such as B-lymphocytes [166, 167]. In contrast, Eom and Choi [8] reported that neither nuclear localization of NF-κB nor the degradation of cytosolic IκB was found in BEAS-2B cells after exposure to SiNP of 20-40 nm, which was unexpected as NF-κB is the major stress response transcription factor that has been reported to respond to a wide variety of environment stressors. This is contradicted by our current and earlier findings [43, 82]. The mechanisms by which SiNP are mediated through NF-κB signalling pathways must therefore be further evaluated.

Other studies have suggested that for maximum expression of pro-inflammatory cytokines, such as IL-6, and IL-8, NF-κB binding must occur simultaneously with other transcription factors such as NF-IL-6. Both NF-κB and NF-IL-6 are located at adjacent sites in the IL-8 [168] and IL-6 [169] promotor region, and contribute to the regulation of the gene expression of these pro-inflammatory cytokines. This has been shown upon exposure to asbestos via the generation of ROS [168]. Similar mechanisms may also be involved for SiNP, but further studies must be assessed.

Taken together, these findings show that the increase in IL-6 and IL-8 responses in BEAS-2B cell cultures exposed to Si10 and Si50 seem to be mediated through an NF-κB-dependent signalling mechanism that may occur through a pathway involving direct phosphorylation of the transcription factor p65 in the absence of IκB-α degradation.

5.5 Involvement of PKC in pro-inflammatory cytokine responses

Because crystalline silica is considered to be an oxidant-generating source as well as an inflammatory agent, it has been suggested that this large-sized silica may have the potential to activate PKC and thus modulate cellular responses [105]. To date, there are no studies done to evaluate the involvement of PKC in the cytotoxic response of silica nanoparticles. However, previous studies have reported that crystalline silica of larger sizes might induce acute injury and chronic pulmonary fibrosis (e.g. silicosis) by activation of PKC that subsequently trigger a ROS-mediated mechanism. This has been demonstrated by Lim et al [130] with alveolar macrophages using PKC inhibitors. The authors showed that crystalline silica particles activated tyrosine kinase and thus phospholipase C (PLC), which in turn triggered the production of DAG and inositol triphosphate (IP_3). While IP_3 increases intracellular Ca^{2+} levels by releasing calcium from the endoplasmatic reticulum, DAG activates PKC. This leads to the generation of ROS through the additional activation of NADPH oxidases [130]. A support for PKC in cytokine formation has been put forward by Kim et al [128], who showed that PKC activation increased the production of pro-inflammatory cytokines, indicating that PKC activation is crucial for the initial defense mechanisms in the airways. Such mechanisms may possibly be activated by silica nanoparticles, because formation of ROS and subsequent oxidative stress have been suggested to contribute to their cytotoxic potential, which is due to their greater surface to mass ratio [8, 22, 111-114].

In accordance with this, our data suggest a partial role for PKC activation in SiNP-induced cytokine responses of IL-6 and IL-8. Si10 and Si50 seemed to have different abilities to induce cytokine responses through PKC signaling pathways. Pre-treatment with a broad PKC inhibitor (GF109203X) caused a more distinct inhibition of Si10-induced IL-6 and IL-8 responses compared to Si50, which might be due to a higher potential of Si10 than Si50 to activate PKC inflammation. This needs, however, to be examined. Furthermore, a greater inhibition of IL-6 than IL-8 may also indicate that PKC is more important for the expression

of IL-6 than IL-8. The complex mechanisms responsible for this are not yet known. One explanation could be due to different promoter structures of the IL-6 and IL-8 genes. Alternatively, PKC might exert its effects on signalling mechanisms far up-stream to the transcriptional machinery.

Several studies indicate that only certain isoforms of PKC mediate signals for IL-8 release, and that different isoforms of PKC may have opposing effects on cytokine production [107]. The broad general PKC-inhibitor that have been used in our study, have the ability to reduce the activity of many different isoforms of PKC. To gain more information of the involvement of the different isoforms, more selective inhibitors have to be used. There are few studies assessing the nanoparticle-induced PKC and other mechanisms of IL-6 responses, but it has been reported that signaling mechanisms regulating IL-8 is not only restricted to this chemokine, but may also be relevant for IL-6 during an inflammatory response [81]. To date, there was not found much literature studying the involvement of PKC, including different isoforms, in SiNP-induced responses. The possibility for Si10 and Si50 to activate different isoforms of PKC might also explain the different ability of GF109203X to inhibit the cytokine responses elicited by these nanoparticles. Given that the release of IL-6 and IL-8 was reduced only to some extent in the present study after pre-treatment of this PKC-inhibitor, it might be suggested that PKC have a partial role in the SiNP-induced pro-inflammatory response.

However, Holian et al [131] demonstrated that in the presence of serum, which was required for crystalline silica-mediated cytokine responses, neither crystalline nor amorphous silica markedly increased the levels of intracellular calcium. Asbestos have been demonstrated to produce superoxide anion through the PKC signaling pathway, but contrary to asbestos, this effect was not seen for crystalline silica-exposed cells, which may indicate that it does not activate PKC. Nevertheless, the same authors demonstrated that crystalline silica might activate tyrosine kinase pathways in the presence of serum, and that crystalline silica is not dependent on elevation of intracellular calcium and PKC activation to cause signal transduction. Thus, further studies must be assessed to determine the involvement of PKC in signaling mechanisms mediating pro-inflammatory responses caused by larger silica particulates, as well as SiNP.

It has been suggested that PKC activation might induce cytokine responses of IL-6, IL-8, IL-1β and TNF-α, and inflammatory response signals through NF-κB pathways in human bronchial epithelial cells [128]. Several studies have shown that crystalline silica can cause an elevation in intracellular calcium *in vitro* [130-132] which is a known activator of NF-κB [133, 134]. It has been suggested that various PKC isoforms also might be involved in the activation of NF-κB, but it is unknown which PKC isozymes might mediate the action of micro-and nano-sized silica particles [130]. PKCζ, which is abundantly expressed in the lungs, is a positive regulator of NF-κB by regulating RelA. PKCζ is also necessary for IKK activation in the lung in response to TNF-α and IL-1β [134], which might in turn increase the production and secretion of IL-6 and IL-8. Whether, the role of PKC is mediated via a NF-kB-mediated mechanism remains to be examined. Furthermore, which PKC-isoforms are involved in the nanoparticle-induced responses should also be clarified.

Possibly PKC activation might exert its role in IL-8 induction by stimulation of AP-1 sites in the IL-8 promotor. Several studies have reported that PKCs might modulate MAPK pathways in different cell types [170-172]. Lounsbury et al [129] demonstrated that inhalation of asbestos in mice increased the production of IP_3 and DAG in respiratory epithelial cells, which may in turn trigger MAPK, activation of fos/jun response genes, and cause injury and proliferation of epithelial cells [129]. These particulates are also associated with various respiratory diseases through the release of ROS and cytokines from alveolar macrophages and epithelial cells [103]. In addition to this, Ding et al [105] demonstrated that that exposure of fractured crystalline silica to murine epidermal cells (JB6 cells) caused an activation of PKC and thus the stimulation of MAPKs p38 and ERK, as well as AP-1. Studies with PKC-inhibitors have indicated that PKCs might function as up-stream regulators for SiNP-induced MAPK/AP-1 cellular signaling, which might be involved in crystalline silica-induced lung diseases [105]. We have previously shown that MAPK, and in particular p38, has an initial role in Si50-induced IL-6 and IL-8 responses in BEAS-2B cells [82]. Furthermore, we have extended these findings by showing that both p38 and JNK has an up-stream role in both Si10- and Si50-induced IL-6 and IL-8 responses [100]. Whether PKC has an upstream role in these cytokine responses via p38-and JNK-mediated mechanism remains to be examined.

6 Conclusions

- Cell densities in culture affected the release of pro-inflammatory cytokines differently after exposure to SiNP, and seemed to be dependent on particle size. The response of Si10 was dependent on cell density, in which an intermediate cell density induced the highest release of IL-6, IL-8 and RANTES. In contrast, Si50 showed a less distinct pattern with respect to cell density as Si10. With respect to cytotoxicity, LDH release was little affected by cell density.

- Compared on a mass basis, Si10 caused higher releases of all pro-inflammatory cytokines compared to Si50. Both Si10 and Si50 induced the greatest release of IL-6 and IL-8, and to a lower extent the release of RANTES, TNF-α and IL-1β. The pattern of cytokine release differed slightly between Si10 and Si50. Si10 induced the cytokine release in the following order, IL-8 > IL-6 >> RANTES > IL-1β > TNF-α (under detection limit). For Si50, the order was IL-6 = IL-8 >> RANTES > IL-1β > TNF-α. The cytotoxicity of SiNP showed concentration-dependent release of LDH with Si10 being significantly more toxic than Si50.

- Both particle sizes of amorphous SiNP caused an increase of mRNA expression of IL-6, IL-8, IL-1β and TNF-α. Si10 caused the highest mRNA expression giving a prolonged and increasing mRNA-production towards 8 hours. At 1.5 hours, gene expression caused by Si50 (100 µg/ml) was approximately similar as observed for Si10 (25 µg/ml). However, the effect was transient for Si50. SiNP exposure caused the highest gene expression of IL-8 and with the following decreasing order IL-6, IL-1β and TNF-α.

- With respect to signaling mechanisms, IL-6 and IL-8 release triggered by Si10 and Si50 were mediated by a NF-κB-linked mechanism. Thus, both SiNPs increased the phosphorylation of p65 and degradation of IκB-α. Furthermore, pre-treatment with the chemical inhibitor PDT-p65 as well as by silencing of NF-κB p65 by siRNA markedly reduced SiNP-induced IL-6 and IL-8.

- SiNP-induced cytokine release of IL-6 and IL-8 seemed to be partially mediated through PKC-dependent mechanisms. However, the role and mechanisms of PKC in mediating pro-inflammatory responses after SiNP-exposure needs to be further examined.

7 Further studies

In this study, we have shown that the pro-inflammatory and cytotoxic potential of SiNP of 10 nm and 50 nm might be partly mediated through PKC signalling mechanisms after pre-treating BEAS-2B cells with a broad PKC-inhibitor. This inhibitor has the ability to reduce the activity of a broad range of PKC isoforms, and will thus not indicate which specific isoforms that might be involved in the SiNP-induced pro-inflammatory response. As previous studies have indicated, certain PKC isoforms might be involved in the activation of NF-κB. Further studies must therefore be assessed to clarify which isoforms are activated through this signalling mechanism after exposure to SiNP. It is also of interest to examine if PKC work in conjunction with MAPKs, and how these pathways are regulated relative to each other. Furthermore, it might also be of interest to determine if TNF-α are regulated through PKC-dependent mechanisms, and examine on a cellular level which receptors are involved in the PKC-mediated signalling pathway (e.g. scavenger receptors).

References

1. Nohynek, G.J., et al., *Safety assessment of personal care products/cosmetics and their ingredients.* Toxicol Appl Pharmacol, 2010. **243**(2): p. 239-59.
2. Warheit, D.B., *Assessing health risks of inhaled nanomaterials: development of pulmonary bioassay hazard studies.* Anal Bioanal Chem, 2010. **398**(2): p. 607-12.
3. Hougaard, K.S., et al., *Chapter 21 - Developmental toxicity of engineered nanoparticles*, in *Reproductive and Developmental Toxicology*, R.C. Gupta, Editor. 2011, Academic Press: San Diego. p. 269-290.
4. Truong, L., et al., *Differential stability of lead sulfide nanoparticles influences biological responses in embryonic zebrafish.* Arch Toxicol, 2011. **85**(7): p. 787-98.
5. Lewinski, N., V. Colvin, and R. Drezek, *Cytotoxicity of nanoparticles.* Small, 2008. **4**(1): p. 26-49.
6. Napierska, D., et al., *The nanosilica hazard: another variable entity.* Part Fibre Toxicol, 2010. **7**(1): p. 39.
7. Rahman, M., et al., *Protein-Nanoparticle Interactions : The Bio-Nano Interface.* Springer, 2013. **15**
8. Eom, H.J. and J. Choi, *SiO(2) Nanoparticles Induced Cytotoxicity by Oxidative Stress in Human Bronchial Epithelial Cell, Beas-2B.* Environ Health Toxicol, 2011. **26**: p. e2011013.
9. Fubini, B., M. Ghiazza, and I. Fenoglio, *Physico-chemical features of engineered nanoparticles relevant to their toxicity.* Nanotoxicology, 2010. **4**: p. 347-63.
10. Mulder, G.J. and L. Dencker, *Pharmaceutical Toxicology*. Pharmaceutical Press. 2006. 161-176.
11. Lu, X., et al., *Right or left: the role of nanoparticles in pulmonary diseases.* Int J Mol Sci, 2014. **15**(10): p. 17577-600.
12. Landsiedel, R., et al., *Application of short-term inhalation studies to assess the inhalation toxicity of nanomaterials.* Part Fibre Toxicol, 2014. **11**: p. 16.
13. Manke, A., S. Luanpitpong, and Y. Rojanasakul, *Potential Occupational Risks Associated with Pulmonary Toxicity of Carbon Nanotubes.* Occup Med Health Aff, 2014. **2**.
14. Chang, L.Y., et al., *8.04 - Alveolar Epithelium in Lung Toxicology*.* Comprehensive Toxicology (Second Edition), 2010: p. 59-91.
15. Mossman, B.T., et al., *Mechanisms of action of inhaled fibers, particles and nanoparticles in lung and cardiovascular diseases.* Part Fibre Toxicol, 2007. **4**: p. 4.
16. Muhlfeld, C., P. Gehr, and B. Rothen-Rutishauser, *Translocation and cellular entering mechanisms of nanoparticles in the respiratory tract.* Swiss Med Wkly, 2008. **138**(27-28): p. 387-91.
17. Gebel, T., et al., *Manufactured nanomaterials: categorization and approaches to hazard assessment.* Arch Toxicol, 2014. **88**(12): p. 2191-211.
18. Nel, A., et al., *Toxic potential of materials at the nanolevel.* Science, 2006. **311**(5761): p. 622-7.
19. Ferreira, A.J., J. Cemlyn-Jones, and C. Robalo Cordeiro, *Nanoparticles, nanotechnology and pulmonary nanotoxicology.* Rev Port Pneumol, 2013. **19**(1): p. 28-37.
20. Yildirimer, L., et al., *Toxicology and clinical potential of nanoparticles.* Nano Today, 2011. **6**(6): p. 585-607.

21. Brook, R.D., et al., *Air pollution and cardiovascular disease: a statement for healthcare professionals from the Expert Panel on Population and Prevention Science of the American Heart Association.* Circulation, 2004. **109**(21): p. 2655-71.
22. Miethling-Graff, R., et al., *Exposure to silver nanoparticles induces size- and dose-dependent oxidative stress and cytotoxicity in human colon carcinoma cells.* Toxicol In Vitro, 2014. **28**(7): p. 1280-9.
23. Oberdorster, G., A. Elder, and A. Rinderknecht, *Nanoparticles and the brain: cause for concern?* J Nanosci Nanotechnol, 2009. **9**(8): p. 4996-5007.
24. Oberdorster, G., et al., *Association of particulate air pollution and acute mortality: involvement of ultrafine particles?* Inhal Toxicol, 1995. **7**(1): p. 111-24.
25. Gosens, I., et al., *Impact of agglomeration state of nano- and submicron sized gold particles on pulmonary inflammation.* Part Fibre Toxicol, 2010. **7**(1): p. 37.
26. Gatoo, M.A., et al., *Physicochemical properties of nanomaterials: implication in associated toxic manifestations.* 2014. **2014**: p. 498420.
27. Oberdorster, G., *Pulmonary effects of inhaled ultrafine particles.* Int Arch Occup Environ Health, 2001. **74**(1): p. 1-8.
28. Andujar, P., et al., *Respiratory effects of manufactured nanoparticles.* Rev Mal Respir, 2011. **28**(8): p. e66-75.
29. Gustafsson, Å., *Nanomaterials: respiratory and immunological effects following inhalation of engineered nanoparticles.* 2014.
30. Gardner, D.E., A.W. Hayes, and J.A. Thomas, *Toxicology of the Lung*. 4. ed. CRC Press. 2006.
31. Schleh, C. and J.M. Hohlfeld, *Interaction of nanoparticles with the pulmonary surfactant system.* Inhal Toxicol, 2009. **21 Suppl 1**: p. 97-103.
32. Hillery, A.M., A.W. Lloyd, and J. Swarbrick, *Drug Delivery and Targeting: For Pharmacists and Pharmaceutical Scientists* Taylor & Francis, 2001.
33. Velden, V.H. and H.F. Versnel, *Bronchial epithelium: morphology, function and pathophysiology in asthma.* Eur Cytokine Netw, 1998. **9**(4): p. 585-97.
34. Sand, O., et al., *Menneskets fysiologi*. 1. ed. Gyldendal Norsk Forlag AS. 2001.
35. Gardner, D.E., J.D. Crapo, and R.O. McClellan, *Toxicology of the Lung*. 3rd ed. CRC Press. 2000.
36. Oberdorster, G., E. Oberdorster, and J. Oberdorster, *Nanotoxicology: an emerging discipline evolving from studies of ultrafine particles.* Environ Health Perspect, 2005. **113**(7): p. 823-39.
37. Watkins III, J.B.W. and C.D. Klaasen, *Casarett & Doull's Essentials of Toxicology*. 2 ed. 2010. 203-214.
38. Daigle, C.C., et al., *Ultrafine particle deposition in humans during rest and exercise.* Inhal Toxicol, 2003. **15**(6): p. 539-52.
39. Aulton, M.E., *Aulton's pharmaceutics : the design and manufacture of medicines*. 3rd ed. ed. 2007, Edinburgh: Churchill Livingstone.
40. Londahl, J., et al., *Measurement techniques for respiratory tract deposition of airborne nanoparticles: a critical review.* J Aerosol Med Pulm Drug Deliv, 2014. **27**(4): p. 229-54.
41. Asgharian, B. and O.T. Price, *Deposition of ultrafine (nano) particles in the human lung.* Inhal Toxicol, 2007. **19**(13): p. 1045-54.
42. Braakhuis, H.M., et al., *Particle size dependent deposition and pulmonary inflammation after short-term inhalation of silver nanoparticles.* Part Fibre Toxicol, 2014. **11**(1): p. 49.

43. Skuland, T., *Silikananopartikler og inflammasjon: En mekanistisk studie av silikananopartikler og deres effekt på cytokinproduksjon og cytokinutskillelse i BEAS-2B celler*. Høgskolen i Telemark, 2012.
44. Geiser, M. and W.G. Kreyling, *Deposition and biokinetics of inhaled nanoparticles.* Part Fibre Toxicol, 2010. **7**: p. 2.
45. Horie, M. and Y. Morimoto, *[Hazard assessment of manufactured nanoparticles: association of in vitro and in vivo examinations]*. J uoeh, 2012. **34**(1): p. 57-64.
46. Oberdorster, G., et al., *Translocation of inhaled ultrafine particles to the brain.* Inhal Toxicol, 2004. **16**(6-7): p. 437-45.
47. Oberdorster, G., J. Ferin, and B.E. Lehnert, *Correlation between particle size, in vivo particle persistence, and lung injury.* Environ Health Perspect, 1994. **102 Suppl 5**: p. 173-9.
48. Schleh, C., et al., *The effect of titanium dioxide nanoparticles on pulmonary surfactant function and ultrastructure.* Respir Res, 2009. **10**: p. 90.
49. Hu, G., et al., *Physicochemical properties of nanoparticles regulate translocation across pulmonary surfactant monolayer and formation of lipoprotein corona.* ACS Nano, 2013. **7**(12): p. 10525-33.
50. Ruge, C.A., et al., *The interplay of lung surfactant proteins and lipids assimilates the macrophage clearance of nanoparticles.* PLoS One, 2012. **7**(7): p. e40775.
51. Dwivedi, M.V., et al., *Size influences the effect of hydrophobic nanoparticles on lung surfactant model systems.* Biophys J, 2014. **106**(1): p. 289-98.
52. Hidalgo, A., A. Cruz, and J. Perez-Gil, *Barrier or carrier? Pulmonary surfactant and drug delivery.* Eur J Pharm Biopharm, 2015.
53. Kasper, J.Y., et al., *Pulmonary surfactant augments cytotoxicity of silica nanoparticles: Studies on an in vitro air-blood barrier model.* Beilstein J Nanotechnol, 2015. **6**: p. 517-28.
54. Muhlfeld, C., et al., *Interactions of nanoparticles with pulmonary structures and cellular responses.* Am J Physiol Lung Cell Mol Physiol, 2008. **294**(5): p. L817-29.
55. Napierska, D., et al., *Size-dependent cytotoxicity of monodisperse silica nanoparticles in human endothelial cells.* Small, 2009. **5**(7): p. 846-53.
56. Totlandsdal, A.I., M. Refsnes, and M. Lag, *Mechanisms involved in ultrafine carbon black-induced release of IL-6 from primary rat epithelial lung cells.* Toxicol In Vitro, 2010. **24**(1): p. 10-20.
57. Nemmar, A., et al., *Passage of inhaled particles into the blood circulation in humans.* Circulation, 2002. **105**(4): p. 411-4.
58. Mills, N.L., et al., *Do inhaled carbon nanoparticles translocate directly into the circulation in humans?* Am J Respir Crit Care Med, 2006. **173**(4): p. 426-31.
59. Brown, J.S., K.L. Zeman, and W.D. Bennett, *Ultrafine particle deposition and clearance in the healthy and obstructed lung.* Am J Respir Crit Care Med, 2002. **166**(9): p. 1240-7.
60. Wiebert, P., et al., *Negligible clearance of ultrafine particles retained in healthy and affected human lungs.* Eur Respir J, 2006. **28**(2): p. 286-90.
61. Kreyling, W.G., et al., *Translocation of ultrafine insoluble iridium particles from lung epithelium to extrapulmonary organs is size dependent but very low.* J Toxicol Environ Health A, 2002. **65**(20): p. 1513-30.
62. Schmid, O., et al., *Dosimetry and toxicology of inhaled ultrafine particles.* Biomarkers, 2009. **14 Suppl 1**: p. 67-73.
63. Geiser, M., *Update on macrophage clearance of inhaled micro- and nanoparticles.* J Aerosol Med Pulm Drug Deliv, 2010. **23**(4): p. 207-17.
64. Weiss, U., *Inflammation.* Nature, 2008. **454**(7203): p. 427-427.

65. *Inflammation.* 2012.
66. Byrne, J.D. and J.A. Baugh, *The significance of nanoparticles in particle-induced pulmonary fibrosis.* Mcgill J Med, 2008. **11**(1): p. 43-50.
67. Bonner, J.C., *Lung fibrotic responses to particle exposure.* Toxicol Pathol, 2007. **35**(1): p. 148-53.
68. Haschek, W.M. and H. Witschi, *Pulmonary fibrosis--a possible mechanism.* Toxicol Appl Pharmacol, 1979. **51**(3): p. 475-87.
69. Kusaka, T., et al., *Effect of silica particle size on macrophage inflammatory responses.* PLoS One, 2014. **9**(3): p. e92634.
70. Finkelstein, M.M., *Silica, silicosis, and lung cancer: a risk assessment.* Am J Ind Med, 2000. **38**(1): p. 8-18.
71. Levine, T.B. and A.B. Levine, *Inflammation.* 2012: p. 192-227.
72. Becher, R., et al., *Rat lung inflammatory responses after in vivo and in vitro exposure to various stone particles.* Inhal Toxicol, 2001. **13**(9): p. 789-805.
73. Fettelschoss, A., et al., *Inflammasome activation and IL-1[beta] target IL-1[alpha] for secretion as opposed to surface expression.(IMMUNOLOGY)(Author abstract)(Report).* Proceedings of the National Academy of Sciences of the United States, 2011. **108**(44): p. 18055.
74. Yazdi, A.S., et al., *Nanoparticles activate the NLR pyrin domain containing 3 (Nlrp3) inflammasome and cause pulmonary inflammation through release of IL-1alpha and IL-1beta.* Proc Natl Acad Sci U S A, 2010. **107**(45): p. 19449-54.
75. Herseth, J.I., et al., *Role of IL-1 beta and COX2 in silica-induced IL-6 release and loss of pneumocytes in co-cultures.* Toxicol In Vitro, 2009. **23**(7): p. 1342-53.
76. Dinarello, C.A., *Proinflammatory cytokines.* Chest, 2000. **118**(2): p. 503-8.
77. Herseth, J.I., et al., *IL-1beta differently involved in IL-8 and FGF-2 release in crystalline silica-treated lung cell co-cultures.* Part Fibre Toxicol, 2008. **5**: p. 16.
78. Holtmann, H., et al., *Induction of interleukin-8 synthesis integrates effects on transcription and mRNA degradation from at least three different cytokine- or stress-activated signal transduction pathways.* Mol Cell Biol, 1999. **19**(10): p. 6742-53.
79. Herseth, J., et al., *IL-1beta as a determinant in silica-induced cytokine responses in monocyte-endothelial cell co-cultures.* Hum Exp Toxicol, 2008. **27**(5): p. 387-99.
80. Gualtieri, M., et al., *Differences in cytotoxicity versus pro-inflammatory potency of different PM fractions in human epithelial lung cells.* Toxicol In Vitro, 2010. **24**(1): p. 29-39.
81. Hoffmann, E., et al., *Multiple control of interleukin-8 gene expression.* J Leukoc Biol, 2002. **72**(5): p. 847-55.
82. Skuland, T., et al., *Silica nanoparticles induce cytokine responses in lung epithelial cells through activation of a p38/TACE/TGF-alpha/EGFR-pathway and NF-kappaBeta signalling.* Toxicol Appl Pharmacol, 2014. **279**(1): p. 76-86.
83. Matsukura, S., et al., *Expression of IL-6, IL-8, and RANTES on human bronchial epithelial cells, NCI-H292, induced by influenza virus A.* J Allergy Clin Immunol, 1996. **98**(6 Pt 1): p. 1080-7.
84. Wilson, D., et al., *Nuclear factor-kappa B is not involved in titanium dioxide-induced inflammation.* J uoeh, 2012. **34**(2): p. 183-91.
85. Kaminska, B., *MAPK signalling pathways as molecular targets for anti-inflammatory therapy--from molecular mechanisms to therapeutic benefits.* Biochim Biophys Acta, 2005. **1754**(1-2): p. 253-62.
86. Ovrevik, J., et al., *p38 and Src-ERK1/2 pathways regulate crystalline silica-induced chemokine release in pulmonary epithelial cells.* Toxicol Sci, 2004. **81**(2): p. 480-90.

87. Lag, M., et al., *Role of mitogen activated protein kinases and protein kinase C in cadmium-induced apoptosis of primary epithelial lung cells.* Toxicology, 2005. **211**(3): p. 253-64.
88. May, M.J., *NF-kappa B : Methods in Molecular Biology* Springer Science, 2015. **1280**.
89. Collins, P.E., C. O'Carroll, and R.J. Carmody, *Measurement of NF-kappaB Transcriptional Activity and Identification of NF-kappaB cis-Regulatory Elements Using Luciferase Assays.* Methods Mol Biol, 2015. **1280**: p. 25-43.
90. Colleran, A., P.E. Collins, and R.J. Carmody, *Assessing Sites of NF-kappaB DNA Binding Using Chromatin Immunoprecipitation.* Methods Mol Biol, 2015. **1280**: p. 47-59.
91. Starokadomskyy, P. and E. Burstein, *Detection of IkappaB Degradation Dynamics and IkappaB-alpha Ubiquitination.* Methods Mol Biol, 2015. **1280**: p. 15-24.
92. Gilmore, T.D., *Introduction to NF-kappaB: players, pathways, perspectives.* Oncogene, 2006. **25**(51): p. 6680-4.
93. Wessel, A.W. and E.P. Hanson, *A Method for the Quantitative Analysis of Stimulation-Induced Nuclear Translocation of the p65 Subunit of NF-kappaB from Patient-Derived Dermal Fibroblasts.* Methods Mol Biol, 2015. **1280**: p. 413-26.
94. Ramaswami, S. and M.S. Hayden, *Electrophoretic Mobility Shift Assay Analysis of NF-kappaB DNA Binding.* Methods Mol Biol, 2015. **1280**: p. 3-13.
95. Collins, P.E., A. Colleran, and R.J. Carmody, *Control of NF-kappaB Subunits by Ubiquitination.* Methods Mol Biol, 2015. **1280**: p. 355-70.
96. Mihalas, A.B. and M.K. Meffert, *IKK Kinase Assay for Assessment of Canonical NF-kappaB Activation in Neurons.* Methods Mol Biol, 2015. **1280**: p. 61-74.
97. Jiang, C. and X. Lin, *Analysis of Epidermal Growth Factor-Induced NF-kappaB Signaling.* Methods Mol Biol, 2015. **1280**: p. 75-102.
98. Shaked, H., M. Guma, and M. Karin, *Analysis of NF-kappaB Activation in Mouse Intestinal Epithelial Cells.* Methods Mol Biol, 2015. **1280**: p. 593-606.
99. Ovrevik, J., et al., *TACE/TGF-alpha/EGFR regulates CXCL8 in bronchial epithelial cells exposed to particulate matter components.* Eur Respir J, 2011. **38**(5): p. 1189-99.
100. Pham, H.L.T., *Pro-inflammatory potential of different sizes of silica nanoparticles in bronchial epithelial lung cells (BEAS-2B).* University of Oslo, 2014.
101. Zhang, L.L., et al., *The protein kinase C (PKC) inhibitors combined with chemotherapy in the treatment of advanced non-small cell lung cancer: meta-analysis of randomized controlled trials.* Clin Transl Oncol, 2014.
102. Boyer, P.D. and E.G. Krebs, *The enzymes : Volume 17 : Control by phosphorylation*. 1986, Academic Press: Orlando.
103. Shukla, A., et al., *Asbestos-induced peribronchiolar cell proliferation and cytokine production are attenuated in lungs of protein kinase C-delta knockout mice.* Am J Pathol, 2007. **170**(1): p. 140-51.
104. Tan, S.L. and P.J. Parker, *Emerging and diverse roles of protein kinase C in immune cell signalling.* Biochem J, 2003. **376**(Pt 3): p. 545-52.
105. Ding, M., et al., *Involvement of protein kinase C in crystalline silica-induced activation of the MAP kinase and AP-1 pathway.* Am J Physiol Lung Cell Mol Physiol, 2006. **290**(2): p. L291-7.
106. Rang, H.P., et al., *Rang and Dale's Pharmacology*. 6. ed. Churchill Livingstone Elsevier. 2007.
107. Refsnes, M., et al., *Mechanisms in fluoride-induced interleukin-8 synthesis in human lung epithelial cells.* Toxicology, 2001. **167**(2): p. 145-58.

108. Stone, V., H. Johnston, and M.J. Clift, *Air pollution, ultrafine and nanoparticle toxicology: cellular and molecular interactions.* IEEE Trans Nanobioscience, 2007. **6**(4): p. 331-40.
109. Park, E.J., et al., *Oxidative stress and apoptosis induced by titanium dioxide nanoparticles in cultured BEAS-2B cells.* Toxicol Lett, 2008. **180**(3): p. 222-9.
110. Rahman, I., S.K. Biswas, and A. Kode, *Oxidant and antioxidant balance in the airways and airway diseases.* Eur J Pharmacol, 2006. **533**(1-3): p. 222-39.
111. Soto, K., K.M. Garza, and L.E. Murr, *Cytotoxic effects of aggregated nanomaterials.* Acta Biomater, 2007. **3**(3): p. 351-8.
112. Chattopadhyay, S., et al., *Toxicity of cobalt oxide nanoparticles to normal cells; an in vitro and in vivo study.* Chem Biol Interact, 2015. **226**: p. 58-71.
113. Nishanth, R.P., et al., *Inflammatory responses of RAW 264.7 macrophages upon exposure to nanoparticles: role of ROS-NFkappaB signaling pathway.* Nanotoxicology, 2011. **5**(4): p. 502-16.
114. Capasso, L., M. Camatini, and M. Gualtieri, *Nickel oxide nanoparticles induce inflammation and genotoxic effect in lung epithelial cells.* Toxicol Lett, 2014. **226**(1): p. 28-34.
115. Hussain, S., et al., *Oxidative stress and proinflammatory effects of carbon black and titanium dioxide nanoparticles: role of particle surface area and internalized amount.* Toxicology, 2009. **260**(1-3): p. 142-9.
116. Foldbjerg, R., D.A. Dang, and H. Autrup, *Cytotoxicity and genotoxicity of silver nanoparticles in the human lung cancer cell line, A549.* Arch Toxicol, 2011. **85**(7): p. 743-50.
117. Perkins, T.N., et al., *Differences in gene expression and cytokine production by crystalline vs. amorphous silica in human lung epithelial cells.* Part Fibre Toxicol, 2012. **9**(1): p. 6.
118. Cho, W.S., et al., *Inflammatory mediators induced by intratracheal instillation of ultrafine amorphous silica particles.* Toxicol Lett, 2007. **175**(1-3): p. 24-33.
119. Sandberg, W.J., et al., *Comparison of non-crystalline silica nanoparticles in IL-1beta release from macrophages.* Part Fibre Toxicol, 2012. **9**: p. 32.
120. Eom, H.J. and J. Choi, *Oxidative stress of silica nanoparticles in human bronchial epithelial cell, Beas-2B.* Toxicol In Vitro, 2009. **23**(7): p. 1326-32.
121. Wottrich, R., S. Diabate, and H.F. Krug, *Biological effects of ultrafine model particles in human macrophages and epithelial cells in mono- and co-culture.* Int J Hyg Environ Health, 2004. **207**(4): p. 353-61.
122. Lin, W., et al., *In vitro toxicity of silica nanoparticles in human lung cancer cells.* Toxicol Appl Pharmacol, 2006. **217**(3): p. 252-9.
123. Barrett, E.G., et al., *Silica-induced chemokine expression in alveolar type II cells is mediated by TNF-alpha.* Am J Physiol, 1998. **275**(6 Pt 1): p. L1110-9.
124. Du, Z., et al., *Cardiovascular toxicity of different sizes amorphous silica nanoparticles in rats after intratracheal instillation.* Cardiovasc Toxicol, 2013. **13**(3): p. 194-207.
125. Skuland, T., et al., *Role of size and surface area for pro-inflammatory responses to silica nanoparticles in epithelial lung cells: importance of exposure conditions.* Toxicol In Vitro, 2014. **28**(2): p. 146-55.
126. Chen, M. and A. von Mikecz, *Formation of nucleoplasmic protein aggregates impairs nuclear function in response to SiO2 nanoparticles.* Exp Cell Res, 2005. **305**(1): p. 51-62.
127. Hornung, V., et al., *Silica crystals and aluminum salts activate the NALP3 inflammasome through phagosomal destabilization.* Nat Immunol, 2008. **9**(8): p. 847-56.

128. Kim, H., et al., *PKC activation induces inflammatory response and cell death in human bronchial epithelial cells.* PLoS One, 2013. **8**(5): p. e64182.
129. Lounsbury, K.M., et al., *Increased localization and substrate activation of protein kinase C delta in lung epithelial cells following exposure to asbestos.* Am J Pathol, 2002. **160**(6): p. 1991-2000.
130. Lim, Y., et al., *Involvement of protein kinase C, phospholipase C, and protein tyrosine kinase pathways in oxygen radical generation by asbestos-stimulated alveolar macrophage.* Environ Health Perspect, 1997. **105 Suppl 5**: p. 1325-7.
131. Holian, A., K. Kelley, and R.F. Hamilton, Jr., *Mechanisms associated with human alveolar macrophage stimulation by particulates.* Environ Health Perspect, 1994. **102 Suppl 10**: p. 69-74.
132. Horie, M., et al., *Comparison of acute oxidative stress on rat lung induced by nano and fine-scale, soluble and insoluble metal oxide particles: NiO and TiO2.* Inhal Toxicol, 2012. **24**(7): p. 391-400.
133. Snow, W.M., et al., *Roles for NF-kappaB and gene targets of NF-kappaB in synaptic plasticity, memory, and navigation.* Mol Neurobiol, 2014. **49**(2): p. 757-70.
134. Diaz-Meco, M.T. and J. Moscat, *The atypical PKCs in inflammation: NF-kappaB and beyond.* Immunol Rev, 2012. **246**(1): p. 154-67.
135. AAT Bioquest®, I., *Product Technical Information Sheet: Amplite™ Colorimetric D-Lactate Dehydrogenase Assay Kit.* 2013.
136. Bihari, P., et al., *Optimized dispersion of nanoparticles for biological in vitro and in vivo studies.* Part Fibre Toxicol, 2008. **5**: p. 14.
137. BioSite, N., *NF-kB p65 (Ser276) Inhibitory Peptide Set Functions as a p65 decoy through phosphorylation on the Ser276 site on the peptide.* 2015.
138. Veranth, J.M., et al., *Effects of cell type and culture media on Interleukin-6 secretion in response to environmental particles.* Toxicol In Vitro, 2008. **22**(2): p. 498-509.
139. Garcia-Canton, C., et al., *Metabolic characterization of cell systems used in in vitro toxicology testing: lung cell system BEAS-2B as a working example.* Toxicol In Vitro, 2013. **27**(6): p. 1719-27.
140. Daly-Burns, B., et al., *A conditionally immortalized cell line model for the study of human prostatic epithelial cell differentiation.* Differentiation, 2007. **75**(1): p. 35-48.
141. Stacey, G., *Primary Cell Cultures and Immortal Cell Lines*, in *eLS*. 2001, John Wiley & Sons, Ltd.
142. Unger, R.E., et al., *In vitro expression of the endothelial phenotype: comparative study of primary isolated cells and cell lines, including the novel cell line HPMEC-ST1.6R.* Microvasc Res, 2002. **64**(3): p. 384-97.
143. Miller, L.A. and E.C. Butcher, *Human airway epithelial monolayers promote selective transmigration of memory T cells: a transepithelial model of lymphocyte migration into the airways.* Am J Respir Cell Mol Biol, 1998. **19**(6): p. 892-900.
144. Ekstrand-Hammarström, B., et al., *Vitamin E down-modulates mitogen-activated protein kinases, nuclear factor-κB and inflammatory responses in lung epithelial cells.* Clinical & Experimental Immunology, 2007. **147**(2): p. 359-369.
145. Ekstrand-Hammarstrom, B., et al., *Human primary bronchial epithelial cells respond differently to titanium dioxide nanoparticles than the lung epithelial cell lines A549 and BEAS-2B.* Nanotoxicology, 2012. **6**(6): p. 623-34.
146. Pintado, C., et al., *Regional difference in inflammatory response to LPS-injection in the brain: role of microglia cell density.* J Neuroimmunol, 2011. **238**(1-2): p. 44-51.
147. Olgart, C. and N. Frossard, *Human lung fibroblasts secrete nerve growth factor: effect of inflammatory cytokines and glucocorticoids.* Eur Respir J, 2001. **18**(1): p. 115-21.

148. Romer, P.S., et al., *Preculture of PBMCs at high cell density increases sensitivity of T-cell responses, revealing cytokine release by CD28 superagonist TGN1412.* Blood, 2011. **118**(26): p. 6772-82.
149. Bhalla, D.K., et al., *Cigarette smoke, inflammation, and lung injury: a mechanistic perspective.* J Toxicol Environ Health B Crit Rev, 2009. **12**(1): p. 45-64.
150. Batt, D.B. and T.M. Roberts, *Cell density modulates protein-tyrosine phosphorylation.* J Biol Chem, 1998. **273**(6): p. 3408-14.
151. Wang, H., et al., *Effect of cigarette smoke on fibroblast-mediated gel contraction is dependent on cell density.* Am J Physiol Lung Cell Mol Physiol, 2003. **284**(1): p. L205-13.
152. Okoturo-Evans, O., et al., *Elucidation of toxicity pathways in lung epithelial cells induced by silicon dioxide nanoparticles.* PLoS One, 2013. **8**(9): p. e72363.
153. Gualtieri, M., et al., *Importance of agglomeration state and exposure conditions for uptake and pro-inflammatory responses to amorphous silica nanoparticles in bronchial epithelial cells.* Nanotoxicology, 2012. **6**(7): p. 700-12.
154. Park, E.J. and K. Park, *Oxidative stress and pro-inflammatory responses induced by silica nanoparticles in vivo and in vitro.* Toxicol Lett, 2009. **184**(1): p. 18-25.
155. Braakhuis, H.M., et al., *Identification of the appropriate dose metric for pulmonary inflammation of silver nanoparticles in an inhalation toxicity study.* Nanotoxicology, 2015: p. 1-11.
156. Warheit, D.B., K.L. Reed, and C.M. Sayes, *A role for nanoparticle surface reactivity in facilitating pulmonary toxicity and development of a base set of hazard assays as a component of nanoparticle risk management.* Inhal Toxicol, 2009. **21 Suppl 1**: p. 61-7.
157. Warheit, D.B., et al., *Health effects related to nanoparticle exposures: environmental, health and safety considerations for assessing hazards and risks.* Pharmacol Ther, 2008. **120**(1): p. 35-42.
158. Waters, K.M., et al., *Macrophage responses to silica nanoparticles are highly conserved across particle sizes.* Toxicol Sci, 2009. **107**(2): p. 553-69.
159. Peeters, P.M., et al., *Silica induces NLRP3 inflammasome activation in human lung epithelial cells.* Part Fibre Toxicol, 2013. **10**: p. 3.
160. Latz, E., *The inflammasomes: mechanisms of activation and function.* Curr Opin Immunol, 2010. **22**(1): p. 28-33.
161. Hirota, J.A., et al., *The airway epithelium nucleotide-binding domain and leucine-rich repeat protein 3 inflammasome is activated by urban particulate matter.* J Allergy Clin Immunol, 2012. **129**(4): p. 1116-25.e6.
162. Rusznak, C., et al., *Effect of cigarette smoke on the permeability and IL-1beta and sICAM-1 release from cultured human bronchial epithelial cells of never-smokers, smokers, and patients with chronic obstructive pulmonary disease.* Am J Respir Cell Mol Biol, 2000. **23**(4): p. 530-6.
163. Silbajoris, R., et al., *Ambient particulate matter induces interleukin-8 expression through an alternative NF-kappaB (nuclear factor-kappa B) mechanism in human airway epithelial cells.* Environ Health Perspect, 2011. **119**(10): p. 1379-83.
164. Refsnes, M., et al., *Differential NF-kappaB and MAPK activation underlies fluoride- and TPA-mediated CXCL8 (IL-8) induction in lung epithelial cells.* J Inflamm Res, 2014. **7**: p. 169-85.
165. Neumann, M. and M. Naumann, *Beyond IkappaBs: alternative regulation of NF-kappaB activity.* Faseb j, 2007. **21**(11): p. 2642-54.
166. Doerre, S. and R.B. Corley, *Constitutive nuclear translocation of NF-kappa B in B cells in the absence of I kappa B degradation.* J Immunol, 1999. **163**(1): p. 269-77.

167. Bohuslav, J., et al., *p53 induces NF-kappaB activation by an IkappaB kinase-independent mechanism involving phosphorylation of p65 by ribosomal S6 kinase 1.* J Biol Chem, 2004. **279**(25): p. 26115-25.
168. Simeonova, P.P. and M.I. Luster, *Asbestos induction of nuclear transcription factors and interleukin 8 gene regulation.* Am J Respir Cell Mol Biol, 1996. **15**(6): p. 787-95.
169. Akira, S., et al., *A nuclear factor for IL-6 expression (NF-IL6) is a member of a C/EBP family.* Embo j, 1990. **9**(6): p. 1897-906.
170. Monick, M., et al., *Respiratory syncytial virus infection results in activation of multiple protein kinase C isoforms leading to activation of mitogen-activated protein kinase.* J Immunol, 2001. **166**(4): p. 2681-7.
171. Sajan, M.P., et al., *Protein kinase C-zeta and phosphoinositide-dependent protein kinase-1 are required for insulin-induced activation of ERK in rat adipocytes.* J Biol Chem, 1999. **274**(43): p. 30495-500.
172. Abe, M.K., et al., *Hydrogen peroxide activates extracellular signal-regulated kinase via protein kinase C, Raf-1, and MEK1.* Am J Respir Cell Mol Biol, 1998. **18**(4): p. 562-9.

Appendix 1: Materials used in the study

Particles	**Manufacturer**
Amourphous silica nanoparticle, 10 nm	Kisker Biotech GmbH & Co, KG, Steinfurt Germany
Amourphous silica nanoparticle, 50 nm	Kisker Biotech GmbH & Co, KG, Steinfurt Germany

Kits	**Manufacturer**
IL-6 Cytoset	Invitrogen, Life Technologies Ltd, UK
IL-8 Cytoset	Invitrogen, Life Technologies Ltd, UK
CCL5/RANTES Duoset	R&D Systems, Minneapolis, 55413 USA
Cytotoxicity Detection Kit (LDH)	Roche Diagnostics Deutschland GmbH 68305 Mannheim, Germany
DC-Protein assay	Bio-Rad Laboratories, Inc., Hercules, CA 94547 USA
SuperSignal WestDura	Thermo Fisher Scientific Inc, Rockford, USA
Re-blot plus	CHEMICON, Millipore, Billerica, MA, USA
PerfectPure RNA Cultured Cell Kit-50	5PRIME GmbH, 40724 Hilden, Germany
High Capacity cDNA Archive Kit	Applied Biosystems, Life Technologies Corporation, California, USA

Antibodies	**Manufacturer**
Anti-p-p65 (1/1000 in 5% BSA)	Cell Signaling Technology, Inc., Danvers, MA 01923, USA

Anti-p65 (1/1000 in 5 % BSA)	Cell Signaling Technology, Inc., Danvers, MA 01923, USA
Anti-IκB-α (1/1000 in 5 % BSA)	Cell Signaling Technology, Inc., Danvers, MA 01923, USA
Anti-β-Actin (1/200 000 in 3 % dry milk)	Sigma-Aldrich, St. Louis, MO, USA
Polyclonal Rabbit Anti-Mouse Immunoglobulins/HRP (1/5000 in 3 % dry milk)	DAKO, Oslo, Norway
Polyclonal Goat Anti-Rabbit Immunoglobulins/HRP (1/2000 in 3 % dry milk)	DAKO, Oslo, Norway

siRNA	**Manufacturer**
SignalSilence NF-κBp65	Cell Signaling Technology, Inc., Danvers, MA 01923, USA
SignalSilence Control siRNA	Cell Signaling, Technology, Inc., Danvers, MA 01923, USA

Chemical inhibitors	**Manufacturer**
GF109203X	Merck Millipore Corporation, Billerica, MA, USA
PDT-p65	Nordic BioSite AB, 183 62 Täby, Sweden

Chemicals, reagents and solutions	**Manufacturer**
LHC-9 medium	Gibco, Life Technologies, Grand Island, NY 14072, USA
DMEM/F12 medium	Gibco, Life Technologies, Grand Island, NY 14072, USA
BSA (albumin, bovine)	Sigma Aldrich, St. Louis, MO, USA

H_2O_2	Merck, Whitehouse Station, NJ, USA
H_2SO_4	
3,3',5,5'-Tetramethylbenzidin (TMB)	Merck, Whitehouse Station, NJ, USA
Leupeptin	Sigma Aldrich, St. Louis, MO, USA
Pepstatin A	Sigma Aldrich, St. Louis, MO, USA
Aprotenin	Sigma Aldrich, St. Louis, MO, USA
PMFS	Sigma Aldrich, St. Louis, MO, USA
Glycerol	Merck, Whitehouse Station, NJ, USA
Sodium dodecyl sulphate (SDS)	Fluka, Sigma-Aldrich, St. Louis, MO, USA
β-mercaptoethanol	Sigma Aldrich, St. Louis, MO, USA
Ammonium persulfate (APS)	Bio-Rad Laboratories, Inc., Hercules, CA 94547 USA
TEMED	Bio-Rad Laboratories, Inc., Hercules, CA 94547 USA
Acrylamide-Bis (37 % solution)	Bio-Rad Laboratories, Inc., Hercules, CA 94547 USA
Sodium chloride	Merck, Whitehouse Station, NJ, USA
Propanol	
Precision Plus Protein Dual Xtra Standards	Bio-Rad Laboratories, Inc., Hercules, CA 94547 USA
ProSieve Color Protein Markers	Lonza Rockland, Inc., Maine, 04841 USA
Trizma hydrochloride	Sigma Aldrich, St. Louis, MO, USA
EDTA	Sigma Aldrich, St. Louis, MO, USA
EGTA	Sigma Aldrich, St. Louis, MO, USA
Sodium pyrophosfat	Sigma Aldrich, St. Louis, MO, USA
Sodium ortovanadat	Sigma Aldrich, St. Louis, MO, USA
Sodium fluoride	Riedel-de Haën, Sigma-Aldrich, St. Louis, MO, USA
Triton-X 100	Sigma Aldrich, St. Louis, MO, USA
β-glycerol phosphate	

Trizma Base	Sigma Aldrich, St. Louis, MO, USA
Albumin bovine serum (BSA)	Sigma Aldrich, St. Louis, MO, USA
Skim milk powder	Fluka, Sigma-Aldrich, St. Louis, MO, USA
Methanol	POCH S.A, Sowinskiego 11, Poland
Tween-20	Sigma Aldrich, St. Louis, MO, USA
1 % bromophenol blue/ Tryptan blue Dye 0,4 %	Bio-Rad Laboratories, Inc., Hercules, CA 94547 USA
30 % acrylamide mix	Bio-Rad Laboratories, Inc., Hercules, CA 94547 USA
HiPerfect	Qiagen GmbH, Hilden, Tyskland

Primers and reagents for Real Time PCR	**Manufacturer**
IL-6 primer/probe	Applied Biosystems, Life Technologies Corporation, California USA
IL-8 primer/probe	Applied Biosystems, Life Technologies Corporation, California USA
TNF-α primer/probe	Applied Biosystems, Life Technologies Corporation, California USA
IL-1β primer/probe	Applied Biosystems, Life Technologies Corporation, California USA
RNase free water	Gibco, Life Technologies, Grand Island, NY 14072, USA
Universal PCR mastermix (Taqman®)	Applied Biosystems, Life Technologies Corporation, California USA

Instruments	**Manufacturer**
Sunrise Absorbance Reader	TECAN Austria GmbH, 5082 Grödig, Austria
Ultrasonic sonicator	Sonics & Materials, Inc. Newtown, USA
Chemi-Doc	Bio-Rad Laboratories, Inc., Hercules, CA 94547 USA

Bioruptor Plus	Diagenode, Denville, NJ, 07834 USA
NanoDrop2000	Thermo Fisher Scientific Inc., Rockford, USA
7500 Fast System Real Time PCR machine	Applied Biosystems, Life Technologies Corporation, California USA
Microscope, Zeis LSM510 Meta confocal	Carl Zeiss S.p.A, Italy
Gene Amp PCR System 2400	Perkin Elmer, Waltham, Massachusetts 02451 USA
TC10™ Automated Cell Counter Biorad	Bio-Rad Laboratories, Inc., Hercules, CA 94547 USA

Equipments	**Manufacturer**
Microtiter plate	Nunc A/S, Roskilde, Denmark
Cell culture bottles	Nunc A/S, Roskilde, Denmark
6-well plate	Corning, Lowell, MA 01851 USA
10 cm dishes	Corning, Lowell, MA 01851 USA
Nitrocellulose Membranes 0,2 µm	Bio-Rad Laboratories, Inc., Hercules, CA 94547 USA
Counting Slides	Bio-Rad Laboratories, Inc., Hercules, CA 94547 USA

Appendix 2: Solutions used in the study

Medium

DMEM/F12

DMEM/F12	6 g
$NAHCO_3$	1.2 g
Distilled water	500 ml

Antibiotics (add to 500 ml DMEM/F12 medium)

AMP	5 ml
Penicillin-Streptomycin	12.5 ml
Amphotericin B	5 ml

Solutions for ELISA

Diluent buffer (Invitrogen, Life technologies)

BSA	5 g
Tween 20	1 ml
Dulbeccos PBS	1000 ml

Blocking/diluent buffer (R&D systems)

BSA	10 g
Dulbeccos PBS	1000 ml

Blocking solution (Invitrogen, Life techonolgies)

BSA	5 g
Dulbeccos PBS	1000 ml

Citrate buffer

Sodium acetate trihydrate	3 g
Distilled water	200 ml

Citric acid is used to adjust pH to 5.5.

TMB

Citrate buffer	11 ml
TMB 6 mg/ml	200 µg
30 % H_2O_2	2.2 µl

Stop solution

H_2SO_4	50 ml
Distilled water	1000 ml

Solutions for Western analysis

5x lysisbuffer	**30 ml**
Tris-HCl 0.5 M pH 7,5	6 ml
Sodium chloride	1.32 g
0,5 M EDTA	300 µl
EGTA	57 mg
Sodium pyrophosphate	167 mg
β-glycerolphosphate	32.4 mg
Sodium orthovanadate	27.6 mg
0,5 M sodium fluoride	300 µl
Triton-x100	1500 µl
Distilled water	add 30 ml

1x lysisbuffer	**5 ml**
5x lysisbuffer	1 ml
10 mg/ml Leupeptin	5 µl
0,1 M PMFS	50 µl
1 mg/ml Pepstatin A	50 µl
10 mg/ml Aprotein	5 µl
Distilled water	3935 µl

10x transfer buffer

Tris-Base	30.3 g
Glycine	144 g
Distilled water	ad 1000 ml

10x electrophoresis buffer

Tris-Base	30 g
Glycine	144 g
SDS	10 g
Distilled water	ad 1000 ml

1x transfer buffer (for immunoblotting)

10x transfer buffer	100 ml
Methanol	200 ml
Distilled water	700 ml

1x electrophoresis buffer (for electrophoresis)

10x electrophoresis buffer	100 ml
Distilled water	900 ml

Ponceau S colour solution

Ponceau S	2 g
Trichloride acetic acid	30 g
Sulfosalicylic acid	30 g
Distilled water	ad 1000 ml

0.5 M Tris-HCl, pH 6.8

Tris-HCl	17.5 g
Tris-Base	1.7 g
Distilled water	ad 250 ml

1.5 M Tris-HCl, pH 8.8

Tris-HCl	9.23 g
Tris-Base	38.5 g
Distilled water	ad 250 ml

10x TBS (washing buffer), pH 7.6

Tris-Base	12 g
Sodium chloride	80 g
Tween-20	10 ml
Distilled water	ad 1000 ml

5x SDS buffer

Tris-HCl 0.5 M, pH 6.8	12,48 ml
SDS	2 g
Mercaptoethanol	5 ml
1 % Bromfenol blue	1 ml
Distilled water	ad 20 ml

Leupeptin 10 mg/ml

Leupeptin (L-2884)	5 mg
H_2O	500 µl

Aprotenin 10 mg/ml

Aprotenin (A-1153)	10 mg
H_2O	1 ml

Pepstatin A 1 mg/ml

Pepstatin	5 mg
DMSO	5000 µl

Dulcobeccos PBS, pH 7.4

Potassium chloride	0.2 g
KH_2PO_4	0.2 g
Sodium chloride	8 g
Na_2HPO_4	1.15 g

10 % polyacrylamide gels	**30 ml**
Distilled water	11.9 ml
30 % acrylamide mix	10.0 ml
1.5 M Tris, pH 8.8	7.5 ml
10 % SDS	300 µl
10 % ammonium persulfate	300 µl
TEMED	12 µl

For a 1.5 mm polyacrylamide gel, one needs 7.5 ml gel solution

Stacking gel

Distilled water	6.1 ml

0.5 M Tris-HCl, pH 6.8	2.5 ml
30 % acrylamide mix	1.3 ml
10 % SDS	100 µl
APS	50 µl
TEMED	10 µl

This is enough for 2 thick gels (1.5 mm) and 2 thin gels (0.75 mm).

Solutions for Real time PCR

Mastermix for cDNA synthesis

Samples and NTC

10 x reverse buffer	2.5 µl
25x dNTP	1 µl
10x random primers	2.5 µl
Multiscribe reverse transcriptase	1.25 µl
Nuclease free water	5.25 µl

NRC

10 x reverse buffer	2.5 µl
25x dNTP	1 µl
10x random primers	2.5 µl
RNase free water	6.5 µl

The total volume for the mastermix in each PCR tube is 12.5 µl.